Measurement of the elliptic anisotropy of charged particles produced in PbPb collisions at $\sqrt{s_{NN}} = 2.76$ TeV

S. Chatrchyan *et al.*[*]
(CMS Collaboration)

(Received 6 April 2012; revised manuscript received 5 November 2012; published 7 January 2013)

The anisotropy of the azimuthal distributions of charged particles produced in $\sqrt{s_{NN}} = 2.76$ TeV PbPb collisions is studied with the CMS experiment at the LHC. The elliptic anisotropy parameter, v_2, defined as the second coefficient in a Fourier expansion of the particle invariant yields, is extracted using the event-plane method, two- and four-particle cumulants, and Lee-Yang zeros. The anisotropy is presented as a function of transverse momentum (p_T), pseudorapidity (η) over a broad kinematic range, $0.3 < p_T < 20$ GeV/c, $|\eta| < 2.4$, and in 12 classes of collision centrality from 0 to 80%. The results are compared to those obtained at lower center-of-mass energies, and various scaling behaviors are examined. When scaled by the geometric eccentricity of the collision zone, the elliptic anisotropy is found to obey a universal scaling with the transverse particle density for different collision systems and center-of-mass energies.

DOI: 10.1103/PhysRevC.87.014902 PACS number(s): 25.75.Gz

I. INTRODUCTION

The azimuthal anisotropy of emitted charged particles is an important feature of the hot, dense medium produced in heavy-ion collisions and has contributed to the suggestion of a strongly coupled quark-gluon plasma (sQGP) being produced in nucleus-nucleus collisions at RHIC [1–5]. In noncentral collisions, the beam direction and the impact parameter vector define a reaction plane for each event. If the nucleon density within the nuclei is continuous, the initial nuclear overlap region is spatially asymmetric with an "almondlike" shape. In this approximation, the impact parameter determines uniquely the initial geometry of the collision, as illustrated in Fig. 1. In a more realistic description, where the position of the individual nucleons that participate in inelastic interactions is considered, the overlap region has a more irregular shape and the event-by-event orientation of the almond fluctuates around the reaction plane. Experimentally, the azimuthal distribution of the particles detected in the final state can be used to determine the "event plane" that contains both the beam direction and the azimuthal direction of maximum particle density. Strong rescattering of the partons in the initial state may lead to local thermal equilibrium and the buildup of anisotropic pressure gradients, which drive a collective anisotropic expansion. The acceleration is greatest in the direction of the largest pressure gradient, that is, along the short axis of the almond. This results in an anisotropic azimuthal distribution of the final-state hadrons. The anisotropy is quantified in terms of a Fourier expansion of the observed particle yields relative to the event-by-event orientation of the event plane [6]:

$$E\frac{d^3N}{d^3p} = \frac{d^3N}{p_T\,dp_T\,dy\,d\varphi} = \frac{1}{2\pi}\frac{d^2N}{p_T\,dp_T\,dy} \times \left(1 + \sum_{n=1}^{\infty} 2v_n(p_T, y)\cos\left[n\left(\varphi - \Psi\right)\right]\right), \quad (1)$$

where φ, E, y, and p_T are the particle's azimuthal angle, energy, rapidity, and transverse momentum, respectively, and Ψ is the event-plane angle. The second coefficient of the expansion, often referred to as the "elliptic flow" strength, carries information about the early collision dynamics [7,8]. The coefficients in the Fourier expansion may depend on p_T, rapidity, and impact parameter. Typically, the measurements are obtained for a particular class of events based on the centrality of the collisions, defined as a fraction of the total inelastic nucleus-nucleus cross section, with 0% denoting the most central collisions with impact parameter $b = 0$ and 100% denoting the most peripheral collisions. Expressions similar to Eq. (1) can be written for the Fourier expansion of the yield integrated over p_T or rapidity:

$$\frac{d^2N}{dy\,d\varphi} = \frac{1}{2\pi}\frac{dN}{dy}\left(1 + \sum_{n=1}^{\infty} 2v_n(y)\cos\left[n\left(\varphi - \Psi\right)\right]\right), \quad (2)$$

and

$$\frac{d^2N}{p_T dp_T\,d\varphi} = \frac{1}{2\pi}\frac{dN}{p_T\,dp_T} \times \left(1 + \sum_{n=1}^{\infty} 2v_n(p_T)\cos\left[n\left(\varphi - \Psi\right)\right]\right). \quad (3)$$

The Fourier coefficients $v_n(y)$ and $v_n(p_T)$ can be obtained by directly analyzing the yields integrated over p_T or rapidity, or from the coefficients of the triple-differential invariant yield in Eq. (1), $v_n(p_T, y)$, by performing the following yield-weighted average over the ranges of transverse momentum

[*]Full author list given at the end of the article.

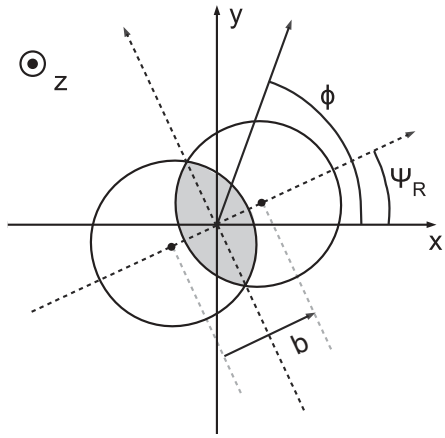

FIG. 1. A schematic diagram of a noncentral nucleus-nucleus collision viewed in the plane orthogonal to the beam. The azimuthal angle φ, the impact parameter vector **b**, and the reaction-plane angle Ψ_R are shown. The event-plane angle Ψ, with respect to which the flow is measured, fluctuates around the reaction-plane angle.

Δp_T and rapidity Δy, from which the particles are taken:

$$v_n(y) = \frac{\int_{\Delta p_T} p_T\, dp_T \frac{d^2N}{p_T\, dp_T\, dy} v_n(p_T, y)}{\int_{\Delta p_T} p_T\, dp_T \frac{d^2N}{p_T\, dp_T\, dy}} \tag{4}$$

or

$$v_n(p_T) = \frac{\int_{\Delta y} dy \frac{d^2N}{p_T\, dp_T\, dy} v_n(p_T, y)}{\int_{\Delta y} dy \frac{d^2N}{p_T\, dp_T\, dy}}. \tag{5}$$

The coefficients of the Fourier expansion of the particles' invariant yield integrated over a broad rapidity and p_T window are often referred to as "integrated flow":

$$\frac{dN}{d\varphi} = \frac{1}{2\pi} N \left(1 + \sum_{n=1}^{\infty} 2v_n \cos\left[n\left(\varphi - \Psi\right)\right]\right), \tag{6}$$

where

$$v_n = \frac{\int_{\Delta y} dy \int_{\Delta p_T} p_T\, dp_T \frac{d^2N}{p_T\, dp_T\, dy} v_n(p_T, y)}{\int_{\Delta y} dy \int_{\Delta p_T} p_T\, dp_T \frac{d^2N}{p_T\, dp_T\, dy}}. \tag{7}$$

In obtaining the Fourier coefficients, the absolute normalization in the particle yields is not important, as long as the particle detection efficiency is constant over the chosen transverse momentum and rapidity range. However, if the efficiency varies, the appropriate efficiency corrections need to be applied. This often leads to a two-step procedure in which first $v_n(p_T, y)$ is obtained in a narrow phase-space window where the efficiency is constant, and then a yield-weighted average is performed using Eqs. (4), (5), or (7), folding in the efficiency-corrected particle spectra. When the particle mass is not determined in the measurement, the pseudorapidity $\eta = -\ln[\tan(\theta/2)]$, with θ being the polar angle, is used instead of the rapidity.

Elliptic flow has been measured at the AGS, SPS, and RHIC. A notable feature in these measurements is that the elliptic flow measured as a function of transverse momentum, $v_2(p_T)$ increases with the nucleon-nucleon center-of-mass energy ($\sqrt{s_{NN}}$) up to about 22 GeV [9,10] and then saturates at a value compatible with predictions from ideal hydrodynamics [11,12]. The most extensive experimental studies have been performed at the highest RHIC energy of $\sqrt{s_{NN}} = 200$ GeV in AuAu collisions [1–3]. First results from PbPb collisions at $\sqrt{s_{NN}} = 2.76$ TeV from the Large Hadron Collider (LHC) [13,14] indicate that there is little or no change in the transverse momentum dependence of the elliptic flow measured at the highest RHIC energy and the LHC, despite the approximately 14-fold increase in the center-of-mass energy. Recent theoretical studies of elliptic flow have focused on quantifying the ratio of the shear viscosity to the entropy density of the produced medium assuming viscous hydrodynamics [15,16] and taking into account a variety of possible initial conditions.

Based on experimental results and the corresponding theoretical descriptions of the data, the underlying physics processes that generate the elliptic anisotropy are thought to vary for different kinematic regions.

(i) *Elliptic flow in the bulk system.* Hadrons produced in soft processes, carrying low transverse momentum ($p_T \lesssim 2$ GeV/c for mesons and $p_T \lesssim 3$ GeV/c for baryons [17–20]), exhibit azimuthal anisotropies that can be attributed to collective flow driven by the pressure gradients in the system. The description of elliptic flow is amenable to hydrodynamic calculations [12,15,21,22]. Comparisons to theory indicate that the flow is primarily generated during an early stage of the system evolution.

(ii) *Recombination region.* At intermediate transverse particle momentum ($2 \lesssim p_T \lesssim 4$ GeV/c), the RHIC data show that the elliptic anisotropies for various identified hadron species approximately follow a common behavior when both the $v_2(p_T)$ value and the p_T of the particle are divided by the number of valence quarks in the hadron [17,18,23]. This behavior is successfully reproduced by models invoking quark recombination as the dominant hadronization mechanism in this momentum range [24–26]. The quark-number scaling of the elliptic flow has been interpreted as evidence that quark degrees of freedom dominate in the early stages of heavy-ion collisions, when the collective flow develops [27]. The quark recombination may involve both thermally produced quarks and quarks originating in jet fragmentation. Therefore, the elliptic anisotropy in the recombination region results from an interplay between the bulk flow of the system and the azimuthal anisotropy in hadron production induced by jet quenching.

(iii) *Jet-fragmentation region.* At intermediate and high transverse momentum ($p_T \gtrsim 3$ GeV/c), where fragments from increasingly harder partons begin to contribute to the particle spectra, anisotropy in the azimuthal distributions may be generated from the stronger jet quenching in the direction of the long axis of the almond-shaped reaction zone [28–31]. It is expected that this mechanism will dominate the elliptic anisotropy of hadrons with momenta in excess of 8 GeV/c. Thus, measurements extending beyond

this p_T range carry information about the path-length dependence of energy loss in the produced medium.

The measurements presented in this paper span the transverse momentum range of $0.3 < p_T < 20$ GeV/c and provide the basis for comparisons to theoretical descriptions of the bulk properties of the system and the quenching of jets. Such comparisons may give insight in determining the transport properties of sQGP, namely, the shear viscosity, and the opacity of the plasma. The theoretical interpretation of the elliptic anisotropy in the recombination region requires identified-hadron measurements that are not included in this analysis.

In ideal hydrodynamics, the integrated elliptic flow is directly proportional to the initial spatial eccentricity of the overlap zone [32]. There are many factors that can change this behavior, including viscosity in the sQGP and the hadronic stages of the system evolution, incomplete thermalization in peripheral collisions, and variations in the equation of state. Event-by-event fluctuations in the overlap zone [33–38] could also influence the experimental results, depending on the method that is used to extract the v_2 signal. Invoking multiple methods with different sensitivities to the initial-state fluctuations is important for disentangling the variety of physics processes that affect the centrality dependence of the elliptic flow. Comparisons to results from lower-energy measurements and explorations of empirical scaling behaviors could provide additional insights into the nature of the matter produced in high-energy heavy-ion collisions.

The pseudorapidity dependence of the elliptic flow, $v_2(\eta)$, provides information on the initial state and the early time development of the collision, constraining the theoretical models and the description of the longitudinal dynamics in the collisions [39,40]. Longitudinal scaling in $v_2(\eta)$ extending over several units of pseudorapidity (extended longitudinal scaling) has been reported at RHIC [41] for a broad range of collision energies ($\sqrt{s_{NN}} = 19.6$–200 GeV). Studies of the evolution of $v_2(\eta)$ from RHIC to LHC energies may have implications for the unified description of sQGP in both energy regimes.

The paper is organized as follows. Section II gives the experimental details of the measurement including the Compact Muon Solenoid (CMS) detector, triggering and event selection, centrality determination, Glauber-model calculations, reconstruction of the charged-particle transverse momentum spectra, methods of measuring the elliptic anisotropy, and the studies of the systematic uncertainties. In Sec. III we present results of v_2 as a function of transverse momentum, centrality, and pseudorapidity and the measurement of the charged-particle transverse momentum spectra. The elliptic flow results are obtained with the event-plane method [6], two- and four-particle cumulants [42], and Lee-Yang zeros [43,44]. The analysis is performed in 12 classes of collision centrality covering the most central 80% of inelastic collisions. We study the eccentricity scaling of v_2 and investigate the differences in the results obtained from different methods, taking into account their sensitivity to initial-state fluctuations. Section IV is devoted to detailed comparisons with results obtained by other experiments at lower energies and the exploration of different scaling behaviors of the elliptic flow. The results of our studies are summarized in Sec. V.

II. EXPERIMENTAL METHOD

A. CMS detector

The central feature of the CMS apparatus is a superconducting solenoid of 6 m internal diameter, providing a 3.8-T field. Within the field volume are a silicon tracker, a crystal electromagnetic calorimeter, and a brass/scintillator hadron calorimeter. Muons are measured in gas-ionization detectors embedded in the steel return yoke. In addition to these detectors, CMS has extensive forward calorimetry. The inner tracker measures charged particles within the pseudorapidity range $|\eta| < 2.5$ and consists of silicon pixel and silicon strip detector modules. The beam scintillation counters (BSCs) are a series of scintillator tiles which are sensitive to almost the full PbPb interaction cross section. These tiles are placed along the beam line at a distance of ± 10.9 and ± 14.4 m from the interaction point and can be used to provide minimum-bias triggers. The forward hadron calorimeter (HF) consists of a steel absorber structure that is composed of grooved plates with quartz fibers inserted into these grooves. The HF calorimeters have a cylindrical shape and are placed at a distance of 11.2 m from the interaction point, covering the pseudorapidity range of $2.9 < |\eta| < 5.2$. A more detailed description of the CMS detector can be found elsewhere [45].

The detector coordinate system has the origin centered at the nominal collision point inside the experiment, with the y axis pointing vertically upward, the x axis pointing radially inward towards the center of the LHC ring, and the z axis pointing along the counterclockwise beam direction.

B. Event selection

The measurements presented are performed by analyzing PbPb collision events recorded by the CMS detector in 2010. From these data, the minimum-bias event sample is collected using coincidences between the trigger signals from both the $+z$ and $-z$ sides of either the BSC or HF. The minimum-bias trigger used for this analysis is required to be in coincidence with the presence of both colliding ion bunches in the interaction region. This requirement suppresses noncollision-related noise, cosmic rays, and beam backgrounds (beam halo and beam-gas collisions). The total hadronic collision rate varied between 1 and 210 Hz, depending on the number of colliding bunches and the bunch intensity.

To obtain a pure sample of inelastic hadronic collisions, several offline selections are applied to the triggered event sample. These selections remove contamination from noncollision beam backgrounds and from ultraperipheral collisions (UPCs) that lead to an electromagnetic breakup of one or both of the Pb nuclei [46]. First, beam-halo events are vetoed based on the BSC timing. Then, to remove UPC and beam-gas events, an offline HF coincidence of at least three towers on each side of the interaction point is required, with a total deposited energy of at least 3 GeV in each tower. A reconstructed primary vertex made of at least two tracks and consistent with the nominal

interaction point position is required. To further reject beam-gas and beam-halo events, the pixel clusters are required to have a length along the beam direction compatible with being produced by particles originating from the primary vertex, as for the study in Ref. [47]. Additionally, a small number of noisy events with uncharacteristic hadron calorimeter responses are removed.

The acceptance of the silicon tracker for $|\eta| > 0.8$ is found to vary significantly with respect to the longitudinal position of the collision point relative to the geometric center of the detector. This event-by-event variance in the tracking efficiency contributes to a systematic bias of the elliptic flow measurements at forward pseudorapidity. To remove this bias, events in this analysis are required to have a longitudinal vertex position within 10 cm of the geometric center of the detector. After all selections, 22.6×10^6 minimum-bias events, corresponding to an integrated luminosity of approximately 3 μb^{-1}, remain in the final sample.

C. Centrality determination and Glauber model calculations

In this analysis, the observable used to determine centrality is the total energy in both HF calorimeters. The distribution of this total energy is used to divide the event sample into 40 centrality bins, each representing 2.5% of the total nucleus-nucleus interaction cross section. The events are then regrouped to form 12 centrality classes used in the analysis: 0–5% (most central), 5–10%, 10–15%, 15–20%, 20–25%, 25–30%, 30–35%, 35–40%, 40–50%, 50–60%, 60–70%, and 70–80% (see Table I). Using Monte Carlo (MC) simulations, it is estimated that the minimum-bias trigger and the event selections include $(97 \pm 3)\%$ of the total inelastic cross section. For the events included in this analysis (0–80% centrality), the trigger is fully efficient.

For each group of events that comprises a centrality class, we evaluate a set of quantities that characterize the initial geometry of the collisions using a MC Glauber model. The Glauber model is a multiple-collision model that treats a nucleus-nucleus collision as an independent sequence of nucleon-nucleon collisions (see Ref. [48] and references therein). The nucleons that participate in inelastic interactions are called "participants." A schematic view of a PbPb collision with an impact parameter $b = 6$ fm, as obtained from the Glauber model, is shown in Fig. 2. The direction and the magnitude of the impact parameter vector and the corresponding reaction-plane angle Ψ_R are the same as in Fig. 1. However, the initial interaction zone as determined by the spatial distribution of the participants (solid circles) is no longer regular in shape and is not necessarily symmetric with respect to the reaction plane. In each event one can evaluate the variances σ_x^2 and σ_y^2, and the covariance $\sigma_{xy} = \langle xy \rangle - \langle x \rangle \langle y \rangle$ of the participant distributions projected on the x and y axes. One can then find a frame x'-y' that minimizes $\sigma_{x'}$, and define a "participant plane" using the beam direction and the x' axis [34,49]. In this frame, the covariance $\sigma_{x'y'}$ of the participant spatial distribution vanishes. To characterize the geometry of the initial state of the collision, we define [34,49] the eccentricity of the participant zone ϵ_{part}, its cumulant moments $\epsilon\{2\}$ and $\epsilon\{4\}$,

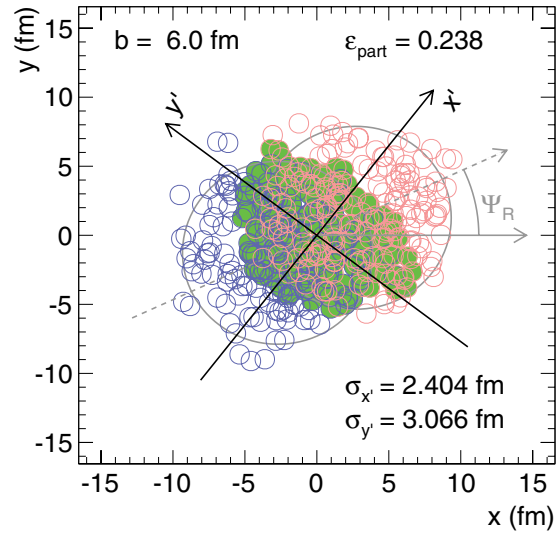

FIG. 2. (Color online) A schematic view of a PbPb collision with an impact parameter $b = 6$ fm, as obtained from the Glauber model. The nucleons that participate in inelastic interactions are marked with solid circles. The x and y coordinates represent the laboratory frame, while x' and y' represent the frame that is aligned with the axes of the ellipse in the participant zone. The participant eccentricity ϵ_{part} and the standard deviations of the participant spatial distribution $\sigma_{y'}$ and $\sigma_{x'}$ from which the transverse overlap area of the two nuclei is calculated are also shown. The angle Ψ_{R} denotes the orientation of the reaction plane.

and the transverse overlap area of the two nuclei S:

$$\epsilon_{\text{part}} \equiv \frac{\sigma_{y'}^2 - \sigma_{x'}^2}{\sigma_{y'}^2 + \sigma_{x'}^2} = \frac{\sqrt{\left(\sigma_y^2 - \sigma_x^2\right)^2 + 4\sigma_{xy}^2}}{\sigma_y^2 + \sigma_x^2}, \tag{8}$$

$$\epsilon\{2\}^2 \equiv \left\langle \epsilon_{\text{part}}^2 \right\rangle, \tag{9}$$

$$\epsilon\{4\}^4 \equiv 2\left\langle \epsilon_{\text{part}}^2 \right\rangle^2 - \left\langle \epsilon_{\text{part}}^4 \right\rangle, \tag{10}$$

and

$$S \equiv \pi \sigma_{x'} \sigma_{y'} = \pi \sqrt{\sigma_x^2 \sigma_y^2 - \sigma_{xy}^2}. \tag{11}$$

In Eqs. (9) and (10), the average is taken over many events from the same centrality interval.

To implement the Glauber model for PbPb collisions at $\sqrt{s_{NN}} = 2.76$ TeV, we utilize the foundation of a published Glauber MC software package TGLAUBERMC [50], which was developed for the PHOBOS Collaboration at RHIC. Standard parameters of the Woods-Saxon function used for modeling the distribution of nucleons in the Pb nuclei are taken from Ref. [51]. The nucleon-nucleon inelastic cross section, which is used to determine how close the nucleon trajectories need to be for an interaction to occur, is taken as 64 ± 5 mb, based on a fit of the existing data for total and elastic cross sections in proton-proton and proton-antiproton collisions [52]. The uncertainties in the parameters involved in these calculations contribute to the systematic uncertainty in N_{part}, S, and ϵ_{part} for a given centrality bin. The connection between the experimentally defined centrality classes using the HF energy distribution and N_{part} from the Glauber model is obtained [53]

TABLE I. For the centrality bins used in the analysis, the average values of the number of participating nucleons, transverse overlap area of the two nuclei, participant eccentricity, and cumulant moments of the participant eccentricity, along with their systematic uncertainties from the Glauber model.

Centrality range (%)	$\langle N_{\text{part}} \rangle$	$\langle S \rangle$ (fm^2)	$\langle \epsilon_{\text{part}} \rangle$	$\epsilon\{2\}$	$\epsilon\{4\}$
0–5	381 ± 2	29.4 ± 1.2	0.074 ± 0.003	0.084 ± 0.003	0.053 ± 0.002
5–10	329 ± 3	26.6 ± 1.1	0.111 ± 0.005	0.128 ± 0.005	0.060 ± 0.003
10–15	283 ± 3	24.0 ± 1.0	0.154 ± 0.007	0.175 ± 0.007	0.122 ± 0.005
15–20	240 ± 3	21.6 ± 1.0	0.198 ± 0.009	0.219 ± 0.009	0.171 ± 0.007
20–25	204 ± 3	19.5 ± 0.9	0.238 ± 0.009	0.262 ± 0.010	0.214 ± 0.008
25–30	171 ± 3	17.5 ± 0.8	0.276 ± 0.010	0.302 ± 0.012	0.253 ± 0.010
30–35	143 ± 3	15.7 ± 0.8	0.312 ± 0.011	0.339 ± 0.012	0.288 ± 0.010
35–40	118 ± 3	14.1 ± 0.7	0.346 ± 0.010	0.375 ± 0.011	0.322 ± 0.009
40–50	86.2 ± 2.8	12.0 ± 0.6	0.395 ± 0.010	0.429 ± 0.011	0.370 ± 0.010
50–60	53.5 ± 2.5	9.4 ± 0.5	0.465 ± 0.008	0.501 ± 0.009	0.437 ± 0.007
60–70	30.5 ± 1.8	7.1 ± 0.4	0.543 ± 0.011	0.581 ± 0.012	0.514 ± 0.010
70–80	15.7 ± 1.1	4.8 ± 0.3	0.630 ± 0.016	0.662 ± 0.017	0.598 ± 0.015

from fully simulated and reconstructed MC events generated with the AMPT [54] event generator. The calculated Glauber model variables for each centrality class are shown in Table I.

D. Reconstruction of the charged-particle transverse momentum distributions and the mean transverse momentum

To determine the transverse momentum distributions of the charged particles produced in the collisions, we first need to reconstruct the particles' trajectories ("tracks") through the 3.8 T solenoidal magnetic field. The tracks are reconstructed by starting with a "seed" comprising two or three reconstructed signals ("hits") in the inner layers of the silicon strip and pixel detectors that are compatible with a helical trajectory of some minimum p_{T} and a selected region around the reconstructed primary vertex or nominal interaction point. This seed is then propagated outward through subsequent layers using a combinatorial Kalman-filter algorithm. Tracking is generally performed in multiple iterations, varying the layers used in the seeding and the parameters used in the pattern recognition and removing duplicate tracks between iterations. This algorithm is described in detail in Ref. [55]. The algorithm used in most of the CMS proton-proton analyses, as well as the tracking detector performance for the 2010 run, are described in Ref. [56].

The six-iteration process used in proton-proton collisions is computationally not feasible in the high-multiplicity environment of very central PbPb collisions. In place of this, a simple two-iteration process is used. The first iteration builds seeds from hits in some combination of three layers in the barrel and end-cap pixel detectors compatible with a trajectory of $p_{\text{T}} > 0.9$ GeV/c and a distance of closest approach to the reconstructed vertex of no more than 0.1 cm in the transverse plane and 0.2 cm longitudinally. These tracks are then filtered using selection criteria based on a minimum number of reconstructed hits, vertex compatibility along the longitudinal direction and in the transverse plane, and low relative uncertainty on the reconstructed momentum.

In the second iteration, seeding is also performed using three layers of the pixel detector, but the minimum transverse momentum requirement is relaxed to $p_{\text{T}} > 0.2$ GeV/c. These tracks are not propagated through the silicon-strip detector, but simply refitted using the transverse position of the beam spot as an additional constraint. These pixel-only tracks are then filtered using selection criteria of vertex compatibility along the longitudinal axis and statistical goodness of fit.

The tracks from both collections are checked for duplicate tracks using the number of hits in common between the two tracks, and duplicates are removed giving preference to the first-iteration tracks. The tracking algorithm may sometimes misidentify tracks by combining silicon detector signals that do not originate from the same charged particle. It is important to keep the proportion of misidentified tracks (referred to as "fake tracks"), or fake rate, as low as possible. To create the final collection, first-iteration tracks with $p_{\text{T}} > 1.5$ GeV/c are combined with second-iteration pixel-only tracks with $p_{\text{T}} < 1.8$ GeV/c. These p_{T} limits were chosen to exclude kinematic regions where a given iteration has a high fake rate. The efficiency and fake rate of this modified tracking collection are found both by using a full MC simulation of PbPb collisions based on the HYDJET event generator [57] and by embedding simulated charged pions into PbPb data events. The efficiency, fake rate, and momentum resolution of this final collection determined by the simulated events from the HYDJET event generator are shown in Fig. 3 for events of five different centrality classes. The abrupt change in efficiency, fake rate, and momentum resolution seen in the figure occurs at the transverse momentum where the two track collections are merged.

The charged-particle transverse momentum distributions are corrected for the loss of acceptance, efficiency, and the contributions from fake tracks. Each detected track is weighted by a factor w_{tr} according to its centrality, transverse momentum, and pseudorapidity:

$$w_{tr}(\text{centrality}, p_{\text{T}}, \eta) = \frac{1 - f}{e}. \tag{12}$$

Here f is the fraction of fake tracks that do not correspond to any charged particle, and e is the absolute tracking efficiency accounting for both geometric detector acceptance

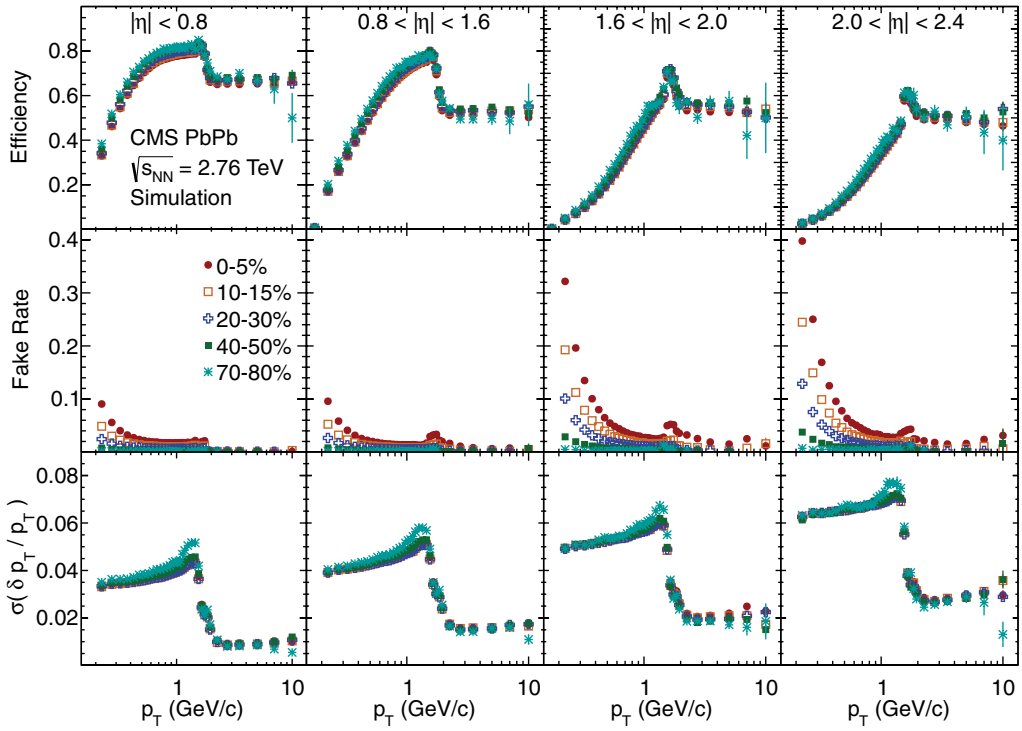

FIG. 3. (Color online) Efficiency (top), fake rate (middle), and momentum resolution (bottom) of charged tracks obtained from HYDJET simulated events in four pseudorapidity regions: $|\eta| < 0.8$, $0.8 < |\eta| < 1.6$, $1.6 < |\eta| < 2.0$, and $2.0 < |\eta| < 2.4$ displayed from left to right, and for the five centrality classes given in the legend.

and algorithmic tracking efficiency. The proportion of multiply reconstructed particles and reconstructed particles from secondary decays is negligible and is not included in the correction factor. The fully corrected transverse momentum distributions are measured in 12 centrality classes over the pseudorapidity range $|\eta| < 2.4$ in bins of $\Delta\eta = 0.4$, as discussed in Sec. III D. These distributions are used in obtaining integrated v_2 values. We also study the evolution of $\langle p_{\mathrm{T}} \rangle$ with pseudorapidity and centrality (Sec. III D) and center-of-mass energy (Sec. IV).

To evaluate $\langle p_{\mathrm{T}} \rangle$, the spectra need to be extrapolated down to $p_{\mathrm{T}} = 0$ GeV/c. The extrapolation is performed using a Tsallis distribution [58–60]:

$$E\frac{d^3N_{\mathrm{ch}}}{dp^3} = \frac{1}{2\pi p_T}\frac{E}{p}\frac{d^2N_{\mathrm{ch}}}{d\eta dp_T} = C\left(1+\frac{E_T}{nT}\right)^{-n}, \quad (13)$$

where $E_T = \sqrt{m^2 + p_{\mathrm{T}}^2} - m$ and m is taken to be the charged pion mass. The measured spectra are fitted in the range $0.3 < p_{\mathrm{T}} < 3.0$ GeV/c, and the fit parameters C, n, and T are determined. The mean transverse momentum is then evaluated using the fit function in the extrapolation region of $0 \leqslant p_{\mathrm{T}} < 0.3$ GeV/c, and the data from the range $0.3 \leqslant p_{\mathrm{T}} \leqslant 6.0$ GeV/c. This method has been previously applied in CMS [47] in the measurement of $\langle p_{\mathrm{T}} \rangle$ in pp collisions at $\sqrt{s} = 7$ TeV.

E. Methods for measuring the anisotropy parameter v_2

Anisotropic flow aims to measure the azimuthal correlations of the particles produced in heavy-ion collisions in relation to the initial geometry of the collisions. Originally, the flow was defined as a correlation of the particle emission angles with the reaction plane [6,7]. More recently, it was recognized [34,49] that the initial geometry is better characterized by the positions of the individual nucleons that participate in inelastic interactions and thus define a participant plane that fluctuates around the reaction plane on an event-by-event basis. Neither the reaction plane nor the participant plane are directly measurable experimentally. Instead, there are several experimental methods that have been developed to evaluate the anisotropic flow based on the final-state particle distributions. In the present analysis, we use the event-plane method, two-particle and four-particle cumulants [42], and the Lee-Yang zeros method [43,44], the last of which is based on correlations involving all the particles in the event.

The anisotropic flow measurements are affected by fluctuations that come from several sources. Statistical fluctuations arise owing to the fact that a finite number of particles is used to determine a reference plane for the flow and the multiplicity fluctuations within the chosen centrality interval. The effect of these fluctuations is to reduce the measured flow signal and is largely compensated for by the resolution corrections described below. Any remaining effects from statistical fluctuations on our measurements are included in the systematic uncertainties (see Sec. II G). Another more important source of fluctuations comes from the event-by-event fluctuations in the participant eccentricity that are present even at fixed N_{part}. These dynamical fluctuations have been shown [34–38] to affect the various methods for estimating the flow differently, because each of them is based on a

different moment of the final-particle momentum distribution. For example, the two-particle cumulant method measures an rms value of the flow that is higher than the mean value. Conversely, the four-particle cumulant and other multiparticle correlation methods return a value that is lower than the mean value. For the event-plane method, the results vary between the mean and the rms value depending on the event-plane resolution, which varies in each centrality interval.

In addition, there exist other sources of correlations in azimuth, such as those from resonance decays, jets, and Bose-Einstein correlations between identical particles. These correlations, which are not related to the participant plane, are called nonflow correlations. The various methods proposed to estimate the magnitude of anisotropic flow have different sensitivities to the nonflow correlations, thus allowing systematic checks on the flow measurements. The multiparticle correlation methods are least affected by nonflow correlations, but they do not work reliably when either the flow anisotropy (v_2) or the multiplicity in the selected phase-space window is small. This happens in the most central and in the most peripheral events [42,43]. Thus, the two-particle cumulant and the event-plane methods provide an extended centrality range, albeit with a larger nonflow contribution.

All four methods used here have been extensively studied and applied in different experiments. Thus, we limit our description in the following subsections only to the features that are specific for our implementations of these methods.

1. Event-plane method

The event-plane method estimates the magnitude of anisotropic flow by reconstructing an "event plane" containing both the beam direction and the direction of the maximal flow determined from the azimuthal distributions of the final-state particles. Under the assumption that the flow is driven by the initial-state asymmetry in the nuclear overlap zone and that there are no other sources of azimuthal correlations in the final-state particles, the event plane is expected to coincide with the participant plane [34] defined in Fig. 2. Recent theoretical calculations [38,61–63] confirm that the event plane and the participant plane are strongly correlated event by event. Because the event plane is determined using a finite number of particles, and detected with finite angular resolution, the measured event-plane angle fluctuates about its true value. As a result, the observed particle azimuthal anisotropy with respect to the event plane is smeared compared to its true value. The true elliptic flow coefficient v_2 in the event-plane method is evaluated by dividing the observed $v_2^{\rm obs}$ value by a resolution correction factor, R, which accounts for the event-plane resolution.

To determine the event-plane resolution correction, a technique that sorts the particles from each event into three subevents based on their pseudorapidity values [6] is used. For subevents A, B, C in three different pseudorapidity windows, the event-plane resolution correction factor R_A for subevent A is found as

$$R_A = \sqrt{\frac{\langle\cos[2(\Psi^A - \Psi^B)]\rangle\langle\cos[2(\Psi^A - \Psi^C)]\rangle}{\langle\cos[2(\Psi^B - \Psi^C)]\rangle}}, \quad (14)$$

where Ψ^A, Ψ^B, and Ψ^C are the event-plane angles determined from the corresponding subevents, and the average is over all events in a selected centrality class used in the v_2 analysis.

In our implementation of the method, the event-plane angle determined for the subevent furthest in η from the track being used in the elliptic flow analysis is used, and the corresponding resolution correction is employed. This selection minimizes the contributions of autocorrelations and other nonflow effects that arise if the particles used in the event-plane determination and those used in the flow analysis are close in phase space.

To achieve the largest pseudorapidity gap possible, two event planes are defined, with calorimeter data covering the pseudorapidity ranges of $-5 < \eta < -3$ and $3 < \eta < 5$, labeled "$HF-$" and "$HF+$", respectively. These pseudorapidity ranges are primarily within the coverage of the HF calorimeters. A third event plane, found using charged particles detected in the tracker in the pseudorapidity range $-0.8 < \eta < 0.8$, is also defined and used in the three-subevent technique for determining the resolution corrections for $HF-$ and $HF+$. The resulting resolution corrections are presented in Fig. 4. Particles detected in the tracker with $\eta > 0$ are then correlated with the $HF-$ event plane, and those with $\eta < 0$ with the $HF+$ plane. In this manner, the minimum pseudorapidity gap between particles used in the event-plane determination and those for which the v_2 signal is measured is 3 units. A two-subevent technique based on $HF-$ and $HF+$, with a resolution parameter defined as $R_{A/B} = \sqrt{\langle\cos[2(\Psi^A - \Psi^B)]\rangle}$, is also implemented and used for systematic studies. The values of $R_{A/B}$ are shown for comparison in Fig. 4.

A standard flattening procedure [64] using a Fourier decomposition of the distribution of the event-plane angles

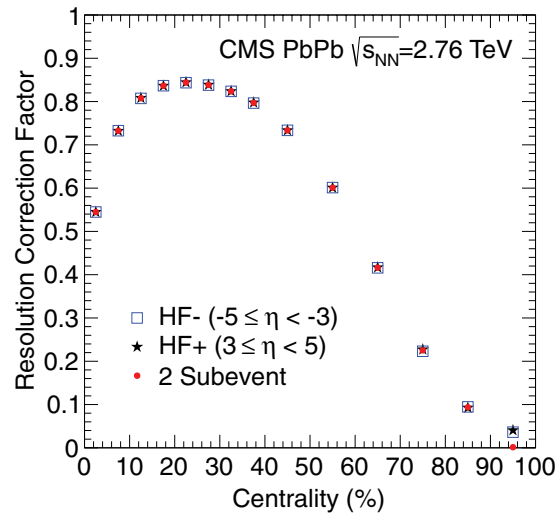

FIG. 4. (Color online) Event-plane resolution correction factors as a function of centrality for the two event planes ($HF-$ and $HF+$) used in determining the elliptic anisotropy parameter v_2. The corrections determined with the three-subevent method used in the analysis are shown as open squares and star symbols. The results from a two-subevent method used in evaluating the systematic uncertainties are shown as solid circles, though they overlap the other points in all but the most peripheral bin.

to 21st order is used to shift the event-by-event plane angle to correct for asymmetries in the event-plane distribution that arise from the detector acceptance and other instrumental effects. Although most of these effects are already accounted for with a correction involving just the first four coefficients in the expansion, the larger order was used for data quality monitoring purposes. For each centrality class in the analysis, the flattening parameters are calculated by grouping events according to the longitudinal location of their primary collision vertex in 5-cm-wide bins.

2. *Cumulant method*

The cumulant method measures flow utilizing a cumulant expansion of multiparticle azimuthal correlations, without determining the orientation of the event plane. The idea is that if the particles are correlated with the event-plane orientation, then there also exist correlations between them. In our analysis, we utilize two- and four-particle correlations. To calculate the cumulants of these correlations, from which the flow coefficient is extracted, we use a generating function of the multiparticle correlations in a complex plane [42]. First, we evaluate the "integrated," or reference, flow by constructing the corresponding generating function including all particles from a broad (p_T, η) window and averaging over the events in a given centrality class. The reference flow may not be corrected for tracking efficiency and should not be equated with the fully corrected integrated flow of the events. Then, the differential flow, that is, the flow in a narrower phase-space window, either in p_T or η, is measured with respect to the reference flow. In the cumulant and Lee-Yang zeros methods, the reference flow serves the same purpose as the determination of the event-plane angle and the resolution correction factors in the event-plane method. In our analysis of $v_2(p_T)$, the p_T and η ranges for the reference flow are $0.3 < p_T < 3$ GeV/c and $|\eta| < 0.8$, respectively. In the analysis of $v_2(\eta)$, the reference flow is obtained for the range $0.3 < p_T < 3$ GeV/c and $|\eta| < 2.4$ to maximize the resolution parameter, which improves as the charged hadron multiplicity M in the selected phase-space window increases. The transverse momentum restriction of $p_T < 3$ GeV/c is imposed to limit the contributions from hadrons originating in jets, and thus reduce the nonflow correlations contributing to the measured elliptic anisotropy parameter. To avoid autocorrelations, the particles used for determining differential flow are not included in evaluating the reference flow. The generating function for the reference flow is calculated at several different points in the complex plane, and we then interpolate between these points. We use three values for the radius parameter, r_0, and seven values for the polar angle, as described in Ref. [42]. The radius parameters are determined according to the detected charged particle multiplicity and the number of events analyzed in each centrality class. Each particle in the differential p_T or η bin is correlated to the particles used for the reference flow through a differential generating function. To account for the fact that the track reconstruction efficiency may vary across the chosen bin, we implement an efficiency correction that is applied as a track-by-track weight in the construction of the differential generating function.

3. *Lee-Yang zeros method*

The Lee-Yang zeros (LYZ) method [43,44] for directly measuring the flow is based on multiparticle correlations involving all particles in the event. It uses the asymptotic behavior of the cumulant expansion to relate the location of the zeros of a complex function to the magnitude of the integrated flow in the system. For a detector with a uniform detection efficiency for all particles in the chosen η and p_T window, it is thus possible to obtain the integrated flow in a simple one-step procedure. Because this is not the case for the CMS measurements presented here, we replace the term "integrated flow" that is used in the literature describing the method [43,44] with "reference flow." In the generating function [i.e., $G^{\theta}(ir)$, where r is the imaginary axis coordinate], the flow vector, constructed from all particles in the event, is projected onto a direction that makes an arbitrary angle θ with respect to the x axis. We use five different projection angles and then average the results over events from the same centrality class to reduce the statistical uncertainties. Subsequently, the minimum of the generating function is found, and the differential flow is determined with respect to the reference flow. There are different ways to define the generating function that involve either a sum or a product of the individual particle contributions. An example is given in Fig. 5, showing how the minimum of the generating function is determined using both definitions. The results presented here are based on the product generating function. In our analysis of $v_2(p_T)$, the p_T and η ranges for the reference flow are $0.3 < p_T < 12$ GeV/c and $|\eta| < 0.8$, respectively. Because the LYZ method is less sensitive to jet-induced charged-particle correlations than the two-particle cumulant method, the p_T range of the tracks included in the determination of the reference flow is not

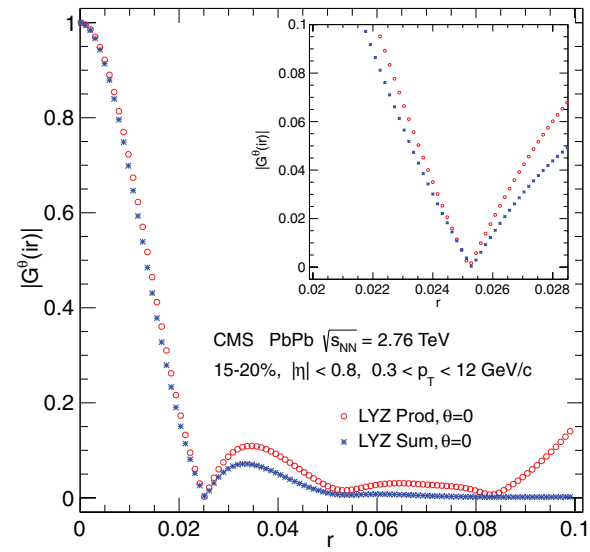

FIG. 5. (Color online) An example of the modulus of the second harmonic LYZ generating function $G^{\theta}(ir)$ as a function of the imaginary axis coordinate r for $\theta = 0$. Both the sum and the product generating functions are shown, calculated from events with centrality 15–20%, $|\eta| < 0.8$, and $0.3 < p_T < 12$ GeV/c. An enlargement of $|G^{\theta}(ir)|$ around its first minimum is shown in the inset.

restricted to low p_T. In the analysis of $v_2(\eta)$, the pseudorapidity range for the particles included in the reference flow is extended to $|\eta| < 2.4$.

The LYZ method is sensitive to multiplicity fluctuations. To evaluate the effects of these fluctuations we perform a toy-model MC study. Event ensembles are generated sampling the multiplicity for each event from Gaussian distributions with mean and rms values comparable to the ones measured in the centrality bins used in the measurement. For each particle, the corresponding p_T, η, and ϕ values are sampled from a realistic input $v_2(p_T, \eta)$ distribution. These events are then analyzed using the same procedure as in the data and the resulting $v_2(p_T, \eta)$ values are compared to the input. We find that the Lee-Yang zeros method tends to underestimate the results if the rms of the multiplicity distribution is more than about 14% of the mean. To keep the systematic uncertainties below 2%, the data are analyzed in 5%-wide centrality classes and then averaged and weighted with the charged-particle yield to obtain results in wider centrality intervals needed for comparisons with other methods. Efficiency corrections are implemented as a track-by-track weight in the differential generating function.

F. Corrections to the anisotropy parameter v_2

In determining the $v_2(p_T)$ distributions for particles detected in the tracker, it is necessary to correct for the influence of misidentified (i.e., "fake") tracks on the measurements. As shown in Sec. II D, the fake-track contribution is particularly significant at low-p_T values and for pseudorapidities $|\eta| > 1.6$. Of particular concern is the observation that the fake tracks can carry a v_2 signal at low p_T similar to that of properly reconstructed (i.e., "real") tracks at a higher p_T. Because the true v_2 signal is very small at low p_T, but increases at higher p_T, the fake tracks may contribute a significant fraction of the measured v_2 signal at low p_T.

Studies using a full MC CMS simulation of PbPb collisions based on the HYDJET event generator [57] indicate that the component of the v_2 signal owing to fake tracks is relatively constant for $p_T < 0.8$ GeV/c, where the fraction of fake tracks is largest. For higher p_T, where the fraction of fake tracks is quite small, the value of v_2 is consistent with the measured value from correctly reconstructed tracks. This suggests the following simple correction scheme. Let $N_{\rm det}(p_T)$ be the number of reconstructed tracks in a given p_T bin, f the fraction of these tracks that are "fake," $N_{\rm true}$ the number of "true" tracks in the p_T bin, and e the efficiency for reconstructing a true track in the bin. Then $N_{\rm det} - fN_{\rm det} = eN_{\rm true}$. The $fN_{\rm det}$ fake tracks are characterized by a constant v_2 value given by $v_2^{\rm fake}$. The $N_{\rm det} - fN_{\rm det}$ real tracks are characterized by $v_2^{\rm real}$. Then the observed value $v_2^{\rm obs}$ of v_2 will be

$$v_2^{\rm obs} = (1 - f)v_2^{\rm real} + f v_2^{\rm fake} \tag{15}$$

and so

$$v_2^{\rm real} = \frac{v_2^{\rm obs} - f v_2^{\rm fake}}{1 - f}. \tag{16}$$

This correction for the fake-track signal is significant only for p_T values less than $\approx$1 GeV/c. In this range, an empirical correction that results in values of v_2 that are independent of the track selection requirements or fraction of fake tracks is applied using $v_2^{\rm fake} = 1.3\,\langle v_2 \rangle$, where the yield-weighted average is performed over the transverse momentum range 0.3 to 3 GeV/c, folding in the efficiency-corrected spectra. This value for $v_2^{\rm fake}$ is also supported by MC studies using HYDJET.

G. Systematic uncertainties

1. *Systematic uncertainties in the measurements of v_2*

The systematic uncertainties in the measurements of v_2 include those common to all methods, as well as method-specific uncertainties. They are evaluated as relative uncertainties and are reported as percentages relative to the measured v_2 values. Because we are reporting the results on v_2 for nonidentified charged particles, it is important to investigate the tracking efficiency as a function of particle species. The tracking efficiencies for charged pions, kaons, protons, and antiprotons are determined using a full simulation of CMS. Subsequently, the value of $v_2(p_T)$ for charged particles is obtained using different assumptions for the p_T dependence of v_2 and the transverse momentum spectra of each particle type, taking into account the corresponding reconstruction efficiencies. The results are compared to those obtained with the assumption of a particle-species-independent efficiency. The uncertainties in the charged particle v_2 results are estimated to be $\lesssim$0.5%, independent of the p_T, η, and centrality ranges. This uncertainty is listed as "Part. composition" in Tables II–IX.

Because the v_2 value changes with centrality, an uncertainty in the centrality determination can lead to a shift in the v_2 measurement. This uncertainty is evaluated by varying the value of the minimum-bias trigger efficiency to include (97 ± 3)% of the total inelastic cross section. The resulting uncertainty on v_2 is of the order 1%, independent of the p_T, η, and centrality ranges. This uncertainty is listed as "Cent. determination" in Tables II–IX.

The kinematic requirements used to select tracks can affect the efficiency of track finding and the relative fraction of fake tracks in an event. The requirements are varied from their default values to estimate the systematic uncertainty. For each set of requirements, corresponding corrections are obtained for the fake-track contribution to the v_2 signal, as described in

TABLE II. Systematic uncertainties in the measurement of $v_2(p_T)$ for $|\eta| < 0.8$ with the event-plane method for different p_T and centrality ranges.

Source	p_T (GeV/c)	Centrality range (%) 0–10	10–70	70–80
Part. composition (%)	All	0.5	0.5	0.5
Cent. determination (%)	All	1.0	1.0	1.0
	<0.3	4.0	2.0	3.0
Corrections (%)	0.3–0.5	2.0	<1.0	2.0
	0.5–22.0	<1.0	<1.0	2.0
Total (%)	<0.3	4.2	2.3	3.2
	0.3–0.5	2.3	1.5	2.3
	0.5–22.0	1.5	1.5	2.3

TABLE III. Systematic uncertainties in the measurement of $v_2(\eta)$ for $0.3 < p_T < 3$ GeV/c with the event-plane method for different η and centrality ranges.

Source	$\lvert\eta\rvert$	Centrality range (%)		
		0–10	10–70	70–80
Part. composition (%)	All	0.5	0.5	0.5
Cent. determination (%)	All	1.0	1.0	1.0
Corrections (%)	0.0–1.6	2.0	<1.0	2.0
	1.6–2.4	4.0	2.0	3.0
Total (%)	0.0–1.6	3.2	1.5	2.3
	1.6–2.4	4.2	2.3	3.2

Sec. II F. For a given centrality and p_T range, the systematic uncertainty is estimated based on the stability of the v_2 value after corrections for fake tracks, independent of the track selection requirements. The uncertainty is found to be directly related to the magnitude of the fake-track contribution, with the final results deemed unreliable when the fake rate is higher than ≈20%. For the results presented in Sec. III, the systematic uncertainties from this source remain below 4% over the entire range of p_T, η, and centrality, and are significantly below this value for $p_T > 0.5$ GeV/c, centrality above 10%, and $|\eta| < 1.6$. The uncertainty in the efficiency corrections is evaluated by determining the efficiency based on the HYDJET model and by embedding simulated pions into PbPb events in data. Although the two resulting efficiencies do have differences, the uncertainty on the v_2 value is small, at most 0.5%. Variations in the v_2 results owing to changing detector conditions throughout the data-taking period are studied by dividing the data into three subgroups and are found to be below 1% for all measurements. The combined uncertainties from the efficiency corrections, fake-track corrections, and variations in detector conditions are listed under "Corrections" in Tables II–IX.

Additional studies of the systematic uncertainty are conducted for each method. In the event-plane method, flattening corrections are obtained using different procedures. The vertex dependence of the flattening parameters is examined and different subevent η gaps are used in obtaining the resolution corrections. The uncertainties from these sources are found to be negligible. The resolution corrections are measured with the three-subevent and two-subevent methods and are found to be consistent within the statistical uncertainties. The statistical uncertainties for the resolution correction factor are less than 1%, except for the most peripheral 70–80% centrality events, where the statistical uncertainty reaches a value of 2%. We include the statistical uncertainties associated with the resolution-correction factors as part of the overall systematic uncertainty on tracking efficiency and fake-track corrections for the event-plane method.

TABLE V. Systematic uncertainties in the measurement of $v_2(\eta)$ for the range $0.3 < p_T < 3$ GeV/c with the two-particle cumulant method for different η and centrality ranges.

Source	$\lvert\eta\rvert$	Centrality range (%)	
		5–10	10–70
Part. composition (%)	All	0.5	0.5
Cent. determination (%)	All	1.0	1.0
Multiplicity fluct. (%)	All	1.5	4.0
r_0 parameter (%)	All	0.2	0.2
Corrections (%)	0.0–1.6	0.8	1
	1.6–2.4	1.5	1.6
Total (%)	0.0–1.6	2.0	4.2
	1.6–2.4	2.4	4.4

In the cumulant method, we examine the numerical stability of the result when the radius parameter r_0 used in the interpolations of the generating function is increased or decreased by half of its central value. The effects of multiplicity fluctuations are studied for the LYZ and the cumulant methods by analyzing the events in finer 2.5% centrality bins and by using a fixed number of particles chosen at random from each event in a given centrality class.

The systematic uncertainties are smallest for the midrapidity region $|\eta| < 0.8$, $p_T > 0.5$ GeV/c, and in the midcentral events (10–40%), and range from 2.0 to 4.5% for the different methods. At low p_T for the most central events and in the forward pseudorapidity region where the fake-track contributions are larger, the uncertainties increase to 2.4–6.8%. Similarly, in the most peripheral events the uncertainties increase mostly owing to multiplicity fluctuations and reach up to 3.2–7%, depending on the experimental method. A summary of the systematic uncertainties is presented in Tables II–IX.

TABLE IV. Systematic uncertainties in the measurement of $v_2(p_T)$ for $|\eta| < 0.8$ with the two-particle cumulant method for different p_T and centrality ranges.

Source	p_T	Centrality range (%)			
	(GeV/c)	0–5	5–10	10–70	70–80
Part. composition (%)	All	0.5	0.5	0.5	0.5
Cent. determination (%)	All	1.0	1.0	1.0	1.0
Multiplicity fluct. (%)	All	0.5	1.5	4.0	4.0
r_0 parameter (%)	All	0.2	0.2	0.2	0.1
Corrections (%)	0.3–0.5	3.8	1.7	0.6	4.0
	0.5–22.0	2.9	2.1	0.6	3.0
Total (%)	0.3–0.5	4.0	2.6	4.2	5.8
	0.5–22.0	3.2	2.9	4.2	5.1

TABLE VI. Systematic uncertainties in the measurement of $v_2(p_T)$ for $|\eta| < 0.8$ with the four-particle cumulant method for different p_T and centrality ranges.

Source	p_T	Centrality range (%)			
	(GeV/c)	5–10	10–40	40–60	60–70
Part. composition (%)	All	0.5	0.5	0.5	0.5
Cent. determination (%)	All	1.0	1.0	1.0	1.0
Multiplicity fluct. (%)	All	5.0	3.0	5.0	5.0
r_0 parameter (%)	All	2.0	3.0	1.0	0.1
Corrections (%)	0.3–0.5	4.1	1.4	3.0	4.5
	0.5–22.0	2.2	1.2	1.1	3.0
Total (%)	0.3–0.5	6.8	4.6	6.0	6.8
	0.5–22.0	5.9	4.5	5.3	6.0

2. *Systematic uncertainties in the measurements of the transverse momentum spectra and the mean transverse momentum* $\langle p_T \rangle$

Several sources of systematic uncertainty are considered in obtaining the inclusive charged-particle transverse momentum distributions and their mean values, $\langle p_T \rangle$. These include the uncertainties in the efficiency and fake-track correction factors, the particle-species-dependent efficiency, and the uncertainty in the minimum-bias trigger efficiency. The effect on the overall normalization of the spectra is considered separately from the smaller effect on the shape of the spectra as a function of p_T. To obtain the mean transverse momentum, different functional forms are used to extrapolate the spectra down to $p_T = 0$, and the p_T range over which the spectra are fitted is varied. The combined point-to-point systematic uncertainties on the spectra are presented as a function of pseudorapidity in Table X. The total normalization uncertainty of the charged-particle spectra measured in each centrality interval is given in Table XI. The systematic uncertainties in the measurement of $\langle p_T \rangle$ in different pseudorapidity intervals are summarized in Table XII.

III. RESULTS

The main results of the analysis using the four methods described above are as follows:

(i) $v_2(p_T)$ at midrapidity $|\eta| < 0.8$;

(ii) integrated v_2 at midrapidity $|\eta| < 0.8$ and $0.3 < p_T < 3$ GeV/c;

(iii) $v_2(\eta)$ for $0.3 < p_T < 3$ GeV/c.

We also measure the charged-particle transverse momentum spectra and their mean p_T for the centrality and pseudorapidity ranges in which the flow is studied.

The flow studies are performed in the 12 centrality classes listed in Table I. Using these results, we examine the scaling of the integrated v_2 with the participant eccentricity, as well as perform comparisons to measurements from other experiments. Centrality classes are regrouped to perform these comparisons, that is, the results of $v_2(p_T)$, $v_2(\eta)$, or integrated v_2 obtained in the finer bins of centrality are averaged over wider bins, weighted using the corresponding $d^2N/dp_T\,d\eta$ spectra. The evolution of the measured elliptic anisotropy as a function of centrality, center-of-mass energy, and transverse particle density is studied. The scaling of $v_2(\eta)$ in the longitudinal dimension is also examined through comparisons to RHIC data.

TABLE VII. Systematic uncertainties in the measurement of $v_2(\eta)$ for the range $0.3 < p_T < 3$ GeV/c with the four-particle cumulant method for different η and centrality ranges.

Source	$\lvert\eta\rvert$	Centrality range (%)		
		5–10	10–40	40–70
Part. composition (%)	All	0.5	0.5	0.5
Cent. determination (%)	All	1.0	1.0	1.0
Multiplicity fluct. (%)	All	5.0	3.0	5.0
r_0 parameter (%)	All	2.0	3.0	1.0
Corrections (%)	0.0–1.6	1.5	1.5	1.5
	1.6–2.4	1.8	2.1	1.9
Total (%)	0.0–1.6	5.8	4.8	5.4
	1.6–2.4	5.8	5.0	5.6

A. Transverse momentum dependence of v_2

In Figs. 6–9, we present the measurement of v_2 for charged particles as a function of transverse momentum at midrapidity, obtained by each analysis method. We use the notation $v_2\{\text{EP}\}$ to refer to the measurement of v_2 using the event-plane method and $v_2\{2\}$, $v_2\{4\}$, $v_2\{\text{LYZ}\}$ to refer to those using the two-particle cumulant, four-particle cumulant, and LYZ methods,

TABLE VIII. Systematic uncertainties in the measurement of $v_2(p_T)$ for $|\eta| < 0.8$ with the LYZ method for different p_T and centrality ranges.

Source	p_T	Centrality range (%)		
	(GeV/c)	5–10	10–40	40–50
Part. composition (%)	All	0.5	0.5	0.5
Cent. determination (%)	All	1.0	1.0	1.0
Multiplicity fluct. (%)	All	0.1	0.9	1.9
Corrections (%)	0.3–0.5	2.5	1.7	0.7
	0.5–22.0	1.5	1.0	0.6
Total (%)	0.3–0.5	2.7	2.2	2.3
	0.5–22.0	1.9	1.8	2.3

TABLE IX. Systematic uncertainties in the measurement of $v_2(\eta)$ for $0.3 < p_T < 3$ GeV/c with the LYZ method for different η and centrality ranges.

Source	$\lvert\eta\rvert$	Centrality range (%)		
		5–10	10–40	40–50
Part. composition (%)	All	0.5	0.5	0.5
Cent. determination (%)	All	1.0	1.0	1.0
Multiplicity fluct. (%)	All	0.1	0.9	1.9
Corrections (%)	0.0–1.6	1.3	1.0	0.8
	1.6–2.4	1.5	1.4	1.3
Total (%)	0.0–1.6	1.7	1.8	2.4
	1.6–2.4	1.9	2.0	2.5

TABLE XI. Normalization uncertainty in the measurement of the charged-particle spectra in different centrality intervals resulting from the uncertainty in the minimum-bias trigger efficiency.

Centrality range (%)	Normalization uncertainty (%)
0–5	0.4
5–10	1.0
10–15	1.7
15–20	2.3
20–25	3.1
25–30	4.1
30–35	5.0
35–40	6.1
40–50	8.0
50–60	12
60–70	16
70–80	21

respectively. Several trends can be observed and related to the physics processes dominating hadron production in different p_T ranges. The value of v_2 increases from central to peripheral collisions up to 40% centrality, as expected if the anisotropy is driven by the spatial anisotropy in the initial state [12,15,21]. The transverse momentum dependence shows a rise of v_2 up to $p_T \approx 3$ GeV/c and then a decrease. As a function of centrality, a tendency for the peak position of the $v_2(p_T)$ distribution to move to higher p_T in more central collisions is observed, with the exception of the results from the most peripheral collisions in the two-particle cumulant and the event-plane methods.

In ideal hydrodynamics the azimuthal anisotropy continuously increases with increasing p_T [12,21]. The deviation of the theory from the RHIC data at $p_T \gtrsim 2$–3 GeV/c has been attributed to incomplete thermalization of the high-p_T hadrons, and the effects of viscosity. Indeed, viscous hydrodynamic calculations [15,16,65] show that the shear viscosity has the effect of reducing the anisotropy at high p_T. At $p_T \gtrsim 8$ GeV/c, where hadron production is dominated by jet fragmentation, the collective-flow effects are expected to disappear [15,21]. Instead, an asymmetry in the azimuthal distribution of hadron emission with respect to the reaction plane could be generated by path-length-dependent parton energy loss [28,30,31]. For events with similar charged-particle suppression [66], but different reaction-zone eccentricity, one might expect that the geometric information would be imprinted in the elliptic anisotropy signal. The top panels of Figs. 6–9 (centrality 0–35%) show a trend that is consistent with this expectation. In more central events, where the eccentricity is smaller, the elliptic anisotropy value is systematically lower. In more peripheral collisions (centrality 35–80%), there is a complex interplay between the reduced energy loss and the increase in eccentricity that influence the $v_2(p_T)$ value in opposite directions. The data presented here provide the basis for future detailed comparisons to theoretical models.

An important consideration in interpreting the $v_2(p_T)$ results is the contribution from nonflow correlations and initial-state eccentricity fluctuations. To aid in assessing the magnitude of these effects and their evolution with the centrality of the collisions, the results of $v_2(p_T)$ obtained by all methods at midrapidity are compared in Fig. 10 for 12 centrality classes. The four methods show differences as expected owing to their sensitivities to nonflow contributions [37,42,43] and eccentricity fluctuations [34,35,38].

The method that is most affected by nonflow correlations is the two-particle cumulant, because of the fact that the reference and the differential flow signals are determined in the same pseudorapidity range. The event-plane method is expected to be similarly affected if dedicated selections are not applied to reduce these contributions. In our analysis, the particles used in the event-plane determination and the particles used to measure the flow are at least 3 units of pseudorapidity apart, which suppresses most nonflow correlations. The differences between the two-particle cumulant and the event-plane methods are most pronounced at high p_T and in peripheral collisions, where jet-induced correlations dominate over the collective flow.

In a collision where M particles are produced, direct k-particle correlations are typically of order $1/M^{k-1}$, so that they become smaller as k increases. Therefore, the

TABLE X. Point-to-point systematic uncertainties in the measurement of the charged-particle spectra in different pseudorapidity intervals.

Source of uncertainty	$\lvert\eta\rvert < 0.8$	$0.8 < \lvert\eta\rvert < 1.2$	$2.0 < \lvert\eta\rvert < 2.4$
Tracking efficiency (%)	5	8	13
Particle composition (%)	1	1	2
Trigger efficiency (%)	3	3	3
Total (%)	6	9	14

TABLE XII. Systematic uncertainty of the mean p_T of charged particles from each source and in total as a function of pseudorapidity.

Source of uncertainty	$\|\eta\| < 0.4$	$0.8 < \|\eta\| < 1.2$	$2.0 < \|\eta\| < 2.4$
Fit function (%)	3	3	4
Trigger efficiency (%)	1.5	1.5	1.5
Tracking efficiency (%)	2	2	2.5
Total (%)	3.9	3.9	4.9

fourth-order cumulant and the LYZ methods are expected to be much less affected by nonflow contributions than the second-order cumulant method [37,42,43]. This trend is seen in our data.

B. Centrality dependence of integrated v_2 and eccentricity scaling

To obtain the integrated v_2 values as a function of centrality at midrapidity, $v_2(p_T)$ measurements are averaged over p_T, weighted by the corresponding charged-particle spectrum. The integration range $0.3 < p_T < 3$ GeV/c is limited to low p_T to maximize the contribution from soft processes, which facilitates comparisons to hydrodynamic calculations.

The centrality dependence of the integrated v_2 at midrapidity $|\eta| < 0.8$ is presented in Fig. 11 for the four methods. The v_2 values increase from central to peripheral collisions, reaching a maximum in the 40–50% centrality range. In the more peripheral collisions, a decrease in v_2 is observed in the event-plane and four-particle cumulant measurements, while the values obtained with the two-particle cumulant method remain constant within their uncertainties. The results for $v_2\{2\}$ are larger than those for $v_2\{EP\}$, while the $v_2\{4\}$ and $v_2\{LYZ\}$ values are smaller. To facilitate a quantitative comparison between the methods, including their respective systematic uncertainties, the bottom panel of Fig. 11 shows the results from the cumulant and the LYZ methods divided by those obtained from the event-plane method. The boxes represent the systematic uncertainty in the ratios, excluding sources of uncertainty common to all methods. The ratios are relatively constant in the 10–60% centrality range, but the differences between the methods increase for the most central and the most peripheral collisions. These findings are similar to results obtained by the STAR experiment at RHIC [67]. Below, we further investigate the differences in the v_2 values returned by each method.

The collective motion of the system, and therefore the anisotropy parameter, depend on the initial shape of the nucleus-nucleus collision area and the fluctuations in the positions of the interacting nucleons. By dividing v_2 by the participant eccentricity, one may potentially remove this dependence across centralities, colliding species, and center-of-mass energies, enabling a comparison of results in terms of the underlying physics driving the flow.

In Fig. 12, we examine the centrality dependence of the eccentricity-scaled anisotropy parameter obtained with the event-plane and cumulant methods at midrapidity, $|\eta| < 0.8$. The participant eccentricity and its cumulant moments are obtained from a Glauber-model simulation, as discussed in Sec. II C. The statistical and systematic uncertainties in the integrated v_2 measurements are added in quadrature and represented by the error bars. The dashed lines show the

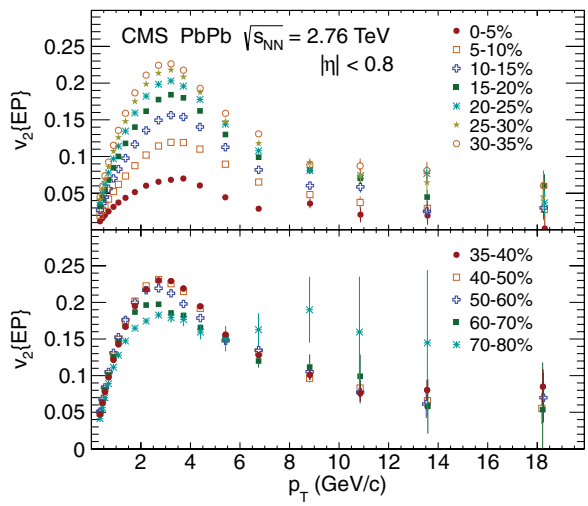

FIG. 6. (Color online) Results from the event-plane (EP) method for v_2 as a function of p_T at midrapidity $|\eta| < 0.8$ for the 12 centrality classes given in the legend. The error bars show the statistical uncertainties only.

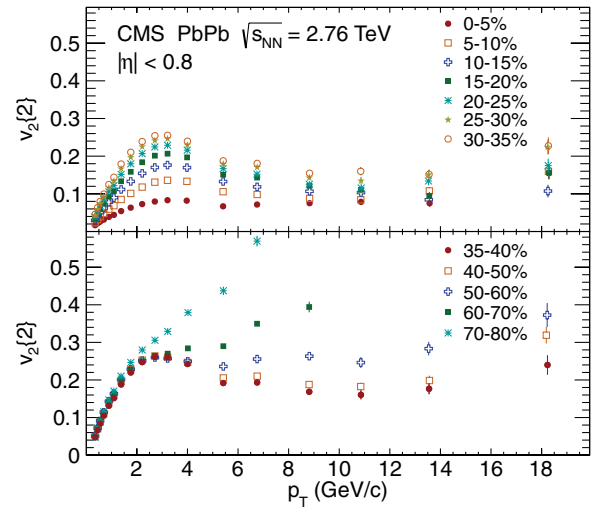

FIG. 7. (Color online) Second-order cumulant results for v_2 as a function of p_T at midrapidity $|\eta| < 0.8$ for the 12 centrality classes given in the legend. The error bars show the statistical uncertainties only.

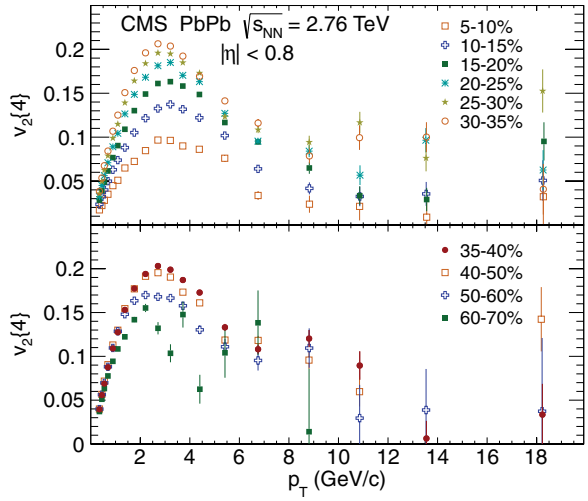

FIG. 8. (Color online) Fourth-order cumulant results for v_2 as a function of p_T at midrapidity $|\eta| < 0.8$ for the ten centrality classes given in the legend. The error bars show the statistical uncertainties only.

systematic uncertainties in the eccentricity determination. In the left panel of Fig. 12, the results from each method are divided by the participant eccentricity, $\epsilon_{\rm part}$. The data show a near-linear decrease from central to peripheral collisions, with differences between methods that were already observed in Fig. 11. In the right panel, the v_2 values for the cumulant measurements are scaled by their respective moments of the participant eccentricity, thus taking into account the corresponding eccentricity fluctuations [34–38]. With this scaling, the two-particle cumulant and the event-plane results become nearly identical, except for the most central and the most peripheral collisions, where the cumulant results are more affected by nonflow contributions. This is expected [37] because in our application of the method there is no separation in rapidity between the particles used for the reference flow and those used in the differential flow measurement. In

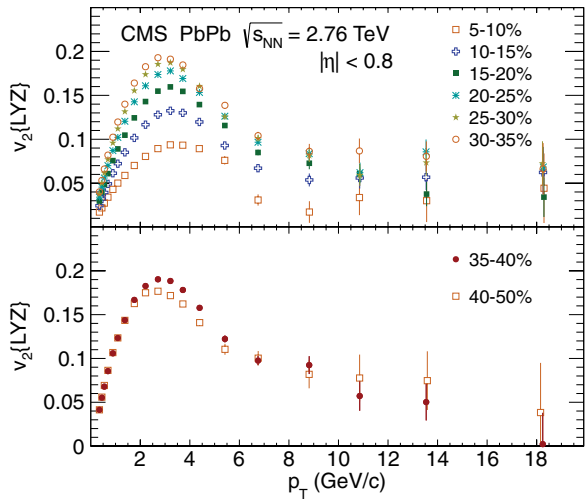

FIG. 9. (Color online) Lee-Yang zeros results for v_2 as a function of p_T at midrapidity $|\eta| < 0.8$ for the eight centrality classes given in the legend. The error bars show the statistical uncertainties only.

the centrality range of 15–40%, the four-particle cumulant measurement of $v_2\{4\}/\epsilon\{4\}$ is also in better agreement with the other two methods. This indicates that the main difference in the results from the different methods could be attributed to their sensitivity to eccentricity fluctuations. In the most central events, where the eccentricity $\epsilon\{4\}$ is very small, and in the most peripheral events, where the fluctuations are large, $v_2\{4\}/\epsilon_2\{4\}$ deviates from the common scaling behavior. For centralities above 50% the differences between the four-particle cumulant method and the other two methods do not seem to be accounted for by the initial-state fluctuations, as described in our implementation of the Glauber model. In this centrality range, the event-by-event fluctuations in the eccentricity are non-Gaussian owing to the underlying Poisson distributions from discrete nucleons [34,38] and are more difficult to model. It has also been suggested [34,37] that when the event-plane resolution is smaller than $\approx$0.6, as is the case for the peripheral collisions studied in CMS, the results from the event-plane method should be evaluated using the two-particle cumulant eccentricity $\epsilon\{2\}$, rather than the participant eccentricity $\epsilon_{\rm part}$. We have used a common definition of eccentricity ($\epsilon_{\rm part}$) for all centrality classes studied in our event-plane analysis. This would lower the measurements of $v_2\{\rm EP\}/\epsilon$ by about 10% in the most peripheral collisions, which is not sufficient to reconcile the differences between the event-plane and the four-particle cumulant results.

Another model of the initial state that has been used in the literature [38,39,68–71], but has not been explored here, is the color glass condensate (CGC) model [72], which takes into account that at very high energies or small values of Bjorken x, the gluon density becomes very large and saturates. The CGC model predicts eccentricities that exceed the Glauber-model eccentricities by an approximately constant factor of around 1.2, with some deviation from this behavior in the most central and most peripheral collisions [38,70]. The results presented here may give further insight into the nature of the initial-state fluctuations, especially in the regions where the eccentricity fluctuations become non-Gaussian.

C. Pseudorapidity dependence of v_2

The pseudorapidity dependence of the anisotropy parameter provides additional constraints on the system evolution in the longitudinal direction. To obtain the $v_2(\eta)$ distribution with the event-plane method, we first measure $v_2(p_T)$ in pseudorapidity bins of $\Delta\eta = 0.4$, and then average the results over the range $0.3 < p_T < 3$ GeV/c, weighting with the efficiency and fake-rate-corrected spectrum.

For the cumulant and LYZ methods, the measurements are done using all particles in the range $|\eta| < 2.4$, and either $0.3 < p_T < 3$ GeV/c or $0.3 < p_T < 12$ GeV/c in the generating function, to obtain the reference flow, and then extracting the pseudorapidity dependence in small pseudorapidity intervals of $\Delta\eta = 0.4$. Tracking efficiency and fake-rate corrections are applied using a track-by-track weight in forming the differential generating functions. As a cross-check, we have confirmed that at midrapidity the values obtained with this method agree with the ones obtained from a direct

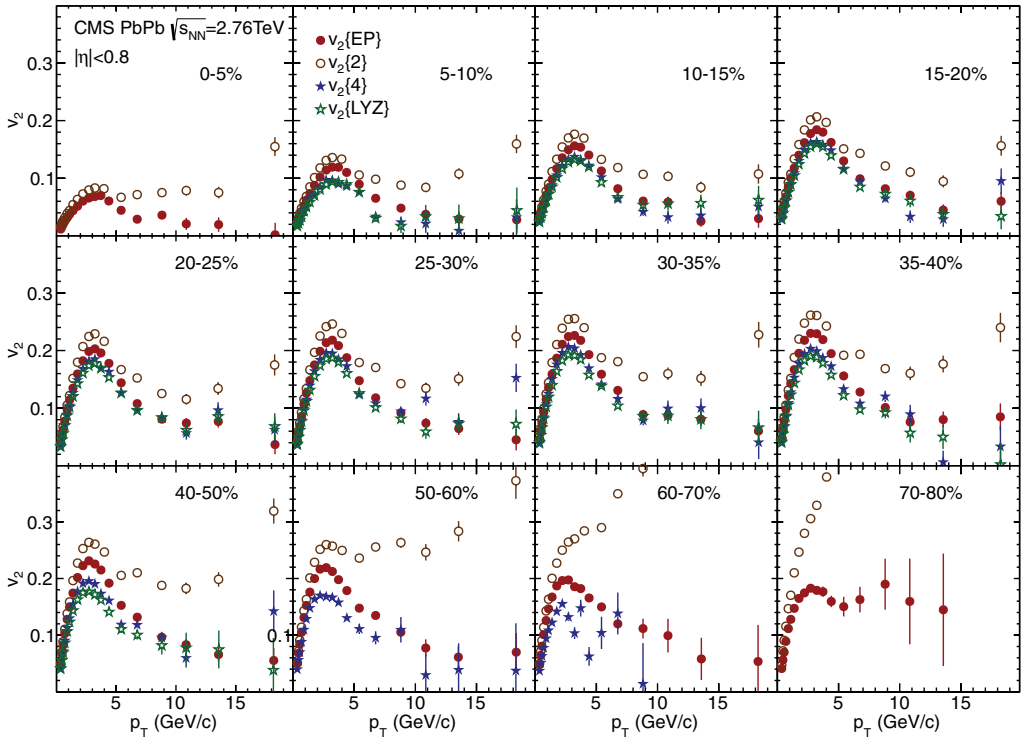

FIG. 10. (Color online) Comparison of the four different methods for determining v_2 as a function of p_T at midrapidity ($|\eta| < 0.8$) for the 12 centrality classes given in the figures. The error bars show the statistical uncertainties only.

yield-weighted average of the $v_2(p_T)$ results from Figs. 7–9, within the stated systematic uncertainties.

As observed at midrapidity ($|\eta| < 0.8$) in Fig. 11, the values of $v_2\{4\}$ and $v_2\{\text{LYZ}\}$ are in agreement and are smaller than $v_2\{2\}$ and $v_2\{\text{EP}\}$. This behavior persists at larger pseudorapidity, as shown in Fig. 13, which suggests that similar nonflow correlations and eccentricity fluctuations affect the results over the full measured pseudorapidity range. The results show that the value of $v_2(\eta)$ is greatest at midrapidity and is constant or decreases very slowly at larger values of $|\eta|$. This behavior is most pronounced in peripheral collisions and for the two-particle cumulant method, which is most affected by nonflow contributions.

To assess whether the observed decrease in $v_2(\eta)$ in the forward pseudorapidity region in peripheral PbPb collisions is attributable to a pseudorapidity dependence in the $v_2(p_T)$ distributions or in the underlying charged-particle spectra, in Fig. 14 we examine the values of $v_2(p_T)$ obtained with the event-plane method for several pseudorapidity intervals in each of the 12 centrality classes shown in Fig. 13. From the most central events up to 35–40% centrality there is no change in the $v_2(p_T)$ distributions with pseudorapidity within the statistical uncertainties. Therefore, any change in the $v_2(\eta)$ distribution can be attributed to changes in the underlying charged-particle transverse momentum spectra. A gradual decrease is observed in the $v_2(p_T)$ values at forward pseudorapidity ($2.0 < |\eta| < 2.4$) in more peripheral events. For the 70–80% centrality class the values of $v_2(p_T)$ decrease by approximately 10% between the central pseudorapidity region $|\eta| < 0.4$ and the forward region $2.0 < |\eta| < 2.4$. Thus, the pseudorapidity dependence in $v_2(\eta)$ for peripheral collisions observed in Fig. 13 is caused by changes in the $v_2(p_T)$ distributions with pseudorapidity, as well as changes in the underlying transverse momentum spectra presented in Sec. III D.

D. Centrality and pseudorapidity dependence of the transverse momentum distributions

Elliptic flow measures the azimuthal anisotropy in the invariant yield of the final-state particles. Therefore, the charged-particle transverse momentum distributions influence the observed results. The soft-particle-production mechanism and the evolution of the expanding nuclear medium are reflected in the low-p_T range of the transverse momentum spectra. In the hydrodynamics calculations, measurements of the pseudorapidity density of charged particles produced in collisions with different centrality constrain the description of the initial entropy and the energy density distribution in the collision zone, while the mean transverse momentum of the particle spectra constrains the final temperature and the radial-flow velocity of the system. With additional input on the equation-of-state that is typically provided by lattice QCD, the hydrodynamics calculations then provide a description of the system evolution from some initial time, when local thermal equilibrium is achieved, to the "freeze-out," when the particle interactions cease.

We have measured the charged-particle transverse momentum spectra for 12 centrality classes over the pseudorapidity range $|\eta| < 2.4$ in bins of $\Delta\eta = 0.4$. Examples of these distributions for the midrapidity ($|\eta| < 0.4$) and forward-rapidity ($2.0 < |\eta| < 2.4$) regions are shown in

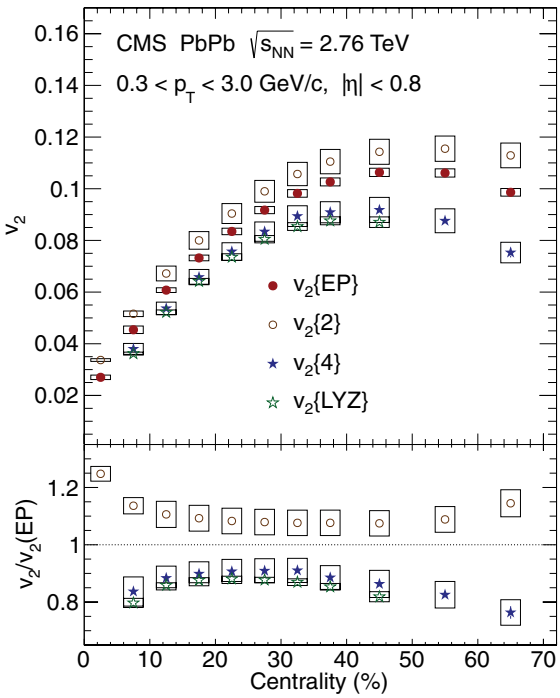

FIG. 11. (Color online) (Top) Integrated v_2 as a function of centrality at midrapidity $|\eta| < 0.8$ for the four methods. The boxes represent the systematic uncertainties. The magnitudes of the statistical uncertainties are smaller than the size of the symbols. (Bottom) The values from three of the methods are divided by the results from the event-plane method. The boxes represent the systematic uncertainties excluding the sources that are common to all methods. The magnitudes of the statistical uncertainties are smaller than the size of the symbols.

Fig. 15. These results extend the measurements of charged-particle spectra previously reported by CMS [66] down to $p_T = 0.3$ GeV/c and to forward pseudorapidity. The measurements presented here are in good agreement with the results in Ref. [66] in their common ranges of p_T, pseudorapidity, and centrality.

The evolution of the charged-particle spectra with centrality and pseudorapidity can be quantified in terms of the mean p_T of the transverse momentum distributions. The values of $\langle p_T \rangle$ as a function of N_{part}, which is derived from the centrality of the event, are shown in Fig. 16. In each pseudorapidity interval, the values of $\langle p_T \rangle$ increase with N_{part} up to $N_{part} \approx 150$ and then saturate, indicating that the freeze-out conditions of the produced system are similar over a broad range of collision centralities (0–35%). This behavior is in contrast to the centrality dependence in the integrated v_2 values at midrapidity shown in Fig. 11 that vary strongly in this centrality range. On the other hand, in more peripheral collisions (centrality greater than 35%) the $v_2(p_T)$ values do not vary much with centrality at low p_T, as shown in the bottom panels of Figs. 6–9, while the spectral shapes change, as indicated by the $\langle p_T \rangle$ measurement. This behavior is qualitatively similar at forward pseudorapidities, as shown in Figs. 14 and 16. These measurements taken together will help in understanding the early time dynamics in the system evolution, which is reflected in the elliptic flow, and the overall evolution through the hadronic stage, which is reflected in the charged-particle spectra.

E. Comparison with other measurements of v_2 at the LHC

Results on the elliptic anisotropy measured in PbPb collisions in $\sqrt{s_{NN}} = 2.76$ TeV have previously been reported by the ALICE [13] and ATLAS [14] experiments. A comparison of $v_2\{2\}$ and $v_2\{4\}$ as a function of p_T in the 40–50% centrality class for $|\eta| < 0.8$ from CMS and ALICE [13] is shown in Fig. 17. The error bars give the statistical uncertainties, and the boxes represent the systematic uncertainties in the CMS measurements. The two measurements are in good agreement over their common p_T range.

A comparison of $v_2(p_T)$ obtained with the event plane method at midrapidity from CMS and ATLAS [14] is presented

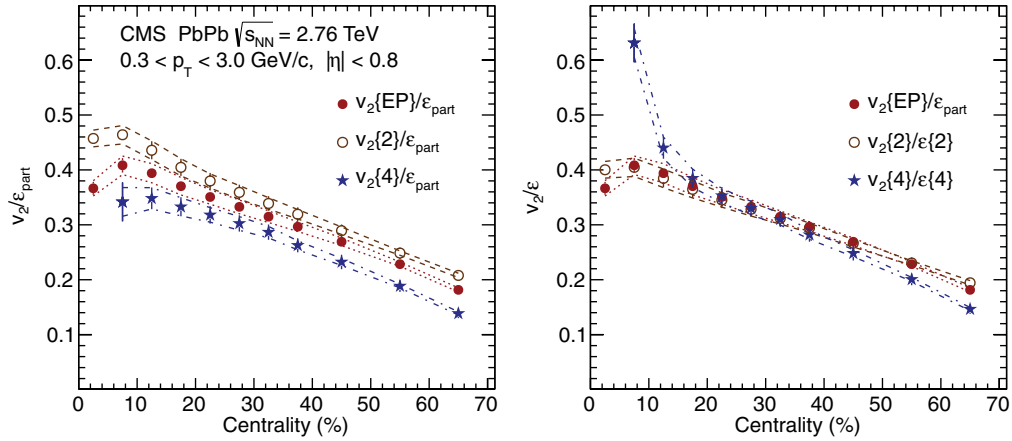

FIG. 12. (Color online) (Left) Centrality dependence of the integrated v_2 divided by the participant eccentricity, ϵ_{part}, obtained at midrapidity $|\eta| < 0.8$ for the event-plane and two- and four-particle cumulant methods. (Right) The measurements of v_2 as a function of centrality are the same as in the left panel, but here the two-particle and four-particle cumulant results are divided by their corresponding moments of the participant eccentricity, $\epsilon\{2\}$ and $\epsilon\{4\}$. In both panels, the error bars show the sum in quadrature of the statistical and systematic uncertainties in the v_2 measurement, and the lines represent the systematic uncertainties in the eccentricity determination.

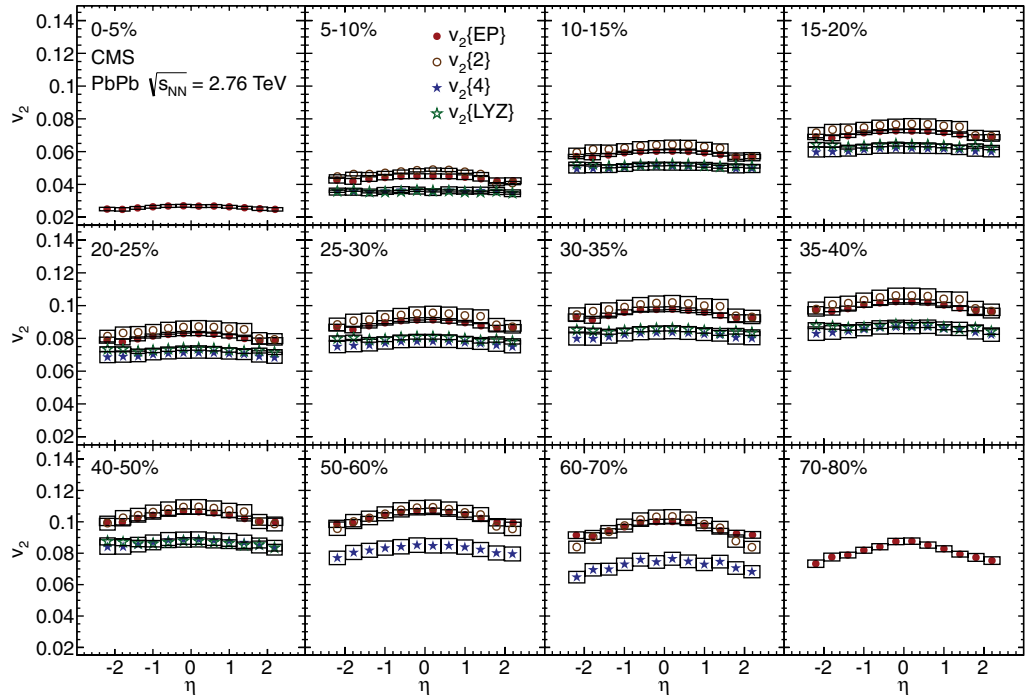

FIG. 13. (Color online) Pseudorapidity dependence of v_2 for $0.3 < p_T < 3$ GeV/c with all four methods in 12 centrality classes. The boxes give the systematic uncertainties. The magnitudes of the statistical uncertainties are smaller than the size of the symbols.

in Fig. 18 for the centrality ranges of the ATLAS measurement. The error bars show the statistical and systematic uncertainties added in quadrature. The results are in good agreement within the statistical and systematic uncertainties.

IV. DISCUSSION

We compare the CMS elliptic flow measurements presented in Sec. III with results obtained at RHIC by the PHENIX, STAR, and PHOBOS experiments. Because each method for

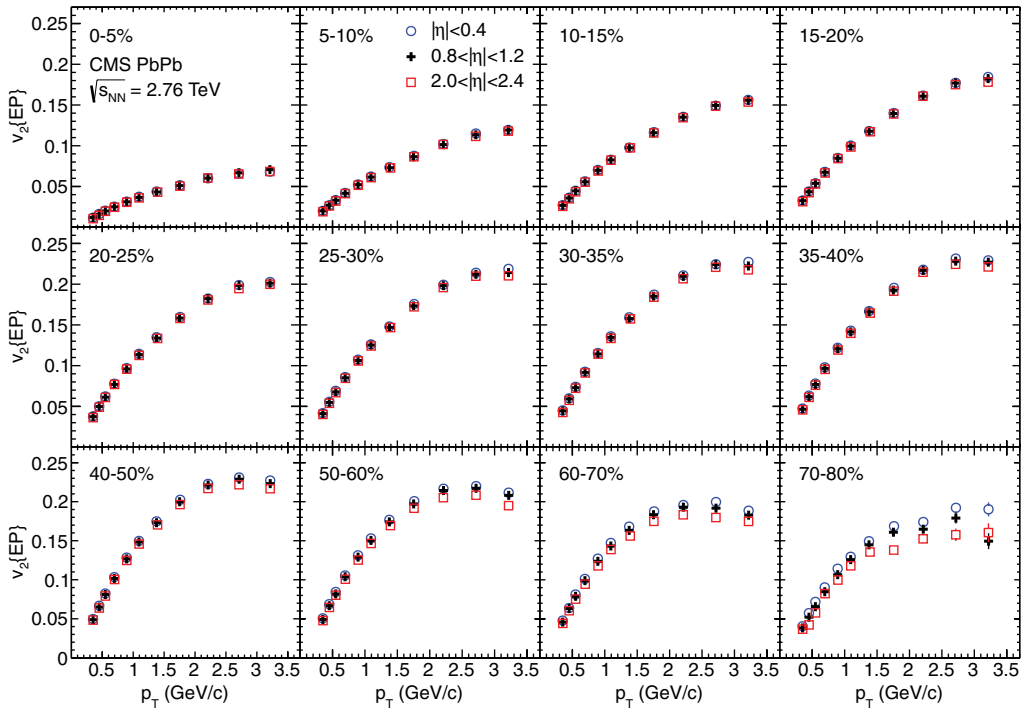

FIG. 14. (Color online) Results from the event-plane method for $v_2(p_T)$ in three pseudorapidity regions and in 12 centrality classes. The error bars show the statistical uncertainties that in most cases have magnitudes smaller than the size of the symbol.

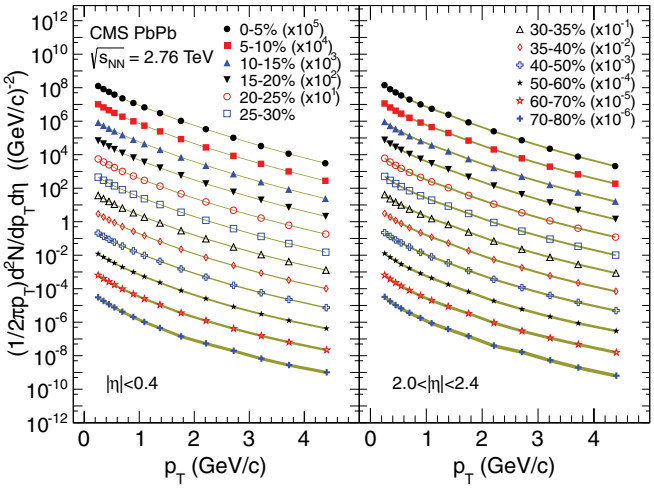

FIG. 15. (Color online) Inclusive charged-particle spectra at midrapidity (left) and forward rapidity (right), for the 12 centrality classes given in the legend. The distributions are offset by arbitrary factors given in the legend for clarity. The shaded bands represent the statistical and systematic uncertainties added in quadrature, including the overall normalization uncertainties from the trigger efficiency estimation.

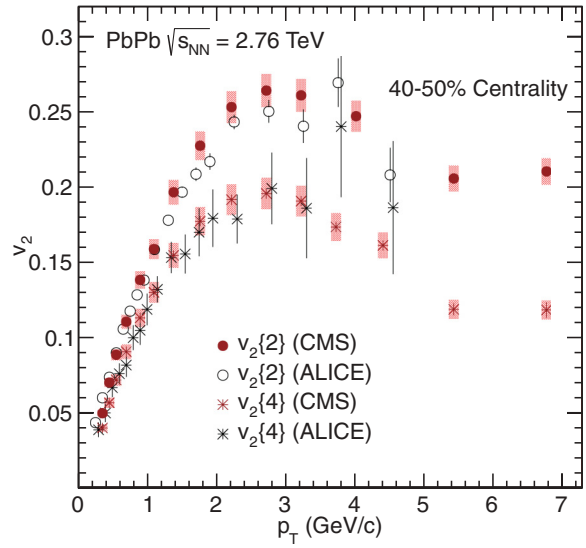

FIG. 17. (Color online) The values of $v_2\{2\}$ and $v_2\{4\}$ obtained with the cumulant method, as a function of p_T from CMS (solid symbols) and ALICE (open symbols) [13], measured in the range $|\eta| < 0.8$ for the 40–50% centrality class. The error bars show the statistical uncertainties, and the boxes give the systematic uncertainties in the CMS measurement.

measuring v_2 has a different sensitivity to nonflow correlations and initial-state fluctuations, we make these comparisons for measurements conducted with the same method and with similar kinematic requirements in the method's implementation. In Fig. 19 the midrapidity measurement of $v_2(p_T)$ with the event-plane method in CMS is compared to results from PHENIX [73] for $\sqrt{s_{NN}} = 200$ GeV AuAu collisions. For the PHENIX measurement, the event plane was determined at forward pseudorapidities, $|\eta| = 3.1$–3.9, while the $v_2(p_T)$ measurement was performed in the pseudorapidity interval $|\eta| < 0.35$, thus providing a separation of at least 2.75 units of pseudorapidity between the charged particles used for the $v_2(p_T)$ analysis and the particles used in the event-plane determination. This procedure is comparable to the CMS approach, where a separation of at least 3 units of pseudorapidity is used. These large pseudorapidity gaps are expected [37] to suppress nonflow contributions in both measurements. The pseudorapidity interval for the CMS measurement is wider, $|\eta| < 0.8$, but because the pseudorapidity dependence of $v_2(\eta)$ was shown to be weak (see Fig. 13), this difference should not influence the comparison of the results. The top panels in Fig. 19 show the measurements of $v_2(p_T)$ from CMS (closed symbols) and PHENIX (open symbols) for several centrality classes. The error bars represent the statistical uncertainties only. The shape of the $v_2(p_T)$ distributions and the magnitude of the signals are similar, in spite of the factor of ≈14 increase in the center-of-mass energy. To facilitate a quantitative comparison of these results, the CMS measurements are fitted with a combination of a fifth-order polynomial function (for $p_T < 3.2$ GeV/c) and a Landau distribution (for $3 < p_T < 7$ GeV/c). There is no physical significance attributed to these functional choices other than an attempt to analytically describe the CMS $v_2(p_T)$ distributions, so that the value of v_2 can be easily compared to results from other experiments, which have been obtained with different p_T binning. The results from the fits are plotted as solid lines in the top panels of Fig. 19. In the bottom panels, the fit function is used to evaluate $v_2(p_T)$ at the p_T values for each data set, and then to form the ratios between the CMS fit values and the PHENIX data, and the CMS fit to the CMS measurements. The error bars represent the statistical uncertainties. The systematic uncertainties from the CMS and PHENIX measurements are added in quadrature and plotted as shaded boxes. The $v_2(p_T)$ values measured by CMS are systematically higher than those from PHENIX in all centrality classes and over the entire transverse momentum range measured by PHENIX. The relative deviations of are the order 10%, except for the most peripheral collisions, where they reach 15%.

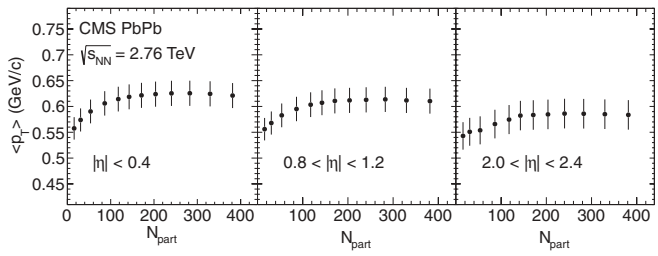

FIG. 16. Mean transverse momentum of the charged-particle spectra as a function of N_{part} in three pseudorapidity intervals marked in the figure. The error bars represent the quadratic sum of the statistical and systematic uncertainties.

A similar comparison is carried out for the two-particle and four-particle cumulant methods. In Fig. 20, the results from the STAR experiment [74] for AuAu collisions at $\sqrt{s_{NN}} =$ 200 GeV in the 20–60% centrality range are compared with the CMS measurements. The pseudorapidity interval for the STAR

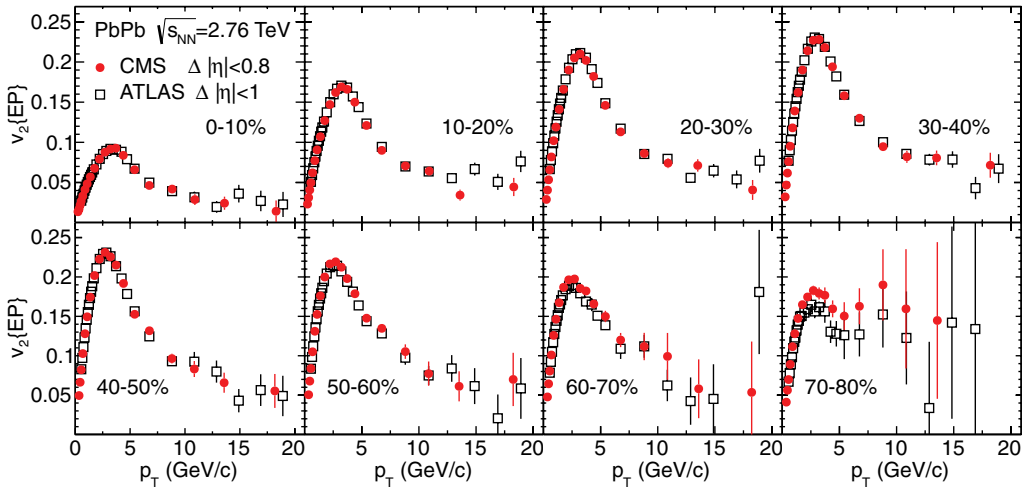

FIG. 18. (Color online) Comparison of results for $v_2(p_T)$ obtained with the event-plane method from CMS (solid symbols) and ATLAS (open symbols) for the centrality classes marked in the figure. The error bars show the statistical and systematic uncertainties added in quadrature.

measurement is $|\eta| < 1.3$, compared to $|\eta| < 0.8$ for CMS. These η ranges are within a pseudorapidity region in which the $v_2(\eta)$ values only weakly depend on the pseudorapidity. The kinematic selections imposed on the charged particles used in determining the reference flow are also similar in the CMS and STAR measurements. The top panels of Fig. 20 show the $v_2(p_T)$ distributions for the two-particle (left) and four-particle (right) cumulant method from both experiments, along with fits to the CMS data (lines). The functional form used for the fit of the CMS $v_2(p_T)$ distributions is the same as the one used in Fig. 19. The bottom panels in Fig. 20 show the ratios of the fits to the CMS data to the actual measurements from CMS and STAR. The error bars represent the statistical uncertainties. The systematic uncertainties from the CMS and STAR measurements are added in quadrature and plotted as shaded boxes. At low p_T, the $v_2(p_T)$ values measured by CMS are larger than in the STAR data, but the relative deviations are smaller than 5% for the four-particle cumulant

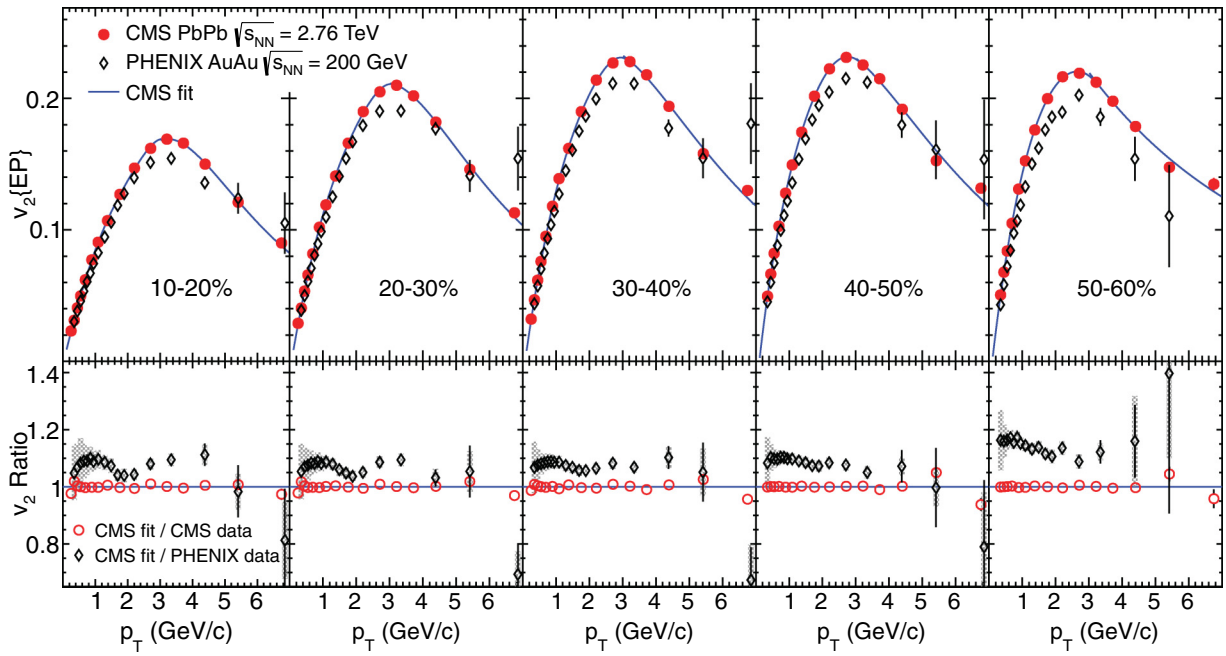

FIG. 19. (Color online) (Top panels) Comparison of $v_2(p_T)$ using the event-plane method as measured by CMS (solid circles) at $\sqrt{s_{NN}} =$ 2.76 TeV, and PHENIX [73] (open diamonds) at $\sqrt{s_{NN}} = 200$ GeV for midrapidity ($|\eta| < 0.8$ and $|\eta| < 0.35$, respectively). The error bars represent the statistical uncertainties. The solid line is a fit to the CMS data. (Bottom panels) Ratios of the CMS fit to the PHENIX data (open diamonds) and to the CMS data (open circles). The error bars show the statistical uncertainties, while the shaded boxes give the quadrature sum of the CMS and PHENIX systematic uncertainties.

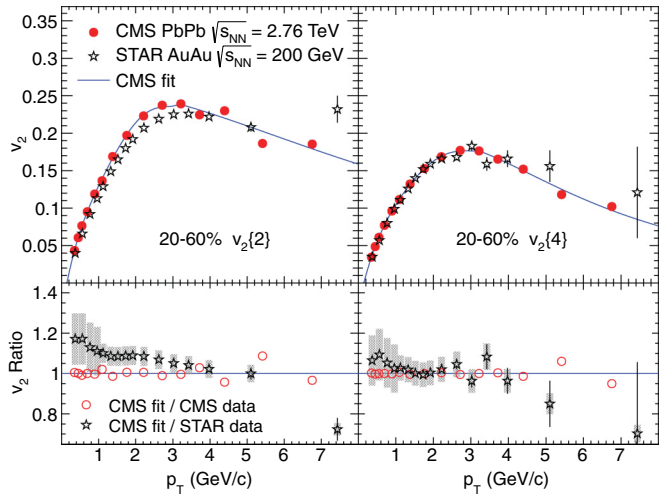

FIG. 20. (Color online) (Top panels) Comparison of $v_2(p_T)$ using the two-particle (left) and the four-particle (right) cumulant method as measured by CMS (solid circles) at $\sqrt{s_{NN}} = 2.76$ TeV, and STAR [74] (open stars) at $\sqrt{s_{NN}} = 200$ GeV at midrapidity ($|\eta| < 0.8$ and $|\eta| < 1.3$, respectively). The error bars represent the statistical uncertainties. The line is a fit to the CMS data. (Bottom panels) Ratios of the CMS fit values to the STAR data (open diamonds) and to the CMS data (open circles). The error bars show the statistical uncertainties, while the shaded boxes give the quadrature sum of the CMS and STAR systematic uncertainties.

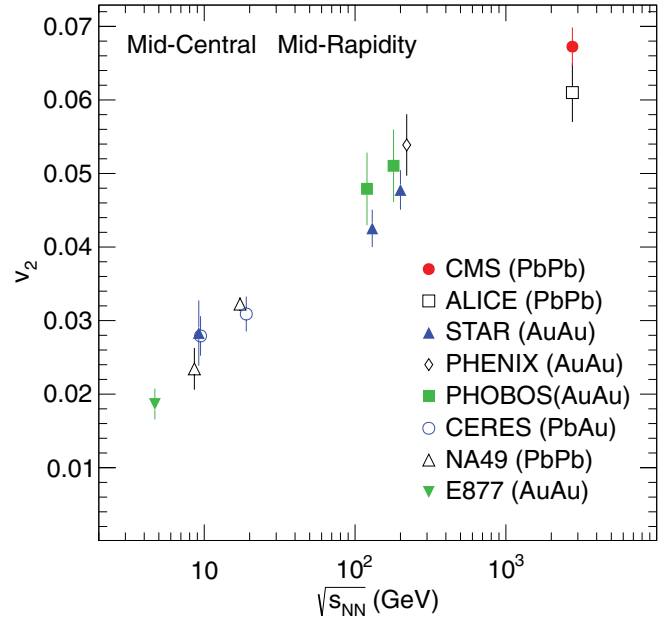

FIG. 21. (Color online) The CMS integrated v_2 values for 20–30% centrality from the range $|\eta| < 0.8$ and $0 < p_T < 3$ GeV/c obtained using the event-plane method is compared as a function of $\sqrt{s_{NN}}$ to results at midrapidity and similar centrality from ALICE [13], STAR [76], PHENIX [23], PHOBOS [49,77,78], NA49 [79], E877 [80], and CERES [81]. The error bars for the lower-energy results represent statistical uncertainties; for the CMS and ALICE measurements the statistical and systematic uncertainties are added in quadrature.

method, and are of the order 10–15% for the two-particle cumulant method. Taken together, the comparisons to the RHIC results in Figs. 19 and 20 indicate only a moderate increase in $v_2(p_T)$ at low p_T from the highest RHIC energy to the LHC, despite the large increase in the center-of-mass energy.

In Fig. 21, we examine the $\sqrt{s_{NN}}$ dependence of the integrated v_2 from midcentral collisions spanning $\sqrt{s_{NN}} = 4.7$ GeV to $\sqrt{s_{NN}} = 2.76$ TeV. The CMS measurement is obtained with the event-plane method in the 20–30% centrality class by extrapolating the $v_2(p_T)$ and the charged-particle spectra down to $p_T = 0$. In the extrapolation it is assumed that $v_2(0) = 0$, and the charged-particle yield is constrained to match the $dN_{ch}/d\eta$ values measured by CMS [75]. The low-energy data are from Refs. [20,23,49,76–81], as compiled in Ref. [79] and tabulated in Ref. [76]. The error bars for the low-energy data represent the statistical uncertainties. For the CMS data the error bar is the quadrature sum of the statistical and systematic uncertainties. The integrated v_2 values increase approximately logarithmically with $\sqrt{s_{NN}}$ over the full energy range, with a 20–30% increase from the highest RHIC energy to that of the LHC. This has contributions from the increase in the mean p_T of the charged-particle spectra with $\sqrt{s_{NN}}$, shown in Fig. 22, and from the moderate increase in the $v_2(p_T)$ distributions at low p_T, shown in Fig. 19. We note that the centrality selections, the collision species, and the methods employed in the integrated v_2 measurements are not identical in all experiments, so the comparison presented in Fig. 21 is only approximate. Further comparisons to results from lower energies are presented in Figs. 23–25.

In ideal hydrodynamics, the eccentricity-scaled elliptic flow is constant over a broad range of impact parameters;

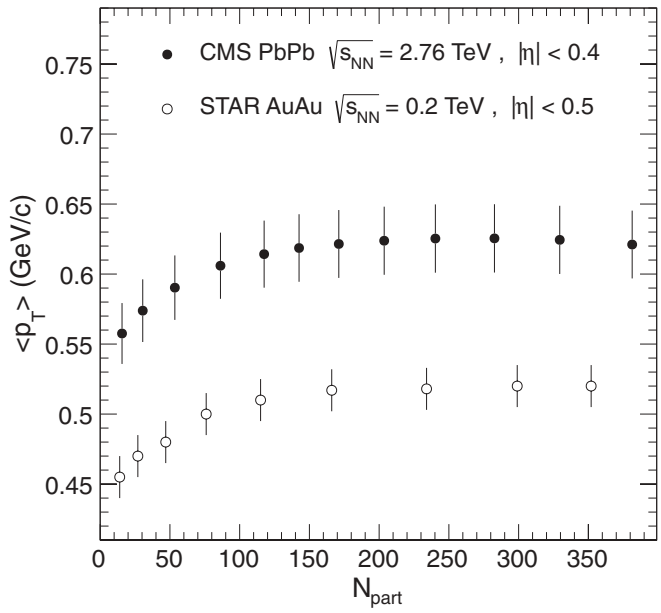

FIG. 22. Mean transverse momentum of the charged-particle spectra as a function of N_{part} measured by CMS in PbPb collisions at $\sqrt{s_{NN}} = 2.76$ TeV (solid circles) and by STAR [82] in AuAu collisions at $\sqrt{s_{NN}} = 200$ GeV (open circles). The error bars represent the quadratic sum of statistical and systematic uncertainties.

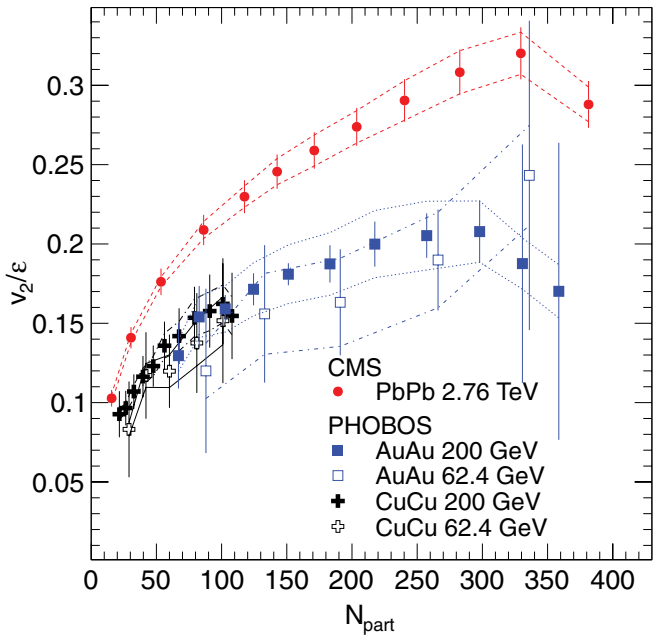

FIG. 23. (Color online) The CMS integrated v_2 values from the event-plane method divided by the participant eccentricity as a function of N_{part} with $|\eta| < 0.8$ and $0 < p_{\text{T}} < 3$ GeV/c. These results are compared with those from PHOBOS [34] for different nuclear species and collision energies. The PHOBOS v_2 values are divided by the cumulant eccentricity $\epsilon\{2\}$ (see text). The error bars give the statistical and systematic uncertainties in the v_2 measurements added in quadrature. The dashed lines represent the systematic uncertainties in the eccentricity determination.

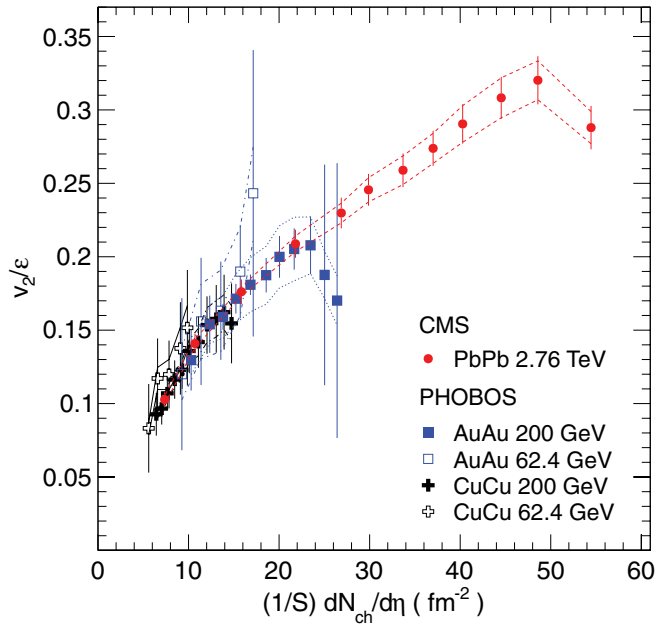

FIG. 24. (Color online) Eccentricity-scaled v_2 as a function of the transverse charged-particle density from CMS and PHOBOS [34]. The error bars include both statistical and systematic uncertainties in v_2. The dashed lines represent the systematic uncertainties in the eccentricity determination.

deviations from this behavior are expected in peripheral collisions, in which the system freezes out before the elliptic flow fully builds up and saturates [32]. A weak centrality and beam-energy dependence is expected through variations in the equation of state. In addition, the system is also affected by viscosity, in both the sQGP and the hadronic stages [22,68,83,84] of its evolution. Therefore, the centrality and $\sqrt{s_{NN}}$ dependence of v_2/ϵ can be used to extract the ratio of the shear viscosity to the entropy density of the system.

In Fig. 23, the integrated v_2 obtained from the event-plane method is divided by the eccentricity of the collisions and plotted as a function of N_{part}, which is derived from the centrality of the event. The result is compared to lower-energy AuAu and CuCu measurements from the PHOBOS experiment [34]. For the CMS measurement, the value of v_2 is divided by the participant eccentricity ϵ_{part} because the event-plane resolution factor shown in Fig. 4 is greater than 0.6 for all but the most central and most peripheral event selections in our analysis. It has been argued [34,37] that for lower-resolution parameters, the event-plane method measures the rms of the azimuthal anisotropy, rather than the mean, and therefore, the relevant eccentricity parameter in this case should be the second-order cumulant eccentricity $\epsilon\{2\} \equiv \sqrt{\langle \epsilon_{\text{part}}^2 \rangle}$. Thus, the comparison with the PHOBOS v_2 results, which were obtained with low event-plane resolution, is done by implementing this scaling using the data from Ref. [34]. An approximately 25% increase in the integrated v_2 scaled by the eccentricity between RHIC and LHC energies is observed and with a similar N_{part} dependence.

It was previously observed [34,79,85] that the v_2/ϵ values obtained in different collision systems and varying beam energies scale with the charged-particle rapidity density per unit transverse overlap area $(1/S)(dN_{\text{ch}}/dy)$, which is proportional to the initial entropy density. In addition, it has been pointed out [69] that in this representation the sensitivity to the modeling of the initial conditions of the heavy-ion collisions is largely removed, thus enabling the extraction of the shear viscosity to the entropy density ratio from the data through the comparison with viscous hydrodynamics calculations. With the factor of 2.1 increase in the charged-particle pseudorapidity density per participant pair, $(dN_{\text{ch}}/d\eta)/(N_{\text{part}}/2)$, from the highest RHIC energy to the LHC [75,86], this scaling behavior can be tested over a much broader range of initial entropy densities. In Fig. 24, we compare the CMS results for v_2/ϵ from the event-plane method to results from the PHOBOS experiment [34] for CuCu and AuAu collisions with $\sqrt{s_{NN}} = 62.4$ and 200 GeV.

At lower energies, the scaling has been examined using the charged-particle rapidity density dN_{ch}/dy [34,79,85]. However, because we do not identify the species of charged particles in this analysis, we perform the comparison using $(1/S)(dN_{\text{ch}}/d\eta)$ to avoid introducing uncertainties related to assumptions about the detailed behavior of the identified particle transverse momentum spectra that are needed to perform this conversion. In Fig. 24, the charged-particle pseudorapidity density $dN_{\text{ch}}/d\eta$ measured by CMS [75] is used, and the value of the integrated v_2 for the ranges

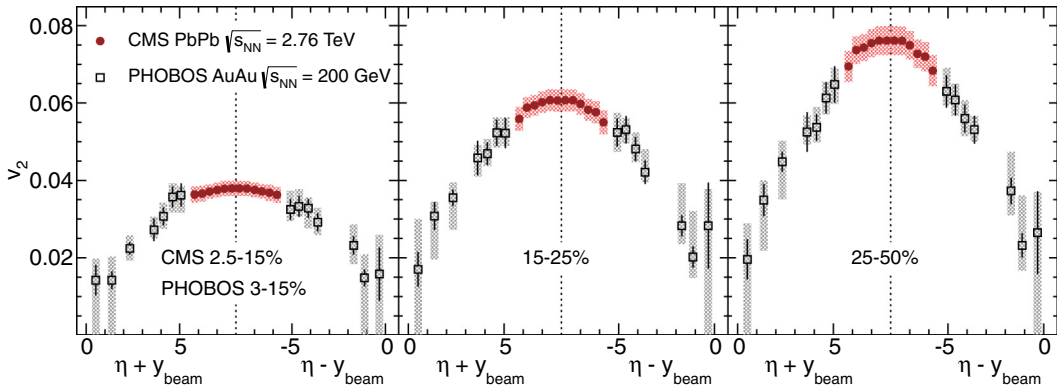

FIG. 25. (Color online) Measurements of v_2 as a function of the pseudorapidity of particles in the rest frame of the colliding nuclei $\eta \pm y_{\rm beam}$ from CMS (solid symbols) and PHOBOS (open symbols) [77] in three centrality intervals. The error bars show the statistical uncertainties and the boxes give the systematic ones.

$0 < p_{\rm T} < 3$ GeV/c and $|\eta| < 0.8$. The transverse nuclear-overlap area S and the participant eccentricity are listed in Table I. The PHOBOS results from Ref. [34] used $dN_{\rm ch}/dy$ and applied two factors to perform the Jacobian transformation from $dN_{\rm ch}/d\eta$: The x axis was scaled by a factor 1.15, and the y axis by 0.9. Both of these factors are reversed to compare the CMS and PHOBOS measurements in Fig. 24. As in Fig. 23, the PHOBOS data are scaled by $\epsilon\{2\}$, while the CMS data are scaled by the participant eccentricity $\epsilon_{\rm part}$, taking into account the event-plane resolution factors in the two measurements. The CMS result extends to very peripheral collisions (70–80% centrality), which allows for a significant overlap in the transverse charged-particle density measured at RHIC and LHC. Despite the large systematic uncertainties quoted for the PHOBOS measurements, the data are in good agreement over the common $(1/S)(dN_{\rm ch}/d\eta)$ range. A smooth increase in v_2/ϵ proportional to the transverse particle density is observed over the entire measured range, except for a small decrease in the most central collisions in both the RHIC and the LHC data. The theoretical predictions [68,71,83] for the $\sqrt{s_{NN}}$ dependence of the transverse-particle-density scaling of v_2/ϵ differ and do not generally predict a universal behavior. The data presented here provide constraints on the model descriptions of the dynamical evolution of the system, and thus should aid the reliable extraction of the transport properties of the hot QCD medium from data.

The $v_2(\eta)$ results can be used to test theoretical descriptions of the longitudinal dynamics in the expanding system, as they have been shown to be sensitive to the choice of the initial conditions, the event-by-event fluctuations in the eccentricity, and the viscosity in the sQGP and the hadronic stages of the system evolution [39,87]. The PHOBOS experiment observed [41] that the elliptic flow measured over a broad range of collision energies ($\sqrt{s_{NN}} = 19.6$, 62.4, 130, and 200 GeV) exhibited longitudinal scaling extending over several units of pseudorapidity when viewed in the rest frame of one of the incident nuclei. A similar phenomenon for soft-particle yields and spectra is known as limiting fragmentation [88]. Furthermore, with increasing $\sqrt{s_{NN}}$, this beam-energy independence of $v_2(\eta)$ was found to extend over an increasingly wider pseudorapidity range [41]. To investigate the potential continuation of extended longitudinal scaling of the elliptic flow to LHC energies, in Fig. 25 we compare the pseudorapidity dependence of $v_2(\eta)$ measured by CMS with that measured by PHOBOS at $\sqrt{s_{NN}} = 200$ GeV in three centrality intervals. Neither the CMS nor the PHOBOS measurements are performed using identified particles. The pseudorapidity η^+ (η^-) of the particles in the rest frame of the nuclei moving in the positive (negative) direction is approximated by $\eta^{\pm} = \eta \pm y_{\rm beam}$, where η is the pseudorapidity of the particles in the center-of-mass frame, and $y_{\rm beam} = \text{arccosh}(E_{\rm lab}/Am_Nc^2) \approx \ln(\sqrt{s_{NN}}\ [\text{GeV}])$, with $E_{\rm lab}$ denoting the energy of the beam in the laboratory frame, A the nuclear mass number, and m_N the nucleon mass. In Fig. 25, the left (right) half of each plot depicts v_2 in the rest frame of the beam moving in the positive (negative) laboratory direction. The PHOBOS $v_2(\eta)$ results are from the hit-based analysis from Fig. 4 in Ref. [77]. The CMS results are obtained with the event-plane method in 0.4-unit-wide bins of pseudorapidity by averaging the corresponding $v_2(p_{\rm T})$ distributions over the range $0 < p_{\rm T} < 3$ GeV/c and folding in the efficiency-corrected charged-particle spectra. A comparable centrality interval (2.5–15% in CMS, and 3–15% in PHOBOS) is analyzed for the most central collisions, while for midcentral (15–25%) and more peripheral (25–50%) collisions, the centrality selections are the same in both experiments. In Fig. 25, the statistical uncertainties are shown as error bars, while the systematic ones are represented by the shaded boxes surrounding the points. The CMS data cover 4.8 units of pseudorapidity, but do not overlap in pseudorapidity with the PHOBOS data when plotted in the rest frames of the colliding nuclei. The CMS results show weaker pseudorapidity dependence than observed in the PHOBOS measurement. The data suggest a nearly boost-invariant region that is several units wide for central events but considerably smaller for peripheral ones. It has been noted [89] that if the QCD matter produced at midrapidity at RHIC is in local equilibrium, then deviations from the triangular shape of $v_2(\eta)$ observed in the PHOBOS measurements [41] would be expected around midrapidity at LHC energies. Detailed comparisons of theoretical calculations to the results presented here can give new insights into the nature of the matter produced at both RHIC and LHC energies.

V. SUMMARY

Detailed measurements of the charged-particle azimuthal anisotropies in $\sqrt{s_{NN}} = 2.76$ TeV PbPb collisions and comparisons to lower collision energy results have been presented. The results cover a broad kinematic range, $0.3 < p_T < 20$ GeV/c, $|\eta| < 2.4$, and 12 centrality classes from 0 to 80%. The measurements employ four different methods that have different sensitivities to fluctuations in the initial conditions and nonflow correlations. The systematic comparison between the methods provides the possibility to explore the underlying physics processes that cause these differences.

The elliptic anisotropy parameter $v_2(p_T)$ for $|\eta| < 0.8$ is found to increase with p_T up to $p_T \approx 3$ GeV/c and then to decrease in the range $3 < p_T < 10$ GeV/c. For transverse momenta of $10 < p_T < 20$ GeV/c, no strong dependence of v_2 on p_T is observed. The study of the high-p_T azimuthal anisotropy in charged-particle production may constrain the theoretical descriptions of parton energy loss and its dependence on the path length traveled through the medium.

The shapes of the $v_2(p_T)$ distributions are found to be similar to those measured at RHIC. At low p_T, only a moderate increase (5–15%) is observed in the comparison between results obtained at the highest RHIC energy and the LHC, despite the large increase in the center-of-mass energy. The integrated v_2 at midrapidity and in midcentral collisions (20–30% centrality) increases approximately logarithmically with $\sqrt{s_{NN}}$. An increase by 20–30% from the highest RHIC energy to that of the LHC is observed, which is mostly attributable to the increase in the mean p_T of the underlying charged-particle spectra. The integrated v_2 signal increases from the most central collisions to the 40–50% centrality range, after which a decrease is observed. Conversely, the values of $\langle p_T \rangle$ increase with N_{part} up to $N_{\text{part}} \approx 150$ (from the most peripheral collisions up to centrality $\approx$35%) and then saturate, indicating similar freeze-out conditions in the more central collisions. The different methods of measuring v_2 give consistent results over a broad range of centrality, when scaled by their respective participant eccentricity moments. Deviations from this scaling are observed in the most central collisions and in peripheral (centrality above 50%) collisions. The eccentricity-scaled v_2 at midrapidity is measured to be approximately linear in the transverse particle density, and a universal scaling is observed in the comparison of results from different collision systems and center-of-mass energies measured at RHIC and the LHC. The value of $v_2(\eta)$ is found to be weakly dependent on pseudorapidity in central collisions; for peripheral collisions the values of $v_2(\eta)$ gradually decrease as the pseudorapidity increases. The results presented here provide further input to the theoretical models of relativistic nucleus-nucleus collisions and will aid in determining the initial conditions of the system, the degree of equilibration, and the transport properties of hot QCD matter produced in heavy-ion collisions.

ACKNOWLEDGMENTS

We congratulate our colleagues in the CERN accelerator departments for the excellent performance of the LHC and thank the technical and administrative staffs at CERN and at other CMS institutes for their contributions to the success of the CMS effort. In addition, we gratefully acknowledge the computing centers and personnel of the Worldwide LHC Computing Grid for delivering so effectively the computing infrastructure essential to our analyses. Finally, we acknowledge the enduring support for the construction and operation of the LHC and the CMS detector provided by the following funding agencies: the Austrian Federal Ministry of Science and Research; the Belgian Fonds de la Recherche Scientifique, and Fonds voor Wetenschappelijk Onderzoek; the Brazilian Funding Agencies (CNPq, CAPES, FAPERJ, and FAPESP); the Bulgarian Ministry of Education, Youth, and Science; CERN; the Chinese Academy of Sciences, Ministry of Science and Technology, and National Natural Science Foundation of China; the Colombian Funding Agency (COLCIENCIAS); the Croatian Ministry of Science, Education, and Sport; the Research Promotion Foundation, Cyprus; the Ministry of Education and Research, Recurrent Financing Contract No. SF0690030s09 and European Regional Development Fund, Estonia; the Academy of Finland, Finnish Ministry of Education and Culture, and Helsinki Institute of Physics; the Institut National de Physique Nucléaire et de Physique des Particules/CNRS, and Commissariat à l'Énergie Atomique et aux Énergies Alternatives/CEA, France; the Bundesministerium für Bildung und Forschung, Deutsche Forschungsgemeinschaft, and Helmholtz-Gemeinschaft Deutscher Forschungszentren, Germany; the General Secretariat for Research and Technology, Greece; the National Scientific Research Foundation, and National Office for Research and Technology, Hungary; the Department of Atomic Energy and the Department of Science and Technology, India; the Institute for Studies in Theoretical Physics and Mathematics, Iran; the Science Foundation, Ireland; the Istituto Nazionale di Fisica Nucleare, Italy; the Korean Ministry of Education, Science, and Technology and the World Class University program of NRF, Korea; the Lithuanian Academy of Sciences; the Mexican Funding Agencies (CINVESTAV, CONACYT, SEP, and UASLP-FAI); the Ministry of Science and Innovation, New Zealand; the Pakistan Atomic Energy Commission; the Ministry of Science and Higher Education and the National Science Centre, Poland; the Fundação para a Ciência e a Tecnologia, Portugal; JINR (Armenia, Belarus, Georgia, Ukraine, Uzbekistan); the Ministry of Education and Science of the Russian Federation, the Federal Agency of Atomic Energy of the Russian Federation, Russian Academy of Sciences, and the Russian Foundation for Basic Research; the Ministry of Science and Technological Development of Serbia; the Secretaría de Estado de Investigación, Desarrollo e Innovación and Programa Consolider-Ingenio 2010, Spain; the Swiss Funding Agencies (ETH Board, ETH Zurich, PSI, SNF, UniZH, Canton Zurich, and SER); the National Science Council, Taipei; the Thailand Center of Excellence in Physics, the Institute for the Promotion of Teaching Science and Technology and National Electronics and Computer Technology Center; the Scientific and Technical Research Council of Turkey, and Turkish Atomic Energy Authority; the Science and Technology Facilities Council, United Kingdom; the US Department of Energy, and the US National Science Foundation. Individuals have received

support from the Marie-Curie program and the European Research Council (European Union); the Leventis Foundation; the A. P. Sloan Foundation; the Alexander von Humboldt Foundation; the Belgian Federal Science Policy Office; the Fonds pour la Formation à la Recherche dans l'Industrie et dans l'Agriculture (FRIA-Belgium); the Agentschap voor Innovatie door Wetenschap en Technologie (IWT-Belgium); the Ministry of Education, Youth, and Sports (MEYS) of Czech Republic; the Council of Science and Industrial Research, India; the Compagnia di San Paolo (Torino); and the HOMING PLUS programme of Foundation for Polish Science, cofinanced from European Union, Regional Development Fund.

[1] K. Adcox *et al.* (PHENIX Collaboration), Nucl. Phys. A **757**, 184 (2005).
[2] J. Adams *et al.* (STAR Collaboration), Nucl. Phys. A **757**, 102 (2005).
[3] B. B. Back *et al.* (PHOBOS Collaboration), Nucl. Phys. A **757**, 28 (2005).
[4] E. V. Shuryak, Nucl. Phys. A **750**, 64 (2005).
[5] M. Gyulassy and L. McLerran, Nucl. Phys. A **750**, 30 (2005).
[6] A. M. Poskanzer and S. A. Voloshin, Phys. Rev. C **58**, 1671 (1998).
[7] J.-Y. Ollitrault, Phys. Rev. D **46**, 229 (1992).
[8] H. Sorge, Phys. Rev. Lett. **82**, 2048 (1999).
[9] S. S. Adler *et al.* (PHENIX Collaboration), Phys. Rev. Lett. **94**, 232302 (2005).
[10] G. Agakishiev *et al.* (STAR Collaboration), Phys. Rev. C **85**, 014901 (2012).
[11] U. Heinz and P. F. Kolb, Nucl. Phys. A **702**, 269 (2002).
[12] P. F. Kolb and U. Heinz, in *Quark-Gluon Plasma*, edited by R. Hwa and X.-N. Wang (World Scientific, Singapore, 2004), p. 634.
[13] K. Aamodt *et al.* (ALICE Collaboration), Phys. Rev. Lett. **105**, 252302 (2010).
[14] G. Aad *et al.* (ATLAS Collaboration), Phys. Lett. B **707**, 330 (2012).
[15] D. A. Teaney, in *Quark-Gluon Plasma 4*, edited by R. Hwa and X.-N. Wang (World Scientific, Singapore, 2010), p. 207.
[16] P. Romatschke, Int. J. Mod. Phys. E **19**, 1 (2010).
[17] S. S. Adler *et al.* (PHENIX Collaboration), Phys. Rev. Lett. **91**, 182301 (2003).
[18] J. Adams *et al.* (STAR Collaboration), Phys. Rev. Lett. **92**, 052302 (2004).
[19] S. Afanasiev *et al.* (PHENIX Collaboration), Phys. Rev. Lett. **99**, 052301 (2007).
[20] B. I. Abelev *et al.* (STAR Collaboration), Phys. Rev. C **75**, 054906 (2007).
[21] P. Huovinen and P. V. Ruuskanen, Annu. Rev. Nucl. Part. Sci. **56**, 163 (2006).
[22] U. W. Heinz, in *Relativistic Heavy Ion Physics, Landolt-Boernstein New Series*, edited by R. Stock (Springer Verlag, New York, 2010), Vol. I/23, Chap. 5.
[23] A. Adare *et al.* (PHENIX Collaboration), Phys. Rev. Lett. **98**, 162301 (2007).
[24] V. Greco, C. M. Ko, and P. Lévai, Phys. Rev. C **68**, 034904 (2003).
[25] R. J. Fries, B. Müller, C. Nonaka, and S. A. Bass, Phys. Rev. C **68**, 044902 (2003).
[26] R. C. Hwa and C. B. Yang, Phys. Rev. C **70**, 024904 (2004).
[27] B. Müller, Nucl. Phys. A **750**, 84 (2005).
[28] M. Gyulassy, I. Vitev, and X.-N. Wang, Phys. Rev. Lett. **86**, 2537 (2001).
[29] S. Afanasiev *et al.* (PHENIX Collaboration), Phys. Rev. C **80**, 054907 (2009).
[30] A. Adare *et al.* (PHENIX Collaboration), Phys. Rev. Lett. **105**, 142301 (2010).
[31] S. A. Bass, C. Gale, A. Majumder, C. Nonaka, G.-Y. Qin, T. Renk, and J. Ruppert, Phys. Rev. C **79**, 024901 (2009).
[32] P. F. Kolb, J. Sollfrank, and U. W. Heinz, Phys. Rev. C **62**, 054909 (2000).
[33] B. Alver *et al.* (PHOBOS Collaboration), Phys. Rev. Lett. **104**, 142301 (2010).
[34] B. Alver *et al.* (PHOBOS Collaboration), Phys. Rev. C **77**, 014906 (2008).
[35] R. S. Bhalerao and J.-Y. Ollitrault, Phys. Lett. B **641**, 260 (2006).
[36] S. A. Voloshin, A. M. Poskanzer, A. Tang, and G. Wang, Phys. Lett. B **659**, 537 (2008).
[37] J.-Y. Ollitrault, A. M. Poskanzer, and S. A. Voloshin, Phys. Rev. C **80**, 014904 (2009).
[38] Z. Qiu and U. W. Heinz, Phys. Rev. C **84**, 024911 (2011).
[39] T. Hirano, U. Heinz, D. Kharzeev, R. Lacey, and Y. Nara, Phys. Lett. B **636**, 299 (2006).
[40] W. Busza, Nucl. Phys. A **854**, 57 (2011).
[41] B. B. Back *et al.* (PHOBOS Collaboration), Phys. Rev. Lett. **94**, 122303 (2005).
[42] N. Borghini, P. M. Dinh, and J.-Y. Ollitrault, Phys. Rev. C **64**, 054901 (2001).
[43] R. S. Bhalerao, N. Borghini, and J.-Y. Ollitrault, Nucl. Phys. A **727**, 373 (2003).
[44] N. Borghini, R. S. Bhalerao, and J.-Y. Ollitrault, J. Phys. G **30**, S1213 (2004).
[45] S. Chatrchyan *et al.* (CMS Collaboration), J. Instrum. **3**, S08004 (2008).
[46] Ø. Djuvsland and J. Nystrand, Phys. Rev. C **83**, 041901 (2011).
[47] V. Khachatryan *et al.* (CMS Collaboration), Phys. Rev. Lett. **105**, 022002 (2010).
[48] M. L. Miller, K. Reygers, S. J. Sanders, and P. Steinberg, Annu. Rev. Nucl. Part. Sci. **57**, 205 (2007).
[49] B. Alver *et al.* (PHOBOS Collaboration), Phys. Rev. Lett. **98**, 242302 (2007).
[50] B. Alver, M. Baker, C. Loizides, and P. Steinberg, arXiv:0805.4411.
[51] H. De Vries, C. W. De Jager, and C. De Vries, Atom. Data Nucl. Data Tables **36**, 495 (1987).
[52] K. Nakamura, K. Hagiwara, H. Murayama, M. Tanabashi, T. Watari, and C. Amsler (Particle Data Group Collaboration), J. Phys. G **37**, 075021 (2010).
[53] S. Chatrchyan *et al.* (CMS Collaboration), Phys. Rev. C **84**, 024906 (2011).
[54] Z.-W. Lin, C. M. Ko, B.-A. Li, B. Zhang, and S. Pal, Phys. Rev. C **72**, 064901 (2005).
[55] W. Adam, B. Mangano, T. Speer, and T. Todorov (CMS Collaboration), CMS Note NOTE-2006-041.
[56] V. Khachatryan, A. Sirunyan, A. Tumasyan, W. Adam, T. Bergauer, and M. Dragicevic (CMS Collaboration), Eur. Phys. J. C **70**, 1165 (2010).

[57] I. P. Lokhtin and A. M. Snigirev, Eur. Phys. J. C **45**, 211 (2006).
[58] C. Tsallis, J. Stat. Phys. **52**, 479 (1988).
[59] G. Wilk and Z. Włodarczyk, Eur. Phys. J. A **40**, 299 (2009).
[60] T. S. Biró, G. Purcsel, and K. Ürmössy, Eur. Phys. J. A **40**, 325 (2009).
[61] H. Holopainen, H. Niemi, and K. J. Eskola, Phys. Rev. C **83**, 034901 (2011).
[62] H. Petersen, G.-Y. Qin, S. A. Bass, and B. Muller, Phys. Rev. C **82**, 041901 (2010).
[63] F. G. Gardim, F. Grassi, M. Luzum, and J.-Y. Ollitrault, Phys. Rev. C **85**, 024908 (2012).
[64] J. Barrette *et al.* (E877 Collaboration), Phys. Rev. C **56**, 3254 (1997).
[65] M. Luzum and P. Romatschke, Phys. Rev. C **78**, 034915 (2008).
[66] S. Chatrchyan *et al.* (CMS Collaboration), Eur. Phys. J. C **72**, 1945 (2012).
[67] B. I. Abelev *et al.* (STAR Collaboration), Phys. Rev. C **77**, 054901 (2008).
[68] T. Hirano, P. Huovinen, and Y. Nara, Phys. Rev. C **83**, 021902 (2011).
[69] H. Song, S. A. Bass, U. Heinz, T. Hirano, and C. Shen, Phys. Rev. Lett. **106**, 192301 (2011).
[70] J. L. Nagle, I. G. Bearden, and W. A. Zajc, New J. Phys. **13**, 075004 (2011).
[71] C. Shen, U. Heinz, P. Huovinen, and H. Song, Phys. Rev. C **84**, 044903 (2011).
[72] H.-J. Drescher and Y. Nara, Phys. Rev. C **76**, 041903 (2007).
[73] S. Afanasiev *et al.* (PHENIX Collaboration), Phys. Rev. C **80**, 024909 (2009).
[74] J. Adams *et al.* (STAR Collaboration), Phys. Rev. Lett. **93**, 252301 (2004).
[75] S. Chatrchyan *et al.* (CMS Collaboration), J. High Energy Phys. 08 (2011) 141.
[76] B. I. Abelev *et al.* (STAR Collaboration), Phys. Rev. C **81**, 024911 (2010).
[77] B. B. Back *et al.* (PHOBOS Collaboration), Phys. Rev. C **72**, 051901 (2005).
[78] B. B. Back *et al.* (PHOBOS Collaboration), Phys. Rev. Lett. **89**, 222301 (2002).
[79] C. Alt *et al.* (PHOBOS Collaboration), Phys. Rev. C **68**, 034903 (2003).
[80] J. Barrette *et al.* (E877 Collaboration), Phys. Rev. C **55**, 1420 (1997).
[81] H. Appelshäuser, D. Adamová, G. Agakichiev, V. Belaga, and P. Braun-Munzinger (CERES Collaboration), Nucl. Phys. A **698**, 253 (2002).
[82] J. Adams *et al.* (STAR Collaboration), Phys. Rev. C **70**, 054907 (2004).
[83] M. Luzum and P. Romatschke, Phys. Rev. Lett. **103**, 262302 (2009).
[84] C. Shen and U. Heinz, Phys. Rev. C **83**, 044909 (2011).
[85] C. Adler *et al.* (STAR Collaboration), Phys. Rev. C **66**, 034904 (2002).
[86] K. Aamodt *et al.* (ALICE Collaboration), Phys. Rev. Lett. **106**, 032301 (2011).
[87] R. Andrade, F. Grassi, Y. Hama, T. Kodama, and O. Socolowski, Jr., Phys. Rev. Lett. **97**, 202302 (2006).
[88] J. Benecke, T. T. Chou, C. N. Yang, and E. Yen, Phys. Rev. **188**, 2159 (1969).
[89] N. Borghini and U. A. Wiedemann, J. Phys. G **35**, 023001 (2008).

S. Chatrchyan,[1] V. Khachatryan,[1] A. M. Sirunyan,[1] A. Tumasyan,[1] W. Adam,[2] T. Bergauer,[2] M. Dragicevic,[2] J. Erö,[2] C. Fabjan,[2] M. Friedl,[2] R. Frühwirth,[2] V. M. Ghete,[2] J. Hammer,[2,a] N. Hörmann,[2] J. Hrubec,[2] M. Jeitler,[2] W. Kiesenhofer,[2] M. Krammer,[2] D. Liko,[2] I. Mikulec,[2] M. Pernicka,[2,b] B. Rahbaran,[2] C. Rohringer,[2] H. Rohringer,[2] R. Schöfbeck,[2] J. Strauss,[2] A. Taurok,[2] F. Teischinger,[2] P. Wagner,[2] W. Waltenberger,[2] G. Walzel,[2] E. Widl,[2] C.-E. Wulz,[2] V. Mossolov,[3] N. Shumeiko,[3] J. Suarez Gonzalez,[3] S. Bansal,[4] K. Cerny,[4] T. Cornelis,[4] E. A. De Wolf,[4] X. Janssen,[4] S. Luyckx,[4] T. Maes,[4] L. Mucibello,[4] S. Ochesanu,[4] B. Roland,[4] R. Rougny,[4] M. Selvaggi,[4] H. Van Haevermaet,[4] P. Van Mechelen,[4] N. Van Remortel,[4] A. Van Spilbeeck,[4] F. Blekman,[5] S. Blyweert,[5] J. D'Hondt,[5] R. Gonzalez Suarez,[5] A. Kalogeropoulos,[5] M. Maes,[5] A. Olbrechts,[5] W. Van Doninck,[5] P. Van Mulders,[5] G. P. Van Onsem,[5] I. Villella,[5] O. Charaf,[6] B. Clerbaux,[6] G. De Lentdecker,[6] V. Dero,[6] A. P. R. Gay,[6] T. Hreus,[6] A. Léonard,[6] P. E. Marage,[6] T. Reis,[6] L. Thomas,[6] C. Vander Velde,[6] P. Vanlaer,[6] V. Adler,[7] K. Beernaert,[7] A. Cimmino,[7] S. Costantini,[7] G. Garcia,[7] M. Grunewald,[7] B. Klein,[7] J. Lellouch,[7] A. Marinov,[7] J. Mccartin,[7] A. A. Ocampo Rios,[7] D. Ryckbosch,[7] N. Strobbe,[7] F. Thyssen,[7] M. Tytgat,[7] L. Vanelderen,[7] P. Verwilligen,[7] S. Walsh,[7] E. Yazgan,[7] N. Zaganidis,[7] S. Basegmez,[8] G. Bruno,[8] L. Ceard,[8] C. Delaere,[8] T. du Pree,[8] D. Favart,[8] L. Forthomme,[8] A. Giammanco,[8,c] J. Hollar,[8] V. Lemaitre,[8] J. Liao,[8] O. Militaru,[8] C. Nuttens,[8] D. Pagano,[8] A. Pin,[8] K. Piotrzkowski,[8] N. Schul,[8] N. Beliy,[9] T. Caebergs,[9] E. Daubie,[9] G. H. Hammad,[9] G. A. Alves,[10] M. Correa Martins Junior,[10] D. De Jesus Damiao,[10] T. Martins,[10] M. E. Pol,[10] M. H. G. Souza,[10] W. L. Aldá Júnior,[11] W. Carvalho,[11] A. Custódio,[11] E. M. Da Costa,[11] C. De Oliveira Martins,[11] S. Fonseca De Souza,[11] D. Matos Figueiredo,[11] L. Mundim,[11] H. Nogima,[11] V. Oguri,[11] W. L. Prado Da Silva,[11] A. Santoro,[11] S. M. Silva Do Amaral,[11] L. Soares Jorge,[11] A. Sznajder,[11] T. S. Anjos,[12,d] C. A. Bernardes,[12,d] F. A. Dias,[12,e] T. R. Fernandez Perez Tomei,[12] E. M. Gregores,[12,d] C. Lagana,[12] F. Marinho,[12] P. G. Mercadante,[12,d] S. F. Novaes,[12] Sandra S. Padula,[12] V. Genchev,[13,a] P. Iaydjiev,[13,a] S. Piperov,[13] M. Rodozov,[13] S. Stoykova,[13] G. Sultanov,[13] V. Tcholakov,[13] R. Trayanov,[13] M. Vutova,[13] A. Dimitrov,[14] R. Hadjiiska,[14] V. Kozhuharov,[14] L. Litov,[14] B. Pavlov,[14] P. Petkov,[14] J. G. Bian,[15] G. M. Chen,[15] H. S. Chen,[15] C. H. Jiang,[15] D. Liang,[15] S. Liang,[15] X. Meng,[15] J. Tao,[15] J. Wang,[15] J. Wang,[15] X. Wang,[15] Z. Wang,[15] H. Xiao,[15] M. Xu,[15] J. Zang,[15] Z. Zhang,[15] C. Asawatangtrakuldee,[16] Y. Ban,[16] S. Guo,[16] Y. Guo,[16] W. Li,[16] S. Liu,[16] Y. Mao,[16] S. J. Qian,[16] H. Teng,[16] S. Wang,[16] B. Zhu,[16] W. Zou,[16] C. Avila,[17] B. Gomez Moreno,[17] A. F. Osorio Oliveros,[17] J. C. Sanabria,[17] N. Godinovic,[18] D. Lelas,[18] R. Plestina,[18,f] D. Polic,[18] I. Puljak,[18,a] Z. Antunovic,[19] M. Dzelalija,[19] M. Kovac,[19] V. Brigljevic,[20] S. Duric,[20] K. Kadija,[20] J. Luetic,[20] S. Morovic,[20]

A. Attikis,[21] M. Galanti,[21] G. Mavromanolakis,[21] J. Mousa,[21] C. Nicolaou,[21] F. Ptochos,[21] P. A. Razis,[21] M. Finger,[22] M. Finger Jr.,[22] Y. Assran,[23,g] S. Elgammal,[23] A. Ellithi Kamel,[23,h] S. Khalil,[23,i] M. A. Mahmoud,[23,j] A. Radi,[23,i] M. Kadastik,[24] M. Müntel,[24] M. Raidal,[24] L. Rebane,[24] A. Tiko,[24] V. Azzolini,[25] P. Eerola,[25] G. Fedi,[25] M. Voutilainen,[25] J. Härkönen,[26] A. Heikkinen,[26] V. Karimäki,[26] R. Kinnunen,[26] M. J. Kortelainen,[26] T. Lampén,[26] K. Lassila-Perini,[26] S. Lehti,[26] T. Lindén,[26] P. Luukka,[26] T. Mäenpää,[26] T. Peltola,[26] E. Tuominen,[26] J. Tuominiemi,[26] E. Tuovinen,[26] D. Ungaro,[26] L. Wendland,[26] K. Banzuzi,[27] A. Korpela,[27] T. Tuuva,[27] M. Besancon,[28] S. Choudhury,[28] M. Dejardin,[28] D. Denegri,[28] B. Fabbro,[28] J. L. Faure,[28] F. Ferri,[28] S. Ganjour,[28] A. Givernaud,[28] P. Gras,[28] G. Hamel de Monchenault,[28] P. Jarry,[28] E. Locci,[28] J. Malcles,[28] L. Millischer,[28] A. Nayak,[28] J. Rander,[28] A. Rosowsky,[28] I. Shreyber,[28] M. Titov,[28] S. Baffioni,[29] F. Beaudette,[29] L. Benhabib,[29] L. Bianchini,[29] M. Bluj,[29,k] C. Broutin,[29] P. Busson,[29] C. Charlot,[29] N. Daci,[29] T. Dahms,[29] L. Dobrzynski,[29] R. Granier de Cassagnac,[29] M. Haguenauer,[29] P. Miné,[29] C. Mironov,[29] C. Ochando,[29] P. Paganini,[29] D. Sabes,[29] R. Salerno,[29] Y. Sirois,[29] C. Veelken,[29] A. Zabi,[29] J.-L. Agram,[30,l] J. Andrea,[30] D. Bloch,[30] D. Bodin,[30] J.-M. Brom,[30] M. Cardaci,[30] E. C. Chabert,[30] C. Collard,[30] E. Conte,[30,l] F. Drouhin,[30,l] C. Ferro,[30] J.-C. Fontaine,[30,l] D. Gelé,[30] U. Goerlach,[30] P. Juillot,[30] M. Karim,[30,l] A.-C. Le Bihan,[30] P. Van Hove,[30] F. Fassi,[31] D. Mercier,[31] S. Beauceron,[32] N. Beaupere,[32] O. Bondu,[32] G. Boudoul,[32] H. Brun,[32] J. Chasserat,[32] R. Chierici,[32,a] D. Contardo,[32] P. Depasse,[32] H. El Mamouni,[32] J. Fay,[32] S. Gascon,[32] M. Gouzevitch,[32] B. Ille,[32] T. Kurca,[32] M. Lethuillier,[32] L. Mirabito,[32] S. Perries,[32] V. Sordini,[32] S. Tosi,[32] Y. Tschudi,[32] P. Verdier,[32] S. Viret,[32] Z. Tsamalaidze,[33] G. Anagnostou,[34] S. Beranek,[34] M. Edelhoff,[34] L. Feld,[34] N. Heracleous,[34] O. Hindrichs,[34] R. Jussen,[34] K. Klein,[34] J. Merz,[34] A. Ostapchuk,[34] A. Perieanu,[34] F. Raupach,[34] J. Sammet,[34] S. Schael,[34] D. Sprenger,[34] H. Weber,[34] B. Wittmer,[34] V. Zhukov,[34,m] M. Ata,[35] J. Caudron,[35] E. Dietz-Laursonn,[35] D. Duchardt,[35] M. Erdmann,[35] A. Güth,[35] T. Hebbeker,[35] C. Heidemann,[35] K. Hoepfner,[35] T. Klimkovich,[35] D. Klingebiel,[35] P. Kreuzer,[35] D. Lanske,[35,b] J. Lingemann,[35] C. Magass,[35] M. Merschmeyer,[35] A. Meyer,[35] M. Olschewski,[35] P. Papacz,[35] H. Pieta,[35] H. Reithler,[35] S. A. Schmitz,[35] L. Sonnenschein,[35] J. Steggemann,[35] D. Teyssier,[35] M. Weber,[35] M. Bontenackels,[36] V. Cherepanov,[36] M. Davids,[36] G. Flügge,[36] H. Geenen,[36] M. Geisler,[36] W. Haj Ahmad,[36] F. Hoehle,[36] B. Kargoll,[36] T. Kress,[36] Y. Kuessel,[36] A. Linn,[36] A. Nowack,[36] L. Perchalla,[36] O. Pooth,[36] J. Rennefeld,[36] P. Sauerland,[36] A. Stahl,[36] M. Aldaya Martin,[37] J. Behr,[37] W. Behrenhoff,[37] U. Behrens,[37] M. Bergholz,[37,n] A. Bethani,[37] K. Borras,[37] A. Burgmeier,[37] A. Cakir,[37] L. Calligaris,[37] A. Campbell,[37] E. Castro,[37] F. Costanza,[37] D. Dammann,[37] G. Eckerlin,[37] D. Eckstein,[37] D. Fischer,[37] G. Flucke,[37] A. Geiser,[37] I. Glushkov,[37] S. Habib,[37] J. Hauk,[37] H. Jung,[37,a] M. Kasemann,[37] P. Katsas,[37] C. Kleinwort,[37] H. Kluge,[37] A. Knutsson,[37] M. Krämer,[37] D. Krücker,[37] E. Kuznetsova,[37] W. Lange,[37] W. Lohmann,[37,n] B. Lutz,[37] R. Mankel,[37] I. Marfin,[37] M. Marienfeld,[37] I.-A. Melzer-Pellmann,[37] A. B. Meyer,[37] J. Mnich,[37] A. Mussgiller,[37] S. Naumann-Emme,[37] J. Olzem,[37] H. Perrey,[37] A. Petrukhin,[37] D. Pitzl,[37] A. Raspereza,[37] P. M. Ribeiro Cipriano,[37] C. Riedl,[37] M. Rosin,[37] J. Salfeld-Nebgen,[37] R. Schmidt,[37,n] T. Schoerner-Sadenius,[37] N. Sen,[37] A. Spiridonov,[37] M. Stein,[37] R. Walsh,[37] C. Wissing,[37] C. Autermann,[38] V. Blobel,[38] S. Bobrovskyi,[38] J. Draeger,[38] H. Enderle,[38] J. Erfle,[38] U. Gebbert,[38] M. Görner,[38] T. Hermanns,[38] R. S. Höing,[38] K. Kaschube,[38] G. Kaussen,[38] H. Kirschenmann,[38] R. Klanner,[38] J. Lange,[38] B. Mura,[38] F. Nowak,[38] N. Pietsch,[38] D. Rathjens,[38] C. Sander,[38] H. Schettler,[38] P. Schleper,[38] E. Schlieckau,[38] A. Schmidt,[38] M. Schröder,[38] T. Schum,[38] M. Seidel,[38] H. Stadie,[38] G. Steinbrück,[38] J. Thomsen,[38] C. Barth,[39] J. Berger,[39] T. Chwalek,[39] W. De Boer,[39] A. Dierlamm,[39] M. Feindt,[39] M. Guthoff,[39,a] C. Hackstein,[39] F. Hartmann,[39] M. Heinrich,[39] H. Held,[39] K. H. Hoffmann,[39] S. Honc,[39] U. Husemann,[39] I. Katkov,[39,m] J. R. Komaragiri,[39] D. Martschei,[39] S. Mueller,[39] Th. Müller,[39] M. Niegel,[39] A. Nürnberg,[39] O. Oberst,[39] A. Oehler,[39] J. Ott,[39] T. Peiffer,[39] G. Quast,[39] K. Rabbertz,[39] F. Ratnikov,[39] N. Ratnikova,[39] S. Röcker,[39] C. Saout,[39] A. Scheurer,[39] F.-P. Schilling,[39] M. Schmanau,[39] G. Schott,[39] H. J. Simonis,[39] F. M. Stober,[39] D. Troendle,[39] R. Ulrich,[39] J. Wagner-Kuhr,[39] T. Weiler,[39] M. Zeise,[39] E. B. Ziebarth,[39] G. Daskalakis,[40] T. Geralis,[40] S. Kesisoglou,[40] A. Kyriakis,[40] D. Loukas,[40] I. Manolakos,[40] A. Markou,[40] C. Markou,[40] C. Mavrommatis,[40] E. Ntomari,[40] L. Gouskos,[41] T. J. Mertzimekis,[41] A. Panagiotou,[41] N. Saoulidou,[41] I. Evangelou,[42] C. Foudas,[42,a] P. Kokkas,[42] N. Manthos,[42] I. Papadopoulos,[42] V. Patras,[42] G. Bencze,[43] C. Hajdu,[43,a] P. Hidas,[43] D. Horvath,[43,o] K. Krajczar,[43,p] B. Radics,[43] F. Sikler,[43,a] V. Veszpremi,[43] G. Vesztergombi,[43,p] N. Beni,[44] S. Czellar,[44] J. Molnar,[44] J. Palinkas,[44] Z. Szillasi,[44] J. Karancsi,[45] P. Raics,[45] Z. L. Trocsanyi,[45] B. Ujvari,[45] S. B. Beri,[46] V. Bhatnagar,[46] N. Dhingra,[46] R. Gupta,[46] M. Jindal,[46] M. Kaur,[46] J. M. Kohli,[46] M. Z. Mehta,[46] N. Nishu,[46] L. K. Saini,[46] A. Sharma,[46] J. Singh,[46] S. P. Singh,[46] S. Ahuja,[47] B. C. Choudhary,[47] A. Kumar,[47] A. Kumar,[47] S. Malhotra,[47] M. Naimuddin,[47] K. Ranjan,[47] V. Sharma,[47] R. K. Shivpuri,[47] S. Banerjee,[48] S. Bhattacharya,[48] S. Dutta,[48] B. Gomber,[48] Sa. Jain,[48] Sh. Jain,[48] R. Khurana,[48] S. Sarkar,[48] A. Abdulsalam,[49] R. K. Choudhury,[49] D. Dutta,[49] S. Kailas,[49] V. Kumar,[49] A. K. Mohanty,[49,a] L. M. Pant,[49] P. Shukla,[49] T. Aziz,[50] S. Ganguly,[50] M. Guchait,[50,q] A. Gurtu,[50] M. Maity,[50,r] G. Majumder,[50] K. Mazumdar,[50] G. B. Mohanty,[50] B. Parida,[50] K. Sudhakar,[50] N. Wickramage,[50] S. Banerjee,[51] S. Dugad,[51] H. Arfaei,[52] H. Bakhshiansohi,[52,s] S. M. Etesami,[52,t] A. Fahim,[52,s] M. Hashemi,[52] H. Hesari,[52] A. Jafari,[52,s] M. Khakzad,[52] A. Mohammadi,[52,u] M. Mohammadi Najafabadi,[52] S. Paktinat Mehdiabadi,[52] B. Safarzadeh,[52,v] M. Zeinali,[52,t] M. Abbrescia,[53a,53b] L. Barbone,[53a,53b] C. Calabria,[53a,53b,a] S. S. Chhibra,[53a,53b] A. Colaleo,[53a] D. Creanza,[53a,53c] N. De Filippis,[53a,53c,a] M. De Palma,[53a,53b] L. Fiore,[53a] G. Iaselli,[53a,53c] L. Lusito,[53a,53b] G. Maggi,[53a,53c] M. Maggi,[53a] B. Marangelli,[53a,53b] S. My,[53a,53c] S. Nuzzo,[53a,53b] N. Pacifico,[53a,53b] A. Pompili,[53a,53b] G. Pugliese,[53a,53c] G. Selvaggi,[53a,53b] L. Silvestris,[53a] G. Singh,[53a,53b] G. Zito,[53a] G. Abbiendi,[54a] A. C. Benvenuti,[54a] D. Bonacorsi,[54a,54b] S. Braibant-Giacomelli,[54a,54b] L. Brigliadori,[54a,54b] P. Capiluppi,[54a,54b] A. Castro,[54a,54b] F. R. Cavallo,[54a] M. Cuffiani,[54a,54b] G. M. Dallavalle,[54a] F. Fabbri,[54a] A. Fanfani,[54a,54b] D. Fasanella,[54a,54b,a] P. Giacomelli,[54a] C. Grandi,[54a] L. Guiducci,[54a] S. Marcellini,[54a] G. Masetti,[54a] M. Meneghelli,[54a,54b,a] A. Montanari,[54a] F. L. Navarria,[54a,54b] F. Odorici,[54a] A. Perrotta,[54a]

F. Primavera,[54a,54b] A. M. Rossi,[54a,54b] T. Rovelli,[54a,54b] G. Siroli,[54a,54b] R. Travaglini,[54a,54b] S. Albergo,[55a,55b] G. Cappello,[55a,55b] M. Chiorboli,[55a,55b] S. Costa,[55a,55b] R. Potenza,[55a,55b] A. Tricomi,[55a,55b] C. Tuve,[55a,55b] G. Barbagli,[56a] V. Ciulli,[56a,56b] C. Civinini,[56a] R. D'Alessandro,[56a,56b] E. Focardi,[56a,56b] S. Frosali,[56a,56b] E. Gallo,[56a] S. Gonzi,[56a,56b] M. Meschini,[56a] S. Paoletti,[56a] G. Sguazzoni,[56a] A. Tropiano,[56a,a] L. Benussi,[57] S. Bianco,[57] S. Colafranceschi,[57,w] F. Fabbri,[57] D. Piccolo,[57] P. Fabbricatore,[58] R. Musenich,[58] A. Benaglia,[59a,59b,a] F. De Guio,[59a,59b] L. Di Matteo,[59a,59b,a] S. Fiorendi,[59a,59b] S. Gennai,[59a,a] A. Ghezzi,[59a,59b] S. Malvezzi,[59a] R. A. Manzoni,[59a,59b] A. Martelli,[59a,59b] A. Massironi,[59a,59b,a] D. Menasce,[59a] L. Moroni,[59a] M. Paganoni,[59a,59b] D. Pedrini,[59a] S. Ragazzi,[59a,59b] N. Redaelli,[59a] S. Sala,[59a] T. Tabarelli de Fatis,[59a,59b] S. Buontempo,[60a] C. A. Carrillo Montoya,[60a,a] N. Cavallo,[60a,x] A. De Cosa,[60a,60b] O. Dogangun,[60a,60b] F. Fabozzi,[60a,x] A. O. M. Iorio,[60a,a] L. Lista,[60a] S. Meola,[60a,y] M. Merola,[60a,60b] P. Paolucci,[60a] P. Azzi,[61a] N. Bacchetta,[61a,a] P. Bellan,[61a,61b] M. Biasotto,[61a,z] D. Bisello,[61a,61b] A. Branca,[61a,a] P. Checchia,[61a] T. Dorigo,[61a] U. Dosselli,[61a] F. Gasparini,[61a,61b] A. Gozzelino,[61a] M. Gulmini,[61a,z] K. Kanishchev,[61a,61c] S. Lacaprara,[61a] I. Lazzizzera,[61a,61c] M. Margoni,[61a,61b] G. Maron,[61a,z] A. T. Meneguzzo,[61a,61b] L. Perrozzi,[61a] N. Pozzobon,[61a,61b] P. Ronchese,[61a,61b] F. Simonetto,[61a,61b] E. Torassa,[61a] M. Tosi,[61a,61b,a] S. Vanini,[61a,61b] M. Gabusi,[62a,62b] S. P. Ratti,[62a,62b] C. Riccardi,[62a,62b] P. Torre,[62a,62b] P. Vitulo,[62a,62b] G. M. Bilei,[63a] L. Fanò,[63a,63b] P. Lariccia,[63a,63b] A. Lucaroni,[63a,63b,a] G. Mantovani,[63a,63b] M. Menichelli,[63a] A. Nappi,[63a,63b] F. Romeo,[63a,63b] A. Saha,[63a] A. Santocchia,[63a,63b] S. Taroni,[63a,63b,a] P. Azzurri,[64a,64c] G. Bagliesi,[64a] T. Boccali,[64a] G. Broccolo,[64a,64c] R. Castaldi,[64a] R. T. D'Agnolo,[64a,64c] R. Dell'Orso,[64a] F. Fiori,[64a,64b,a] L. Foà,[64a,64c] A. Giassi,[64a] A. Kraan,[64a] F. Ligabue,[64a,64c] T. Lomtadze,[64a] L. Martini,[64a,aa] A. Messineo,[64a,64b] F. Palla,[64a] F. Palmonari,[64a] A. Rizzi,[64a,64b] A. T. Serban,[64a,bb] P. Spagnolo,[64a] P. Squillacioti,[64a,a] R. Tenchini,[64a] G. Tonelli,[64a,64b,a] A. Venturi,[64a,a] P. G. Verdini,[64a] L. Barone,[65a,65b] F. Cavallari,[65a] D. Del Re,[65a,65b,a] M. Diemoz,[65a] C. Fanelli,[65a,65b] M. Grassi,[65a,a] E. Longo,[65a,65b] P. Meridiani,[65a,a] F. Micheli,[65a,65b] S. Nourbakhsh,[65a] G. Organtini,[65a,65b] F. Pandolfi,[65a,65b] R. Paramatti,[65a] S. Rahatlou,[65a,65b] M. Sigamani,[65a] L. Soffi,[65a,65b] N. Amapane,[66a,66b] R. Arcidiacono,[66a,66c] S. Argiro,[66a,66b] M. Arneodo,[66a,66c] C. Biino,[66a] C. Botta,[66a,66b] N. Cartiglia,[66a] R. Castello,[66a,66b] M. Costa,[66a,66b] N. Demaria,[66a] A. Graziano,[66a,66b] C. Mariotti,[66a,a] S. Maselli,[66a] E. Migliore,[66a,66b] V. Monaco,[66a,66b] M. Musich,[66a,a] M. M. Obertino,[66a,66c] N. Pastrone,[66a] M. Pelliccioni,[66a] A. Potenza,[66a,66b] A. Romero,[66a,66b] M. Ruspa,[66a,66c] R. Sacchi,[66a,66b] V. Sola,[66a,66b] A. Solano,[66a,66b] A. Staiano,[66a] A. Vilela Pereira,[66a] S. Belforte,[67a] F. Cossutti,[67a] G. Della Ricca,[67a,67b] B. Gobbo,[67a] M. Marone,[67a,67b,a] D. Montanino,[67a,67b,a] A. Penzo,[67a] A. Schizzi,[67a,67b] S. G. Heo,[68] T. Y. Kim,[68] S. K. Nam,[68] S. Chang,[69] J. Chung,[69] D. H. Kim,[69] G. N. Kim,[69] D. J. Kong,[69] H. Park,[69] S. R. Ro,[69] D. C. Son,[69] T. Son,[69] J. Y. Kim,[70] Zero J. Kim,[70] S. Song,[70] H. Y. Jo,[71] S. Choi,[72] D. Gyun,[72] B. Hong,[72] M. Jo,[72] H. Kim,[72] T. J. Kim,[72] K. S. Lee,[72] D. H. Moon,[72] S. K. Park,[72] E. Seo,[72] M. Choi,[73] S. Kang,[73] H. Kim,[73] J. H. Kim,[73] C. Park,[73] I. C. Park,[73] S. Park,[73] G. Ryu,[73] Y. Cho,[74] Y. Choi,[74] Y. K. Choi,[74] J. Goh,[74] M. S. Kim,[74] E. Kwon,[74] B. Lee,[74] J. Lee,[74] S. Lee,[74] H. Seo,[74] I. Yu,[74] M. J. Bilinskas,[75] I. Grigelionis,[75] M. Janulis,[75] A. Juodagalvis,[75] H. Castilla-Valdez,[76] E. De La Cruz-Burelo,[76] I. Heredia-de La Cruz,[76] R. Lopez-Fernandez,[76] R. Magaña Villalba,[76] J. Martínez-Ortega,[76] A. Sánchez-Hernández,[76] L. M. Villasenor-Cendejas,[76] S. Carrillo Moreno,[77] F. Vazquez Valencia,[77] H. A. Salazar Ibarguen,[78] E. Casimiro Linares,[79] A. Morelos Pineda,[79] M. A. Reyes-Santos,[79] D. Krofcheck,[80] A. J. Bell,[81] P. H. Butler,[81] R. Doesburg,[81] S. Reucroft,[81] H. Silverwood,[81] M. Ahmad,[82] M. I. Asghar,[82] H. R. Hoorani,[82] S. Khalid,[82] W. A. Khan,[82] T. Khurshid,[82] S. Qazi,[82] M. A. Shah,[82] M. Shoaib,[82] G. Brona,[83] K. Bunkowski,[83] M. Cwiok,[83] W. Dominik,[83] K. Doroba,[83] A. Kalinowski,[83] M. Konecki,[83] J. Krolikowski,[83] H. Bialkowska,[84] B. Boimska,[84] T. Frueboes,[84] R. Gokieli,[84] M. Górski,[84] M. Kazana,[84] K. Nawrocki,[84] K. Romanowska-Rybinska,[84] M. Szleper,[84] G. Wrochna,[84] P. Zalewski,[84] N. Almeida,[85] P. Bargassa,[85] A. David,[85] P. Faccioli,[85] P. G. Ferreira Parracho,[85] M. Gallinaro,[85] P. Musella,[85] J. Seixas,[85] J. Varela,[85] P. Vischia,[85] S. Afanasiev,[86] I. Belotelov,[86] P. Bunin,[86] M. Gavrilenko,[86] I. Golutvin,[86] A. Kamenev,[86] V. Karjavin,[86] G. Kozlov,[86] A. Lanev,[86] A. Malakhov,[86] P. Moisenz,[86] V. Palichik,[86] V. Perelygin,[86] S. Shmatov,[86] V. Smirnov,[86] A. Volodko,[86] A. Zarubin,[86] S. Evstyukhin,[87] V. Golovtsov,[87] Y. Ivanov,[87] V. Kim,[87] P. Levchenko,[87] V. Murzin,[87] V. Oreshkin,[87] I. Smirnov,[87] V. Sulimov,[87] L. Uvarov,[87] S. Vavilov,[87] A. Vorobyev,[87] An. Vorobyev,[87] Yu. Andreev,[88] A. Dermenev,[88] S. Gninenko,[88] N. Golubev,[88] M. Kirsanov,[88] N. Krasnikov,[88] V. Matveev,[88] A. Pashenkov,[88] D. Tlisov,[88] A. Toropin,[88] V. Epshteyn,[89] M. Erofeeva,[89] V. Gavrilov,[89] M. Kossov,[89,a] N. Lychkovskaya,[89] V. Popov,[89] G. Safronov,[89] S. Semenov,[89] V. Stolin,[89] E. Vlasov,[89] A. Zhokin,[89] A. Belyaev,[90] E. Boos,[90] A. Ershov,[90] A. Gribushin,[90] V. Klyukhin,[90] O. Kodolova,[90] V. Korotkikh,[90] I. Lokhtin,[90] A. Markina,[90] S. Obraztsov,[90] M. Perfilov,[90] S. Petrushanko,[90] L. Sarycheva,[90,b] V. Savrin,[90] A. Snigirev,[90] I. Vardanyan,[90] V. Andreev,[91] M. Azarkin,[91] I. Dremin,[91] M. Kirakosyan,[91] A. Leonidov,[91] G. Mesyats,[91] S. V. Rusakov,[91] A. Vinogradov,[91] I. Azhgirey,[92] I. Bayshev,[92] S. Bitioukov,[92] V. Grishin,[92,a] V. Kachanov,[92] D. Konstantinov,[92] A. Korablev,[92] V. Krychkine,[92] V. Petrov,[92] R. Ryutin,[92] A. Sobol,[92] L. Tourtchanovitch,[92] S. Troshin,[92] N. Tyurin,[92] A. Uzunian,[92] A. Volkov,[92] P. Adzic,[93,cc] M. Djordjevic,[93] M. Ekmedzic,[93] D. Krpic,[93,cc] J. Milosevic,[93] M. Aguilar-Benitez,[94] J. Alcaraz Maestre,[94] P. Arce,[94] C. Battilana,[94] E. Calvo,[94] M. Cerrada,[94] M. Chamizo Llatas,[94] N. Colino,[94] B. De La Cruz,[94] A. Delgado Peris,[94] C. Diez Pardos,[94] D. Domínguez Vázquez,[94] C. Fernandez Bedoya,[94] J. P. Fernández Ramos,[94] A. Ferrando,[94] J. Flix,[94] M. C. Fouz,[94] P. Garcia-Abia,[94] O. Gonzalez Lopez,[94] S. Goy Lopez,[94] J. M. Hernandez,[94] M. I. Josa,[94] G. Merino,[94] J. Puerta Pelayo,[94] I. Redondo,[94] L. Romero,[94] J. Santaolalla,[94] M. S. Soares,[94] C. Willmott,[94] C. Albajar,[95] G. Codispoti,[95] J. F. de Trocóniz,[95] J. Cuevas,[96] J. Fernandez Menendez,[96] S. Folgueras,[96] I. Gonzalez Caballero,[96] L. Lloret Iglesias,[96] J. Piedra Gomez,[96,dd] J. M. Vizan Garcia,[96] J. A. Brochero Cifuentes,[97] I. J. Cabrillo,[97] A. Calderon,[97] S. H. Chuang,[97] J. Duarte Campderros,[97] M. Felcini,[97,ee] M. Fernandez,[97] G. Gomez,[97] J. Gonzalez Sanchez,[97] C. Jorda,[97] P. Lobelle Pardo,[97] A. Lopez Virto,[97] J. Marco,[97] R. Marco,[97] C. Martinez Rivero,[97] F. Matorras,[97] F.J. Munoz Sanchez,[97]

T. Rodrigo,[97] A. Y. Rodríguez-Marrero,[97] A. Ruiz-Jimeno,[97] L. Scodellaro,[97] M. Sobron Sanudo,[97] I. Vila,[97] R. Vilar Cortabitarte,[97] D. Abbaneo,[98] E. Auffray,[98] G. Auzinger,[98] P. Baillon,[98] A. H. Ball,[98] D. Barney,[98] C. Bernet,[98,f] G. Bianchi,[98] P. Bloch,[98] A. Bocci,[98] A. Bonato,[98] H. Breuker,[98] T. Camporesi,[98] G. Cerminara,[98] T. Christiansen,[98] J. A. Coarasa Perez,[98] D. D'Enterria,[98] A. De Roeck,[98] S. Di Guida,[98] M. Dobson,[98] N. Dupont-Sagorin,[98] A. Elliott-Peisert,[98] B. Frisch,[98] W. Funk,[98] G. Georgiou,[98] M. Giffels,[98] D. Gigi,[98] K. Gill,[98] D. Giordano,[98] M. Giunta,[98] F. Glege,[98] R. Gomez-Reino Garrido,[98] P. Govoni,[98] S. Gowdy,[98] R. Guida,[98] M. Hansen,[98] P. Harris,[98] C. Hartl,[98] J. Harvey,[98] B. Hegner,[98] A. Hinzmann,[98] V. Innocente,[98] P. Janot,[98] K. Kaadze,[98] E. Karavakis,[98] K. Kousouris,[98] P. Lecoq,[98] P. Lenzi,[98] C. Lourenço,[98] T. Mäki,[98] M. Malberti,[98] L. Malgeri,[98] M. Mannelli,[98] L. Masetti,[98] F. Meijers,[98] S. Mersi,[98] E. Meschi,[98] R. Moser,[98] M. U. Mozer,[98] M. Mulders,[98] E. Nesvold,[98] M. Nguyen,[98] T. Orimoto,[98] L. Orsini,[98] E. Palencia Cortezon,[98] E. Perez,[98] A. Petrilli,[98] A. Pfeiffer,[98] M. Pierini,[98] M. Pimiä,[98] D. Piparo,[98] G. Polese,[98] L. Quertenmont,[98] A. Racz,[98] W. Reece,[98] J. Rodrigues Antunes,[98] G. Rolandi,[98,ff] T. Rommerskirchen,[98] C. Rovelli,[98,gg] M. Rovere,[98] H. Sakulin,[98] F. Santanastasio,[98] C. Schäfer,[98] C. Schwick,[98] I. Segoni,[98] S. Sekmen,[98] A. Sharma,[98] P. Siegrist,[98] P. Silva,[98] M. Simon,[98] P. Sphicas,[98,hh] D. Spiga,[98] M. Spiropulu,[98,e] M. Stoye,[98] A. Tsirou,[98] G. I. Veres,[98,p] J. R. Vlimant,[98] H. K. Wöhri,[98] S. D. Worm,[98,ii] W. D. Zeuner,[98] W. Bertl,[99] K. Deiters,[99] W. Erdmann,[99] K. Gabathuler,[99] R. Horisberger,[99] Q. Ingram,[99] H. C. Kaestli,[99] S. König,[99] D. Kotlinski,[99] U. Langenegger,[99] F. Meier,[99] D. Renker,[99] T. Rohe,[99] J. Sibille,[99,jj] L. Bäni,[100] P. Bortignon,[100] M. A. Buchmann,[100] B. Casal,[100] N. Chanon,[100] Z. Chen,[100] A. Deisher,[100] G. Dissertori,[100] M. Dittmar,[100] M. Dünser,[100] J. Eugster,[100] K. Freudenreich,[100] C. Grab,[100] P. Lecomte,[100] W. Lustermann,[100] A. C. Marini,[100] P. Martinez Ruiz del Arbol,[100] N. Mohr,[100] F. Moortgat,[100] C. Nägeli,[100,kk] P. Nef,[100] F. Nessi-Tedaldi,[100] L. Pape,[100] F. Pauss,[100] M. Peruzzi,[100] F. J. Ronga,[100] M. Rossini,[100] L. Sala,[100] A. K. Sanchez,[100] A. Starodumov,[100,ll] B. Stieger,[100] M. Takahashi,[100] L. Tauscher,[100,b] A. Thea,[100] K. Theofilatos,[100] D. Treille,[100] C. Urscheler,[100] R. Wallny,[100] H. A. Weber,[100] L. Wehrli,[100] E. Aguilo,[101] C. Amsler,[101] V. Chiochia,[101] S. De Visscher,[101] C. Favaro,[101] M. Ivova Rikova,[101] B. Millan Mejias,[101] P. Otiougova,[101] P. Robmann,[101] H. Snoek,[101] S. Tupputi,[101] M. Verzetti,[101] Y. H. Chang,[102] K. H. Chen,[102] A. Go,[102] C. M. Kuo,[102] S. W. Li,[102] W. Lin,[102] Z. K. Liu,[102] Y. J. Lu,[102] D. Mekterovic,[102] A. P. Singh,[102] R. Volpe,[102] S. S. Yu,[102] P. Bartalini,[103] P. Chang,[103] Y. H. Chang,[103] Y. W. Chang,[103] Y. Chao,[103] K. F. Chen,[103] C. Dietz,[103] U. Grundler,[103] W.-S. Hou,[103] Y. Hsiung,[103] K. Y. Kao,[103] Y. J. Lei,[103] R.-S. Lu,[103] D. Majumder,[103] E. Petrakou,[103] X. Shi,[103] J. G. Shiu,[103] Y. M. Tzeng,[103] M. Wang,[103] A. Adiguzel,[104] M. N. Bakirci,[104,mm] S. Cerci,[104,nn] C. Dozen,[104] I. Dumanoglu,[104] E. Eskut,[104] S. Girgis,[104] G. Gokbulut,[104] I. Hos,[104] E. E. Kangal,[104] G. Karapinar,[104] A. Kayis Topaksu,[104] G. Onengut,[104] K. Ozdemir,[104] S. Ozturk,[104,oo] A. Polatoz,[104] K. Sogut,[104,pp] D. Sunar Cerci,[104,nn] B. Tali,[104,nn] H. Topakli,[104,mm] L. N. Vergili,[104] M. Vergili,[104] I. V. Akin,[105] T. Aliev,[105] B. Bilin,[105] S. Bilmis,[105] M. Deniz,[105] H. Gamsizkan,[105] A. M. Guler,[105] K. Ocalan,[105] A. Ozpineci,[105] M. Serin,[105] R. Sever,[105] U. E. Surat,[105] M. Yalvac,[105] E. Yildirim,[105] M. Zeyrek,[105] M. Deliomeroglu,[106] E. Gülmez,[106] B. Isildak,[106] M. Kaya,[106,qq] O. Kaya,[106,qq] S. Ozkorucuklu,[106,rr] N. Sonmez,[106,ss] K. Cankocak,[107] L. Levchuk,[108] F. Bostock,[109] J. J. Brooke,[109] E. Clement,[109] D. Cussans,[109] H. Flacher,[109] R. Frazier,[109] J. Goldstein,[109] M. Grimes,[109] G. P. Heath,[109] H. F. Heath,[109] L. Kreczko,[109] S. Metson,[109] D. M. Newbold,[109,ii] K. Nirunpong,[109] A. Poll,[109] S. Senkin,[109] V. J. Smith,[109] T. Williams,[109] L. Basso,[110,tt] A. Belyaev,[110,tt] C. Brew,[110] R. M. Brown,[110] D. J. A. Cockerill,[110] J. A. Coughlan,[110] K. Harder,[110] S. Harper,[110] J. Jackson,[110] B. W. Kennedy,[110] E. Olaiya,[110] D. Petyt,[110] B. C. Radburn-Smith,[110] C. H. Shepherd-Themistocleous,[110] I. R. Tomalin,[110] W. J. Womersley,[110] R. Bainbridge,[111] G. Ball,[111] R. Beuselinck,[111] O. Buchmuller,[111] D. Colling,[111] N. Cripps,[111] M. Cutajar,[111] P. Dauncey,[111] G. Davies,[111] M. Della Negra,[111] W. Ferguson,[111] J. Fulcher,[111] D. Futyan,[111] A. Gilbert,[111] A. Guneratne Bryer,[111] G. Hall,[111] Z. Hatherell,[111] J. Hays,[111] G. Iles,[111] M. Jarvis,[111] G. Karapostoli,[111] L. Lyons,[111] A.-M. Magnan,[111] J. Marrouche,[111] B. Mathias,[111] R. Nandi,[111] J. Nash,[111] A. Nikitenko,[111,ll] A. Papageorgiou,[111] J. Pela,[111,a] M. Pesaresi,[111] K. Petridis,[111] M. Pioppi,[111,uu] D. M. Raymond,[111] S. Rogerson,[111] N. Rompotis,[111] A. Rose,[111] M. J. Ryan,[111] C. Seez,[111] P. Sharp,[111,b] A. Sparrow,[111] A. Tapper,[111] M. Vazquez Acosta,[111] T. Virdee,[111] S. Wakefield,[111] N. Wardle,[111] T. Whyntie,[111] M. Barrett,[112] M. Chadwick,[112] J. E. Cole,[112] P. R. Hobson,[112] A. Khan,[112] P. Kyberd,[112] D. Leggat,[112] D. Leslie,[112] W. Martin,[112] I. D. Reid,[112] P. Symonds,[112] L. Teodorescu,[112] M. Turner,[112] K. Hatakeyama,[113] H. Liu,[113] T. Scarborough,[113] C. Henderson,[114] P. Rumerio,[114] A. Avetisyan,[115] T. Bose,[115] C. Fantasia,[115] A. Heister,[115] J. St. John,[115] P. Lawson,[115] D. Lazic,[115] J. Rohlf,[115] D. Sperka,[115] L. Sulak,[115] J. Alimena,[116] S. Bhattacharya,[116] D. Cutts,[116] A. Ferapontov,[116] U. Heintz,[116] S. Jabeen,[116] G. Kukartsev,[116] G. Landsberg,[116] M. Luk,[116] M. Narain,[116] D. Nguyen,[116] M. Segala,[116] T. Sinthuprasith,[116] T. Speer,[116] K. V. Tsang,[116] R. Breedon,[117] G. Breto,[117] M. Calderon De La Barca Sanchez,[117] S. Chauhan,[117] M. Chertok,[117] J. Conway,[117] R. Conway,[117] P. T. Cox,[117] J. Dolen,[117] R. Erbacher,[117] M. Gardner,[117] R. Houtz,[117] W. Ko,[117] A. Kopecky,[117] R. Lander,[117] O. Mall,[117] T. Miceli,[117] R. Nelson,[117] D. Pellett,[117] B. Rutherford,[117] M. Searle,[117] J. Smith,[117] M. Squires,[117] M. Tripathi,[117] R. Vasquez Sierra,[117] V. Andreev,[118] D. Cline,[118] R. Cousins,[118] J. Duris,[118] S. Erhan,[118] P. Everaerts,[118] C. Farrell,[118] J. Hauser,[118] M. Ignatenko,[118] C. Plager,[118] G. Rakness,[118] P. Schlein,[118,b] J. Tucker,[118] V. Valuev,[118] M. Weber,[118] J. Babb,[119] R. Clare,[119] M. E. Dinardo,[119] J. Ellison,[119] J. W. Gary,[119] F. Giordano,[119] G. Hanson,[119] G. Y. Jeng,[119,vv] H. Liu,[119] O. R. Long,[119] A. Luthra,[119] H. Nguyen,[119] S. Paramesvaran,[119] J. Sturdy,[119] S. Sumowidagdo,[119] R. Wilken,[119] S. Wimpenny,[119] W. Andrews,[120] J. G. Branson,[120] G. B. Cerati,[120] S. Cittolin,[120] D. Evans,[120] F. Golf,[120] A. Holzner,[120] R. Kelley,[120] M. Lebourgeois,[120] J. Letts,[120] I. Macneill,[120] B. Mangano,[120] J. Muelmenstaedt,[120] S. Padhi,[120] C. Palmer,[120] G. Petrucciani,[120] M. Pieri,[120] R. Ranieri,[120] M. Sani,[120] V. Sharma,[120] S. Simon,[120] E. Sudano,[120] M. Tadel,[120] Y. Tu,[120] A. Vartak,[120] S. Wasserbaech,[120,ww] F. Würthwein,[120] A. Yagil,[120] J. Yoo,[120] D. Barge,[121] R. Bellan,[121] C. Campagnari,[121] M. D'Alfonso,[121] T. Danielson,[121] K. Flowers,[121] P. Geffert,[121] J. Incandela,[121]

C. Justus,[121] P. Kalavase,[121] S. A. Koay,[121] D. Kovalskyi,[121,a] V. Krutelyov,[121] S. Lowette,[121] N. Mccoll,[121] V. Pavlunin,[121] F. Rebassoo,[121] J. Ribnik,[121] J. Richman,[121] R. Rossin,[121] D. Stuart,[121] W. To,[121] C. West,[121] A. Apresyan,[122] A. Bornheim,[122] Y. Chen,[122] E. Di Marco,[122] J. Duarte,[122] M. Gataullin,[122] Y. Ma,[122] A. Mott,[122] H. B. Newman,[122] C. Rogan,[122] V. Timciuc,[122] P. Traczyk,[122] J. Veverka,[122] R. Wilkinson,[122] Y. Yang,[122] R. Y. Zhu,[122] B. Akgun,[123] R. Carroll,[123] T. Ferguson,[123] Y. Iiyama,[123] D. W. Jang,[123] Y. F. Liu,[123] M. Paulini,[123] H. Vogel,[123] I. Vorobiev,[123] J. P. Cumalat,[124] B. R. Drell,[124] C. J. Edelmaier,[124] W. T. Ford,[124] A. Gaz,[124] B. Heyburn,[124] E. Luiggi Lopez,[124] J. G. Smith,[124] K. Stenson,[124] K. A. Ulmer,[124] S. R. Wagner,[124] L. Agostino,[125] J. Alexander,[125] A. Chatterjee,[125] N. Eggert,[125] L. K. Gibbons,[125] B. Heltsley,[125] W. Hopkins,[125] A. Khukhunaishvili,[125] B. Kreis,[125] N. Mirman,[125] G. Nicolas Kaufman,[125] J. R. Patterson,[125] A. Ryd,[125] E. Salvati,[125] W. Sun,[125] W. D. Teo,[125] J. Thom,[125] J. Thompson,[125] J. Vaughan,[125] Y. Weng,[125] L. Winstrom,[125] P. Wittich,[125] D. Winn,[126] S. Abdullin,[127] M. Albrow,[127] J. Anderson,[127] L. A. T. Bauerdick,[127] A. Beretvas,[127] J. Berryhill,[127] P. C. Bhat,[127] I. Bloch,[127] K. Burkett,[127] J. N. Butler,[127] V. Chetluru,[127] H. W. K. Cheung,[127] F. Chlebana,[127] V. D. Elvira,[127] I. Fisk,[127] J. Freeman,[127] Y. Gao,[127] D. Green,[127] O. Gutsche,[127] A. Hahn,[127] J. Hanlon,[127] R. M. Harris,[127] J. Hirschauer,[127] B. Hooberman,[127] S. Jindariani,[127] M. Johnson,[127] U. Joshi,[127] B. Kilminster,[127] B. Klima,[127] S. Kunori,[127] S. Kwan,[127] D. Lincoln,[127] R. Lipton,[127] L. Lueking,[127] J. Lykken,[127] K. Maeshima,[127] J. M. Marraffino,[127] S. Maruyama,[127] D. Mason,[127] P. McBride,[127] K. Mishra,[127] S. Mrenna,[127] Y. Musienko,[127,xx] C. Newman-Holmes,[127] V. O'Dell,[127] O. Prokofyev,[127] E. Sexton-Kennedy,[127] S. Sharma,[127] W. J. Spalding,[127] L. Spiegel,[127] P. Tan,[127] L. Taylor,[127] S. Tkaczyk,[127] N. V. Tran,[127] L. Uplegger,[127] E. W. Vaandering,[127] R. Vidal,[127] J. Whitmore,[127] W. Wu,[127] F. Yang,[127] F. Yumiceva,[127] J. C. Yun,[127] D. Acosta,[128] P. Avery,[128] D. Bourilkov,[128] M. Chen,[128] S. Das,[128] M. De Gruttola,[128] G. P. Di Giovanni,[128] D. Dobur,[128] A. Drozdetskiy,[128] R. D. Field,[128] M. Fisher,[128] Y. Fu,[128] I. K. Furic,[128] J. Gartner,[128] J. Hugon,[128] B. Kim,[128] J. Konigsberg,[128] A. Korytov,[128] A. Kropivnitskaya,[128] T. Kypreos,[128] J. F. Low,[128] K. Matchev,[128] P. Milenovic,[128,yy] G. Mitselmakher,[128] L. Muniz,[128] R. Remington,[128] A. Rinkevicius,[128] P. Sellers,[128] N. Skhirtladze,[128] M. Snowball,[128] J. Yelton,[128] M. Zakaria,[128] V. Gaultney,[129] L. M. Lebolo,[129] S. Linn,[129] P. Markowitz,[129] G. Martinez,[129] J. L. Rodriguez,[129] T. Adams,[130] A. Askew,[130] J. Bochenek,[130] J. Chen,[130] B. Diamond,[130] S. V. Gleyzer,[130] J. Haas,[130] S. Hagopian,[130] V. Hagopian,[130] M. Jenkins,[130] K. F. Johnson,[130] H. Prosper,[130] V. Veeraraghavan,[130] M. Weinberg,[130] M. M. Baarmand,[131] B. Dorney,[131] M. Hohlmann,[131] H. Kalakhety,[131] I. Vodopiyanov,[131] M. R. Adams,[132] I. M. Anghel,[132] L. Apanasevich,[132] Y. Bai,[132] V. E. Bazterra,[132] R. R. Betts,[132] J. Callner,[132] R. Cavanaugh,[132] C. Dragoiu,[132] O. Evdokimov,[132] E. J. Garcia-Solis,[132] L. Gauthier,[132] C. E. Gerber,[132] D. J. Hofman,[132] S. Khalatyan,[132] F. Lacroix,[132] M. Malek,[132] C. O'Brien,[132] C. Silkworth,[132] D. Strom,[132] N. Varelas,[132] U. Akgun,[133] E. A. Albayrak,[133] B. Bilki,[133,zz] K. Chung,[133] W. Clarida,[133] F. Duru,[133] S. Griffiths,[133] C. K. Lae,[133] J.-P. Merlo,[133] H. Mermerkaya,[133,aaa] A. Mestvirishvili,[133] A. Moeller,[133] J. Nachtman,[133] C. R. Newsom,[133] E. Norbeck,[133] J. Olson,[133] Y. Onel,[133] F. Ozok,[133] S. Sen,[133] E. Tiras,[133] J. Wetzel,[133] T. Yetkin,[133] K. Yi,[133] B. A. Barnett,[134] B. Blumenfeld,[134] S. Bolognesi,[134] D. Fehling,[134] G. Giurgiu,[134] A. V. Gritsan,[134] Z. J. Guo,[134] G. Hu,[134] P. Maksimovic,[134] S. Rappoccio,[134] M. Swartz,[134] A. Whitbeck,[134] P. Baringer,[135] A. Bean,[135] G. Benelli,[135] O. Grachov,[135] R. P. Kenny Iii,[135] M. Murray,[135] D. Noonan,[135] V. Radicci,[135] S. Sanders,[135] R. Stringer,[135] G. Tinti,[135] J. S. Wood,[135] V. Zhukova,[135] A. F. Barfuss,[136] T. Bolton,[136] I. Chakaberia,[136] A. Ivanov,[136] S. Khalil,[136] M. Makouski,[136] Y. Maravin,[136] S. Shrestha,[136] I. Svintradze,[136] J. Gronberg,[137] D. Lange,[137] D. Wright,[137] A. Baden,[138] M. Boutemeur,[138] B. Calvert,[138] S. C. Eno,[138] J. A. Gomez,[138] N. J. Hadley,[138] R. G. Kellogg,[138] M. Kirn,[138] T. Kolberg,[138] Y. Lu,[138] M. Marionneau,[138] A. C. Mignerey,[138] A. Peterman,[138] K. Rossato,[138] A. Skuja,[138] J. Temple,[138] M. B. Tonjes,[138] S. C. Tonwar,[138] E. Twedt,[138] G. Bauer,[139] J. Bendavid,[139] W. Busza,[139] E. Butz,[139] I. A. Cali,[139] M. Chan,[139] V. Dutta,[139] G. Gomez Ceballos,[139] M. Goncharov,[139] K. A. Hahn,[139] Y. Kim,[139] M. Klute,[139] Y.-J. Lee,[139] W. Li,[139] P. D. Luckey,[139] T. Ma,[139] S. Nahn,[139] C. Paus,[139] D. Ralph,[139] C. Roland,[139] G. Roland,[139] M. Rudolph,[139] G. S. F. Stephans,[139] F. Stöckli,[139] K. Sumorok,[139] K. Sung,[139] D. Velicanu,[139] E. A. Wenger,[139] R. Wolf,[139] B. Wyslouch,[139] S. Xie,[139] M. Yang,[139] Y. Yilmaz,[139] A. S. Yoon,[139] M. Zanetti,[139] S. I. Cooper,[140] P. Cushman,[140] B. Dahmes,[140] A. De Benedetti,[140] G. Franzoni,[140] A. Gude,[140] J. Haupt,[140] S. C. Kao,[140] K. Klapoetke,[140] Y. Kubota,[140] J. Mans,[140] N. Pastika,[140] R. Rusack,[140] M. Sasseville,[140] A. Singovsky,[140] N. Tambe,[140] J. Turkewitz,[140] L. M. Cremaldi,[141] R. Kroeger,[141] L. Perera,[141] R. Rahmat,[141] D. A. Sanders,[141] E. Avdeeva,[142] K. Bloom,[142] S. Bose,[142] J. Butt,[142] D. R. Claes,[142] A. Dominguez,[142] M. Eads,[142] P. Jindal,[142] J. Keller,[142] I. Kravchenko,[142] J. Lazo-Flores,[142] H. Malbouisson,[142] S. Malik,[142] G. R. Snow,[142] U. Baur,[143] A. Godshalk,[143] I. Iashvili,[143] S. Jain,[143] A. Kharchilava,[143] A. Kumar,[143] S. P. Shipkowski,[143] K. Smith,[143] G. Alverson,[144] E. Barberis,[144] D. Baumgartel,[144] M. Chasco,[144] J. Haley,[144] D. Trocino,[144] D. Wood,[144] J. Zhang,[144] A. Anastassov,[145] A. Kubik,[145] N. Mucia,[145] N. Odell,[145] R. A. Ofierzynski,[145] B. Pollack,[145] A. Pozdnyakov,[145] M. Schmitt,[145] S. Stoynev,[145] M. Velasco,[145] S. Won,[145] L. Antonelli,[146] D. Berry,[146] A. Brinkerhoff,[146] M. Hildreth,[146] C. Jessop,[146] D. J. Karmgard,[146] J. Kolb,[146] K. Lannon,[146] W. Luo,[146] S. Lynch,[146] N. Marinelli,[146] D. M. Morse,[146] T. Pearson,[146] R. Ruchti,[146] J. Slaunwhite,[146] N. Valls,[146] J. Warchol,[146] M. Wayne,[146] M. Wolf,[146] J. Ziegler,[146] B. Bylsma,[147] L. S. Durkin,[147] C. Hill,[147] R. Hughes,[147] P. Killewald,[147] K. Kotov,[147] T. Y. Ling,[147] D. Puigh,[147] M. Rodenburg,[147] C. Vuosalo,[147] G. Williams,[147] B. L. Winer,[147] N. Adam,[148] E. Berry,[148] P. Elmer,[148] D. Gerbaudo,[148] V. Halyo,[148] P. Hebda,[148] J. Hegeman,[148] A. Hunt,[148] E. Laird,[148] D. Lopes Pegna,[148] P. Lujan,[148] D. Marlow,[148] T. Medvedeva,[148] M. Mooney,[148] J. Olsen,[148] P. Piroué,[148] X. Quan,[148] A. Raval,[148] H. Saka,[148] D. Stickland,[148] C. Tully,[148] J. S. Werner,[148] A. Zuranski,[148] J. G. Acosta,[149] X. T. Huang,[149] A. Lopez,[149] H. Mendez,[149] S. Oliveros,[149] J. E. Ramirez Vargas,[149] A. Zatserklyaniy,[149] E. Alagoz,[150] V. E. Barnes,[150] D. Benedetti,[150] G. Bolla,[150] D. Bortoletto,[150] M. De Mattia,[150] A. Everett,[150] Z. Hu,[150] M. Jones,[150] O. Koybasi,[150] M. Kress,[150] A. T. Laasanen,[150] N. Leonardo,[150]

V. Maroussov,[150] P. Merkel,[150] D. H. Miller,[150] N. Neumeister,[150] I. Shipsey,[150] D. Silvers,[150] A. Svyatkovskiy,[150] M. Vidal Marono,[150] H. D. Yoo,[150] J. Zablocki,[150] Y. Zheng,[150] S. Guragain,[151] N. Parashar,[151] A. Adair,[152] C. Boulahouache,[152] V. Cuplov,[152] K. M. Ecklund,[152] F. J. M. Geurts,[152] B. P. Padley,[152] R. Redjimi,[152] J. Roberts,[152] J. Zabel,[152] B. Betchart,[153] A. Bodek,[153] Y. S. Chung,[153] R. Covarelli,[153] P. de Barbaro,[153] R. Demina,[153] Y. Eshaq,[153] A. Garcia-Bellido,[153] P. Goldenzweig,[153] Y. Gotra,[153] J. Han,[153] A. Harel,[153] S. Korjenevski,[153] D. C. Miner,[153] D. Vishnevskiy,[153] M. Zielinski,[153] A. Bhatti,[154] R. Ciesielski,[154] L. Demortier,[154] K. Goulianos,[154] G. Lungu,[154] S. Malik,[154] C. Mesropian,[154] S. Arora,[155] A. Barker,[155] J. P. Chou,[155] C. Contreras-Campana,[155] E. Contreras-Campana,[155] D. Duggan,[155] D. Ferencek,[155] Y. Gershtein,[155] R. Gray,[155] E. Halkiadakis,[155] D. Hidas,[155] D. Hits,[155] A. Lath,[155] S. Panwalkar,[155] M. Park,[155] R. Patel,[155] V. Rekovic,[155] A. Richards,[155] J. Robles,[155] K. Rose,[155] S. Salur,[155] S. Schnetzer,[155] C. Seitz,[155] S. Somalwar,[155] R. Stone,[155] S. Thomas,[155] G. Cerizza,[156] M. Hollingsworth,[156] S. Spanier,[156] Z. C. Yang,[156] A. York,[156] R. Eusebi,[157] W. Flanagan,[157] J. Gilmore,[157] T. Kamon,[157,bbb] V. Khotilovich,[157] R. Montalvo,[157] I. Osipenkov,[157] Y. Pakhotin,[157] A. Perloff,[157] J. Roe,[157] A. Safonov,[157] T. Sakuma,[157] S. Sengupta,[157] I. Suarez,[157] A. Tatarinov,[157] D. Toback,[157] N. Akchurin,[158] J. Damgov,[158] P. R. Dudero,[158] C. Jeong,[158] K. Kovitanggoon,[158] S. W. Lee,[158] T. Libeiro,[158] Y. Roh,[158] I. Volobouev,[158] E. Appelt,[159] D. Engh,[159] C. Florez,[159] S. Greene,[159] A. Gurrola,[159] W. Johns,[159] P. Kurt,[159] C. Maguire,[159] A. Melo,[159] P. Sheldon,[159] B. Snook,[159] S. Tuo,[159] J. Velkovska,[159] M. W. Arenton,[160] M. Balazs,[160] S. Boutle,[160] B. Cox,[160] B. Francis,[160] J. Goodell,[160] R. Hirosky,[160] A. Ledovskoy,[160] C. Lin,[160] C. Neu,[160] J. Wood,[160] R. Yohay,[160] S. Gollapinni,[161] R. Harr,[161] P. E. Karchin,[161] C. Kottachchi Kankanamge Don,[161] P. Lamichhane,[161] A. Sakharov,[161] M. Anderson,[162] M. Bachtis,[162] D. Belknap,[162] L. Borrello,[162] D. Carlsmith,[162] M. Cepeda,[162] S. Dasu,[162] L. Gray,[162] K. S. Grogg,[162] M. Grothe,[162] R. Hall-Wilton,[162] M. Herndon,[162] A. Hervé,[162] P. Klabbers,[162] J. Klukas,[162] A. Lanaro,[162] C. Lazaridis,[162] J. Leonard,[162] R. Loveless,[162] A. Mohapatra,[162] I. Ojalvo,[162] G. A. Pierro,[162] I. Ross,[162] A. Savin,[162] W. H. Smith,[162] and J. Swanson[162]

(CMS Collaboration)

[1]*Yerevan Physics Institute, Yerevan, Armenia*
[2]*Institut für Hochenergiephysik der OeAW, Wien, Austria*
[3]*National Centre for Particle and High Energy Physics, Minsk, Belarus*
[4]*Universiteit Antwerpen, Antwerpen, Belgium*
[5]*Vrije Universiteit Brussel, Brussel, Belgium*
[6]*Université Libre de Bruxelles, Bruxelles, Belgium*
[7]*Ghent University, Ghent, Belgium*
[8]*Université Catholique de Louvain, Louvain-la-Neuve, Belgium*
[9]*Université de Mons, Mons, Belgium*
[10]*Centro Brasileiro de Pesquisas Fisicas, Rio de Janeiro, Brazil*
[11]*Universidade do Estado do Rio de Janeiro, Rio de Janeiro, Brazil*
[12]*Instituto de Fisica Teorica, Universidade Estadual Paulista, Sao Paulo, Brazil*
[13]*Institute for Nuclear Research and Nuclear Energy, Sofia, Bulgaria*
[14]*University of Sofia, Sofia, Bulgaria*
[15]*Institute of High Energy Physics, Beijing, China*
[16]*State Key Lab. of Nucl. Phys. and Tech., Peking University, Beijing, China*
[17]*Universidad de Los Andes, Bogota, Colombia*
[18]*Technical University of Split, Split, Croatia*
[19]*University of Split, Split, Croatia*
[20]*Institute Rudjer Boskovic, Zagreb, Croatia*
[21]*University of Cyprus, Nicosia, Cyprus*
[22]*Charles University, Prague, Czech Republic*
[23]*Academy of Scientific Research and Technology of the Arab Republic of Egypt, Egyptian Network of High Energy Physics, Cairo, Egypt*
[24]*National Institute of Chemical Physics and Biophysics, Tallinn, Estonia*
[25]*Department of Physics, University of Helsinki, Helsinki, Finland*
[26]*Helsinki Institute of Physics, Helsinki, Finland*
[27]*Lappeenranta University of Technology, Lappeenranta, Finland*
[28]*DSM/IRFU, CEA/Saclay, Gif-sur-Yvette, France*
[29]*Laboratoire Leprince-Ringuet, Ecole Polytechnique, IN2P3-CNRS, Palaiseau, France*
[30]*Institut Pluridisciplinaire Hubert Curien, Université de Strasbourg, Université de Haute Alsace Mulhouse, CNRS/IN2P3, Strasbourg, France*
[31]*Centre de Calcul de l'Institut National de Physique Nucleaire et de Physique des Particules (IN2P3), Villeurbanne, France*
[32]*Université de Lyon, Université Claude Bernard Lyon 1, CNRS-IN2P3, Institut de Physique Nucléaire de Lyon, Villeurbanne, France*
[33]*Institute of High Energy Physics and Informatization, Tbilisi State University, Tbilisi, Georgia*
[34]*RWTH Aachen University, I. Physikalisches Institut, Aachen, Germany*
[35]*RWTH Aachen University, III. Physikalisches Institut A, Aachen, Germany*

[36]*RWTH Aachen University, III. Physikalisches Institut B, Aachen, Germany*
[37]*Deutsches Elektronen-Synchrotron, Hamburg, Germany*
[38]*University of Hamburg, Hamburg, Germany*
[39]*Institut für Experimentelle Kernphysik, Karlsruhe, Germany*
[40]*Institute of Nuclear Physics "Demokritos", Aghia Paraskevi, Greece*
[41]*University of Athens, Athens, Greece*
[42]*University of Ioánnina, Ioánnina, Greece*
[43]*KFKI Research Institute for Particle and Nuclear Physics, Budapest, Hungary*
[44]*Institute of Nuclear Research ATOMKI, Debrecen, Hungary*
[45]*University of Debrecen, Debrecen, Hungary*
[46]*Panjab University, Chandigarh, India*
[47]*University of Delhi, Delhi, India*
[48]*Saha Institute of Nuclear Physics, Kolkata, India*
[49]*Bhabha Atomic Research Centre, Mumbai, India*
[50]*Tata Institute of Fundamental Research - EHEP, Mumbai, India*
[51]*Tata Institute of Fundamental Research - HECR, Mumbai, India*
[52]*Institute for Research in Fundamental Sciences (IPM), Tehran, Iran*
[53a]*INFN Sezione di Bari, Bari, Italy*
[53b]*Università di Bari, Bari, Italy*
[53c]*Politecnico di Bari, Bari, Italy*
[54a]*INFN Sezione di Bologna, Bologna, Italy*
[54b]*Università di Bologna, Bologna, Italy*
[55a]*INFN Sezione di Catania, Catania, Italy*
[55b]*Università di Catania, Catania, Italy*
[56a]*INFN Sezione di Firenze, Firenze, Italy*
[56b]*Università di Firenze, Firenze, Italy*
[57]*INFN Laboratori Nazionali di Frascati, Frascati, Italy*
[58]*INFN Sezione di Genova, Genova, Italy*
[59a]*INFN Sezione di Milano-Bicocca, Milano, Italy*
[59b]*Università di Milano-Bicocca, Milano, Italy*
[60a]*INFN Sezione di Napoli, Napoli, Italy*
[60b]*Università di Napoli "Federico II", Napoli, Italy*
[61a]*INFN Sezione di Padova, Padova, Italy*
[61b]*Università di Padova, Padova, Italy*
[61c]*Università di Trento (Trento), Padova, Italy*
[62a]*INFN Sezione di Pavia, Pavia, Italy*
[62b]*Università di Pavia, Pavia, Italy*
[63a]*INFN Sezione di Perugia, Perugia, Italy*
[63b]*Università di Perugia, Perugia, Italy*
[64a]*INFN Sezione di Pisa, Pisa, Italy*
[64b]*Università di Pisa, Pisa, Italy*
[64c]*Scuola Normale Superiore di Pisa, Pisa, Italy*
[65a]*INFN Sezione di Roma, Roma, Italy*
[65b]*Università di Roma "La Sapienza", Roma, Italy*
[66a]*INFN Sezione di Torino, Torino, Italy*
[66b]*Università di Torino, Torino, Italy*
[66c]*Università del Piemonte Orientale (Novara), Torino, Italy*
[67a]*INFN Sezione di Trieste, Trieste, Italy*
[67b]*Università di Trieste, Trieste, Italy*
[68]*Kangwon National University, Chunchon, Korea*
[69]*Kyungpook National University, Daegu, Korea*
[70]*Chonnam National University, Institute for Universe and Elementary Particles, Kwangju, Korea*
[71]*Konkuk University, Seoul, Korea*
[72]*Korea University, Seoul, Korea*
[73]*University of Seoul, Seoul, Korea*
[74]*Sungkyunkwan University, Suwon, Korea*
[75]*Vilnius University, Vilnius, Lithuania*
[76]*Centro de Investigacion y de Estudios Avanzados del IPN, Mexico City, Mexico*

[77] *Universidad Iberoamericana, Mexico City, Mexico*
[78] *Benemerita Universidad Autonoma de Puebla, Puebla, Mexico*
[79] *Universidad Autónoma de San Luis Potosí, San Luis Potosí, Mexico*
[80] *University of Auckland, Auckland, New Zealand*
[81] *University of Canterbury, Christchurch, New Zealand*
[82] *National Centre for Physics, Quaid-I-Azam University, Islamabad, Pakistan*
[83] *Institute of Experimental Physics, Faculty of Physics, University of Warsaw, Warsaw, Poland*
[84] *Soltan Institute for Nuclear Studies, Warsaw, Poland*
[85] *Laboratório de Instrumentação e Física Experimental de Partículas, Lisboa, Portugal*
[86] *Joint Institute for Nuclear Research, Dubna, Russia*
[87] *Petersburg Nuclear Physics Institute, Gatchina (St Petersburg), Russia*
[88] *Institute for Nuclear Research, Moscow, Russia*
[89] *Institute for Theoretical and Experimental Physics, Moscow, Russia*
[90] *Moscow State University, Moscow, Russia*
[91] *P.N. Lebedev Physical Institute, Moscow, Russia*
[92] *State Research Center of Russian Federation, Institute for High Energy Physics, Protvino, Russia*
[93] *University of Belgrade, Faculty of Physics and Vinca Institute of Nuclear Sciences, Belgrade, Serbia*
[94] *Centro de Investigaciones Energéticas Medioambientales y Tecnológicas (CIEMAT), Madrid, Spain*
[95] *Universidad Autónoma de Madrid, Madrid, Spain*
[96] *Universidad de Oviedo, Oviedo, Spain*
[97] *Instituto de Física de Cantabria (IFCA), CSIC-Universidad de Cantabria, Santander, Spain*
[98] *CERN, European Organization for Nuclear Research, Geneva, Switzerland*
[99] *Paul Scherrer Institut, Villigen, Switzerland*
[100] *Institute for Particle Physics, ETH Zurich, Zurich, Switzerland*
[101] *Universität Zürich, Zurich, Switzerland*
[102] *National Central University, Chung-Li, Taiwan*
[103] *National Taiwan University (NTU), Taipei, Taiwan*
[104] *Cukurova University, Adana, Turkey*
[105] *Middle East Technical University, Physics Department, Ankara, Turkey*
[106] *Bogazici University, Istanbul, Turkey*
[107] *Istanbul Technical University, Istanbul, Turkey*
[108] *National Scientific Center, Kharkov Institute of Physics and Technology, Kharkov, Ukraine*
[109] *University of Bristol, Bristol, United Kingdom*
[110] *Rutherford Appleton Laboratory, Didcot, United Kingdom*
[111] *Imperial College, London, United Kingdom*
[112] *Brunel University, Uxbridge, United Kingdom*
[113] *Baylor University, Waco, USA*
[114] *The University of Alabama, Tuscaloosa, USA*
[115] *Boston University, Boston, USA*
[116] *Brown University, Providence, USA*
[117] *University of California, Davis, Davis, USA*
[118] *University of California, Los Angeles, Los Angeles, USA*
[119] *University of California, Riverside, Riverside, USA*
[120] *University of California, San Diego, La Jolla, USA*
[121] *University of California, Santa Barbara, Santa Barbara, USA*
[122] *California Institute of Technology, Pasadena, USA*
[123] *Carnegie Mellon University, Pittsburgh, USA*
[124] *University of Colorado at Boulder, Boulder, USA*
[125] *Cornell University, Ithaca, USA*
[126] *Fairfield University, Fairfield, USA*
[127] *Fermi National Accelerator Laboratory, Batavia, USA*
[128] *University of Florida, Gainesville, USA*
[129] *Florida International University, Miami, USA*
[130] *Florida State University, Tallahassee, USA*
[131] *Florida Institute of Technology, Melbourne, USA*
[132] *University of Illinois at Chicago (UIC), Chicago, USA*
[133] *The University of Iowa, Iowa City, USA*
[134] *Johns Hopkins University, Baltimore, USA*

[135]*The University of Kansas, Lawrence, USA*
[136]*Kansas State University, Manhattan, USA*
[137]*Lawrence Livermore National Laboratory, Livermore, USA*
[138]*University of Maryland, College Park, USA*
[139]*Massachusetts Institute of Technology, Cambridge, USA*
[140]*University of Minnesota, Minneapolis, USA*
[141]*University of Mississippi, University, USA*
[142]*University of Nebraska-Lincoln, Lincoln, USA*
[143]*State University of New York at Buffalo, Buffalo, USA*
[144]*Northeastern University, Boston, USA*
[145]*Northwestern University, Evanston, USA*
[146]*University of Notre Dame, Notre Dame, USA*
[147]*The Ohio State University, Columbus, USA*
[148]*Princeton University, Princeton, USA*
[149]*University of Puerto Rico, Mayaguez, USA*
[150]*Purdue University, West Lafayette, USA*
[151]*Purdue University Calumet, Hammond, USA*
[152]*Rice University, Houston, USA*
[153]*University of Rochester, Rochester, USA*
[154]*The Rockefeller University, New York, USA*
[155]*Rutgers, the State University of New Jersey, Piscataway, USA*
[156]*University of Tennessee, Knoxville, USA*
[157]*Texas A&M University, College Station, USA*
[158]*Texas Tech University, Lubbock, USA*
[159]*Vanderbilt University, Nashville, USA*
[160]*University of Virginia, Charlottesville, USA*
[161]*Wayne State University, Detroit, USA*
[162]*University of Wisconsin, Madison, USA*

[a]CERN, European Organization for Nuclear Research, Geneva, Switzerland
[b]Deceased
[c]National Institute of Chemical Physics and Biophysics, Tallinn, Estonia
[d]Universidade Federal do ABC, Santo Andre, Brazil
[e]California Institute of Technology, Pasadena, USA
[f]Laboratoire Leprince-Ringuet, Ecole Polytechnique, IN2P3-CNRS, Palaiseau, France
[g]Suez Canal University, Suez, Egypt
[h]Cairo University, Cairo, Egypt
[i]British University, Cairo, Egypt
[j]Fayoum University, El-Fayoum, Egypt
[k]Soltan Institute for Nuclear Studies, Warsaw, Poland
[l]Université de Haute-Alsace, Mulhouse, France
[m]Moscow State University, Moscow, Russia
[n]Brandenburg University of Technology, Cottbus, Germany
[o]Institute of Nuclear Research ATOMKI, Debrecen, Hungary
[p]Eötvös Loránd University, Budapest, Hungary
[q]Tata Institute of Fundamental Research - HECR, Mumbai, India
[r]University of Visva-Bharati, Santiniketan, India
[s]Sharif University of Technology, Tehran, Iran
[t]Isfahan University of Technology, Isfahan, Iran
[u]Shiraz University, Shiraz, Iran
[v]Plasma Physics Research Center, Science and Research Branch, Islamic Azad University, Teheran, Iran
[w]Facoltà Ingegneria Università di Roma, Roma, Italy
[x]Università della Basilicata, Potenza, Italy
[y]Università degli Studi Guglielmo Marconi, Roma, Italy
[z]Laboratori Nazionali di Legnaro dell' INFN, Legnaro, Italy
[aa]Università degli studi di Siena, Siena, Italy
[bb]University of Bucharest, Bucuresti-Magurele, Romania
[cc]Faculty of Physics of University of Belgrade, Belgrade, Serbia
[dd]University of Florida, Gainesville, USA
[ee]University of California, Los Angeles, Los Angeles, USA

[ff]Scuola Normale e Sezione dell' INFN, Pisa, Italy
[gg]INFN Sezione di Roma (a); Università di Roma "La Sapienza" (b), Roma, Italy
[hh]University of Athens, Athens, Greece
[ii]Rutherford Appleton Laboratory, Didcot, United Kingdom
[jj]The University of Kansas, Lawrence, USA
[kk]Paul Scherrer Institut, Villigen, Switzerland
[ll]Institute for Theoretical and Experimental Physics, Moscow, Russia
[mm]Gaziosmanpasa University, Tokat, Turkey
[nn]Adiyaman University, Adiyaman, Turkey
[oo]The University of Iowa, Iowa City, USA
[pp]Mersin University, Mersin, Turkey
[qq]Kafkas University, Kars, Turkey
[rr]Suleyman Demirel University, Isparta, Turkey
[ss]Ege University, Izmir, Turkey
[tt]School of Physics and Astronomy, University of Southampton, Southampton, United Kingdom
[uu]INFN Sezione di Perugia (a); Università di Perugia (b), Perugia, Italy
[vv]University of Sydney, Sydney, Australia
[ww]Utah Valley University, Orem, USA
[xx]Institute for Nuclear Research, Moscow, Russia
[yy]University of Belgrade, Faculty of Physics and Vinca Institute of Nuclear Sciences, Belgrade, Serbia
[zz]Argonne National Laboratory, Argonne, USA
[aaa]Erzincan University, Erzincan, Turkey
[bbb]Kyungpook National University, Daegu, Korea